Dissertation

submitted to the

Combined Faculty of Natural Sciences and Mathematics

of the Ruperto Carola University Heidelberg, Germany

for the degree of

Doctor of Natural Sciences

Presented by

M.Sc. David Weigt

born in: Hildesheim, Germany

Oral examination: March 29, 2019

Development of cellular metabolite-based MALDI mass spectrometry assays for drug discovery

Referees: Prof. Dr. Britta Brügger

Prof. Dr. Carsten Hopf

ABBREVIATIONS

ACN	Acetonitrile
ADMET	Absorption, distribution, metabolism, excretion and toxicity
ALL	Acute lymphoblastic leukemia
AMP	Absorption mode processing
ATT	6-Aza-2-thiothymine
AU	Arbitrary unit
CDP	Cytidine diphosphate
CV	Coefficient of variation
CML	Chronic myelogenous leukemia
CoA	Coenzyme A
Da	Dalton
DHB	2,5 dihydroxybenzoic acid
DMSO	Dimethyl sulfoxide
EDTA	Ethylenediaminetetraacetic acid
ESI	Electrospray ionization
FASN	Fatty acid synthase
FCS	Fetal calf serum
FDA	Food and drug administration
FTICR	Fourier transform ion cyclotron resonance
GCP	Good clinical practice
GIST	Gastrointestinal stromal tumor
GMP	Good manufacturing practice
h	Hour
HDAC	Histone deacetylase
HEPES	4-(2-hydroxyethyl)-1-piperazineethanesulfonic acid
HPLC	High performance liquid chromatography
HTS	High-throughput screening
H_2O	Water (HPLC quality)
IC	Intact cell
IC50	Half maximal inhibitory concentration
IMDM	Iscove's modified Dulbecco's medium
IND	Investigational new drug
LC	Liquid chromatography
m	Mass
min	Minute
ml	Milliliter
m/z	Mass-to-charge
µl	Microliter
MALDI	Matrix-assisted laser desorption / ionization
Malonyl-CoA	Malonyl-coenzyme A
MS	Mass spectrometry

MSE	Matrix suppression effect
MSI	Mass spectrometry imaging
MTP	MALDI target plate
Nd:YAG	Neodymium-doped yttrium aluminum garnet
NMR	Nuclear magnetic resonance
PBS	Phosphate buffered saline
PC	Phosphatidyl-choline
PCA	Principal component analysis
PD	Pharmacodynamics
PDD	Phenotypic drug discovery
PEN/STREP	Penicillin-streptomycin
PK	Pharmacokinetic
pKa	Negative logarithm of the acid dissociation constant
ppm	Parts per million
rpm	Revolutions per minute
RPMI	Roswell park memorial institute medium
R&D	Research and development
S/N	Signal-to-noise ratio
s	Second
T	Tesla
TDD	Target-based drug discovery
TOF	Time of flight
TOFA	5-(tetradecyloxy)-2-furancarboxylic acid
TFA	Trifluoroacetic acid
UV	Ultraviolet
WC	Whole cell

TABLE OF CONTENTS

SUMMARY

Due to their speed and lack of photonic interferences MALDI MS assays have a great potential to support drug discovery. Previous work demonstrated the feasibility of whole cell-based MALDI MS assays for abundant pharmacodynamics protein markers. Analogous assays for metabolites, which are of interest for phenotypic and mechanistic drug profiling studies due to their potentially high dynamic range, have been missing. In this thesis a score-based method development approach was implemented to develop a metabolite-based whole cell MALDI MS fingerprinting workflow. The final workflow enabled optimized discrimination of three cancer cell lines by principal component analysis. This MS fingerprinting workflow was used for development of the first metabolite-based phenotypic MALDI MS assay, in this case to monitor BCR-Abl tyrosine kinase inhibition in K562 leukemia cells. To add to the strength of this workflow, a data processing pipeline was developed in R programming language for the automated extraction of drug-sensitive *m/z* features. This data processing pipeline enabled the extraction of metabolite concentration-response markers that were structurally characterized by ultra-high resolution MALDI-FTICR MS/MS. To this end, heme B, a known marker for erythropoiesis in K562 cells, was identified as a suitable phenotypic marker of redifferentiation of these leukemia cells. The potassium adduct of the membrane lipid phosphatidylcholine (36:1) enabled to compare potencies of different tyrosine kinase inhibitors. In the second part of this thesis, the first MALDI MS-based mechanistic cell assay was developed, using inhibitors of the fatty acid synthase (FASN) as an example. Here, the employment of a ^{13}C-labelled internal isotope standard enabled standardized monitoring of cellular malonyl-CoA accumulation upon FASN inhibition. Automation enabled assays in 96-well format. The dynamic range of the signal readout and Z-factors suggested excellent assay performance. Exploratory, unbiased data analysis followed by MS/MS structural characterization revealed CDP-choline as a generalized marker for lipid pathway inhibition, which not only responds to confirmed FASN inhibitors but also to the acetyl-CoA carboxylase inhibitor TOFA. The assay confirmed publications highlighting BI 99179 and GSK2194069 as potent FASN inhibitors but also gave evidence that a third inhibitor, triclosan, which also was published as a FASN inhibitor, indeed affects the lipid synthesis pathway at one synthetic step, but most likely not FASN activity. In conclusion, this thesis demonstrated that metabolite-based MALDI MS cell assays – both phenotypic and mechanistic - are feasible, standardizable, and automatable, and that they generate robust data useful for chemical biology work or compound profiling in drug discovery. Future work is likely going to focus on scaling up the throughput of MALDI MS cell assays by miniaturization and automation as well as expanding the repertoire of metabolic enzymes targetable by MALDI MS cell assays.

ZUSAMMENFASSUNG

Aufgrund ihrer Schnelligkeit und des Fehlens photonischer Interferenzen haben Matrix-unterstützte Laser-Desorptions-/Ionisations (MALDI) Massenspektrometrie (MS) -Assays ein großes Potenzial, die Entdeckung neuer Wirkstoffe zu unterstützen. In früheren Arbeiten wurde die Durchführbarkeit von MALDI MS-Zellassays für abundante pharmakodynamische Proteinmarker gezeigt. Bislang gab es jedoch keine analogen Assays für Metabolite, die aufgrund ihres potentiell hohen dynamischen Bereichs für phänotypisches und mechanistisches Wirkstoff-Profiling von Interesse sind. In dieser Dissertation wurde ein kennzahlenbasierter Ansatz zur Methodenentwicklung implementiert, um einen metabolitbasierten MALDI MS-Fingerprinting-Workflow für ganze Zellen zu entwickeln. Der finale Workflow ermöglichte die optimierte Unterscheidung von drei Krebszelllinien mittels Hauptkomponentenanalyse (PCA). Der MS-Fingerprinting-Workflow wurde für die Entwicklung des ersten metabolitenbasierten, phänotypischen MALDI MS-Assays verwendet, in diesem Fall, um die Inhibition der BCR-Abl-Tyrosinkinase in K562-Leukämiezellen zu messen. Um die Leistungsfähigkeit des Workflows zu erhöhen, wurde mit Hilfe der Programmierumgebung R eine Datenverarbeitungspipeline zur automatisierten Extraktion von wirkstoffsensitiven *m/z*-Werten entwickelt. Diese Datenverarbeitungspipeline ermöglichte die Extraktion von Metabolit-Konzentrations-Wirkungs-Markern, die mittels ultrahochauflösender MALDI-FTICR MS/MS strukturell charakterisiert wurden. Häm B, ein bekannter Marker für Erythropoese in K562-Zellen, wurde als geeigneter phänotypischer Marker für die Redifferenzierung dieser Leukämiezellen identifiziert. Das Kaliumaddukt des Membranlipids, Phosphatidylcholin (36:1), ermöglichte den Vergleich der Potenzen verschiedener Tyrosinkinase-Inhibitoren. Im zweiten Teil dieser Arbeit wurde am Beispiel der Inhibition der Fettsäuresynthase (FASN) der erste auf MALDI MS basierende mechanistische Zellassay entwickelt. Die Verwendung eines ^{13}C-markierten Standards ermöglichte eine standardisierte Überwachung der zellulären Malonyl-CoA-Akkumulation nach FASN-Inhibition. Automatisierung ermöglichte die Durchführung des Assays im 96-Well-Format. Der dynamische Bereich des Signals sowie der Z-Faktor deuteten auf einen hervorragenden Assay hin. Explorative Datenanalyse gefolgt von MS/MS-Strukturcharakterisierung ergab, dass CDP-Cholin als genereller Marker für die Inhibition der Phospholipid-Biosynthese fungiert, der nicht nur auf bestätigte FASN-Inhibitoren, sondern auch auf den Acetyl-CoA-Carboxylase-Inhibitor TOFA anspricht. Der Assay bestätigte Publikationen, in denen BI 99179 und GSK2194069 als potente FASN-Inhibitoren hervorgehoben wurden, wies jedoch auch darauf hin, dass ein weiterer Inhibitor, Triclosan, der ebenfalls als FASN-Inhibitor veröffentlicht wurde, tatsächlich die Lipidsynthese an einem Syntheseschritt beeinflusst, jedoch nicht die FASN-Aktivität. Zusammenfassend konnte in dieser Arbeit gezeigt werden, dass - sowohl phänotypische als auch mechanistische -

metabolitbasierte MALDI-MS-Zellassays durchführbar, standardisierbar und automatisierbar sind und robuste Daten liefern, die für die chemische Biologie oder das Wirkstoffprofiling nützlich sind. Zukünftige Arbeiten werden sich voraussichtlich auf die Erhöhung des Durchsatzes von MALDI MS-Zellassays durch Miniaturisierung und Automatisierung sowie die Erweiterung des Repertoires an Enzymreaktion, die durch MALDI-MS-Zellassays nachverfolgt werden können, fokussieren.

1 INTRODUCTION

1.1 MASS SPECTROMETRY

Mass spectrometry (MS) is an analytical technique used to ionize chemical species and sort them based on their mass-to-charge ratio (*m/z*). Mass spectra are typically plots of *m/z* values against their ion intensities and can be used to determine the isotopic distribution of an atom or molecule [1], the chemical structure of a molecule [2], or a species or molecule specific pattern also called fingerprint [3].

A mass spectrometer typically consists of an ion source to ionize gaseous, liquid or solid samples, a mass-analyzer to separate the ions by *m/z* in an electric or magnetic field, and a detector to detect charged molecules [4]. If the formation of gas phase ions involves extensive fragmentation of the analyte, the ionization technique is referred to as 'hard', whereas ionization techniques without extensive fragmentation are referred to as 'soft' [5].

Accurate mass measurements require a high mass resolution to rule out the interference with signals corresponding to ions of different elemental compositions. Mass resolution is defined as the closest distance between two distinguishable peaks of equal width and height [6]. The term resolving power is defined as the quotient of the mass resolution and the measured *m/z*. Mass accuracy, is defined as the quotient of the *m/z* measurement error (Δm) and the true *m/z*. Mass accuracy is typically measured in parts per million (ppm).

To date, a wide variety of methods to transfer charged ions into the gas phase have been described. Among these methods matrix-assisted laser desorption / ionization (MALDI) has become an irreplaceable part in biological science [7].

1.1.1 BASICS OF MALDI MS

MALDI is a relatively impurity tolerant and sensitive ionization method that is characterized by relatively little fragmentation of the analyte [8]. Prerequisite for MALDI is the incorporation of the analyte molecules into a crystalline matrix. The analyte is desorbed from the target plate by irradiating matrix:analyte co-crystals with a pulsed laser beam. After the desorption and ionization, the analyte molecules are separated according to their respective *m/z* values in the mass analyzer [9]. Although the MALDI ionization process is not fully understood, two descriptive models have found scientific acceptance:

The **Gas Phase Protonation model** proposes two steps that lead to the formation of analyte ions. In the first step, laser irradiation produces matrix ions through photoionization. In the second step, the charge is transferred to the neutral analyte molecules [9, 10].

The **Lucky Survivor model** proposes that the extent of ionization depends on the solvent and matrix used during sample preparation. According to the model, the solvent and matrix transfer charges to the analyte. Subsequently, the charged analyte is incorporated into the matrix crystal. Laser induced desorption releases charged clusters of analyte and matrix into the gas phase. Charge transfer among analyte and counterions might either result in quantitatively neutralized clusters that are not detectable. In cases of charge excess due to charge separation during the disruption of the matrix crystal, the lack of counterions favors the formation of charged analytes – the lucky survivors [9, 11]. It might well be possible that both models are involved in the formation of analyte ions (**Fig. 1.1.1**) [10].

Time of flight (TOF) analysis is well suited for the pulsed ion generation by MALDI. The generated ions are accelerated in an electric field (**Fig. 1.1.2 A**). The time required to pass a flight tube (*tof*) is dependent on the mass (*m*) and the charge of the particle (*q*):

$$tof = k\sqrt{\frac{m}{q}}$$

where *k* is a proportionality factor, that includes among other the length of ion source and flight tube as well as the extraction potential. TOF measurements can be applied over a broad mass range since the analyzer can be operated in both linear (2 - >100 kDa) and reflector mode (0 – 2000 Da) [12]. In linear mode the ions are directly accelerated towards the detector. In reflector mode the accelerated ions are redirected in an ion mirror (reflector) at the end of the flight tube to compensate slight differences in kinetic energy. Thereby mass resolution and accuracy are increased.

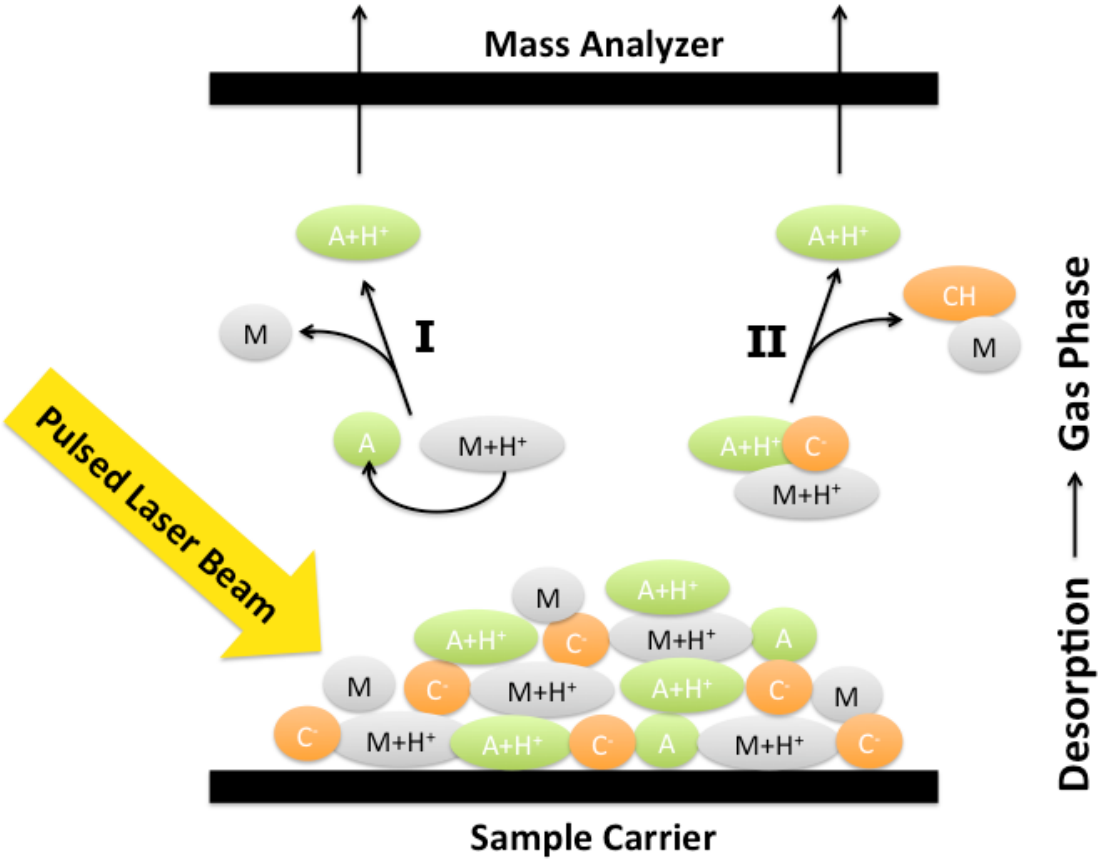

Figure 1.1.1: The MALDI process. The analyte is embedded into a MALDI matrix on a sample carrier. A pulsed laser beam irradiates the sample. Two complementary models are used to describe the subsequent desorption and ionization: I) According to the Gas Phase Protonation model, neutral analyte molecules are charged by gas phase collisions with charged matrix-molecules. II) The lucky survivor model proposes that the charged analyte breaks out of a cluster of ions that predominantly neutralize each other. The charged analytes enter the mass analyzer. Note that the model is not only valid for the generation of positively charged ions (as illustrated) but also for negatively charged ions.

MALDI-TOF MS has been applied to a broad range of biological analytes like proteins in linear mode as well as peptides, glycans, lipids and metabolites in reflector mode. Typical mass resolutions in linear and reflector mode are 5,000 and 20,000, respectively. For higher mass resolutions of 100,000 and above, the MALDI sources are coupled to mass analyzers like the Fourier Transform (FT) Ion Cyclotron Resonance (ICR) analyzer [13].

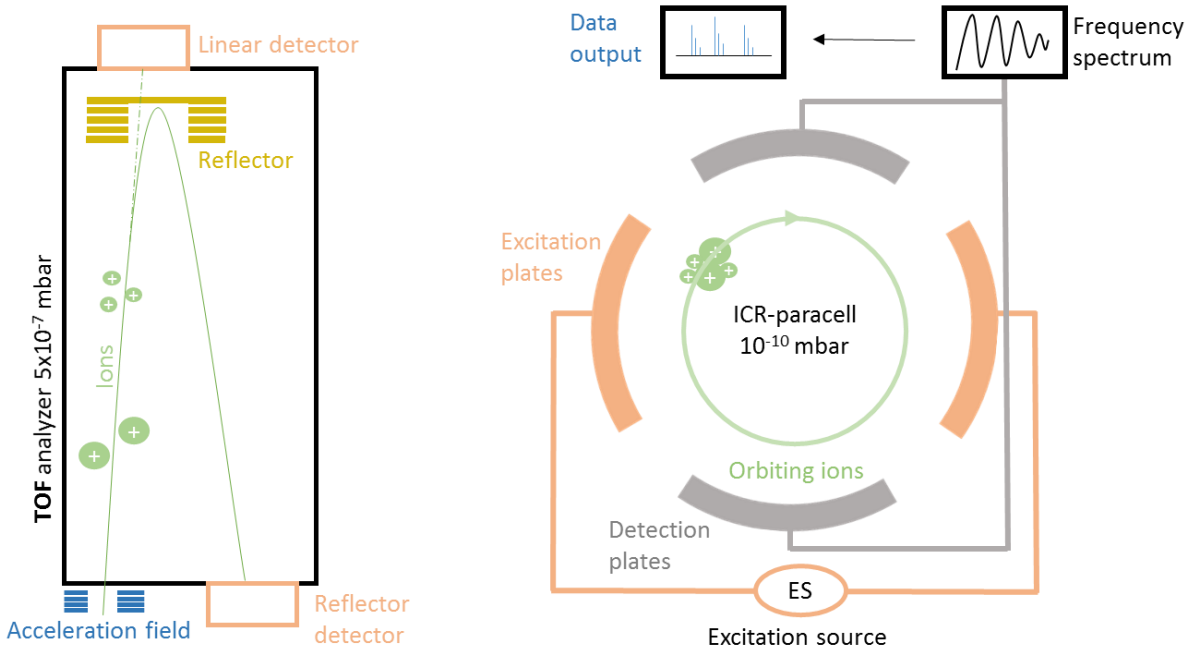

Figure 1.1.2: Common mass analyzers combined with MALDI. A) During a MALDI-TOF measurement, gas phase ions enter the TOF analyzer upon acceleration in an electric field. For linear ion mode measurements, ions directly pass the flight tube towards the linear detector. For measurements in reflector ion mode, an ion mirror, i. e. reflector, is interposed prior to the linear detector. Low molecular mass molecules are redirected and describe an inverted U-shaped flight pass towards the reflector detector. B) During a MALDI-FTICR measurement ions enter a strong magnetic field, in which they are kept on circular trajectories through excitation to their cyclotron resonance frequency. The movement of charged molecules in a magnetic field induces a voltage at the detection plates. The obtained frequency spectrum can be converted into a mass spectrum through Fourier transformation.

In FTICR MS charged particles, e.g. ions, are trapped in an orthogonal magnetic field between two electric plates (Penning Trap) by a force called “Lorentz Force“ (**Fig. 1.1.2 B**). An instrument that excites these circulating ions to larger trajectories by an oscillating electric field is called ICR mass spectrometer. The frequency at which an ion moves in a magnetic field is characteristic for its mass and can be measured by electrodes. The measured signal is a superposition of sine waves, called free induction decay (FID). Fourier transformation of the FID results in a mass spectrum [14].

1.1.2 HISTORICAL VIEW ON THE DEVELOPMENT OF MALDI MS

In the early 1910s, Joseph John Thomson invented an instrument that was able to measure the electron to mass ratio (*e/m*) and thereby indirectly enabled to determine the mass of *e*. Thomson was awarded the Nobel Prize in Physics in 1906 for investigating the electron[1]. Together with Francis Aston, who was awarded the Nobel Prize in Chemistry in 1922, Thomson built the first mass spectrometer that was able to measure the mass of charged atoms [15]. In the beginning of the 20th century mass spectrometry was mainly used to separate elemental isotopes which was of particular importance for the separation of ^{235}U, the isotope suitable for nuclear fission from ^{238}U in the nuclear weapons program during World War II [16].

In 1985, Karas, Bachmann and Hillenkamp demonstrated that the addition of small UV-absorbent molecules as a matrix facilitates the detection of non-absorbing molecules [17]. The great advantage of this method is an almost fragmentation free, soft ionization. The development of MALDI for nonvolatile molecules advanced the use of TOF mass analyzers, which until then were only of interest for the rather exotic studies on charged atoms [18].

In 2002, the Nobel Prize in Chemistry was awarded one fourth to Koichi Tanaka for the "development of soft desorption ionization methods for mass spectrometric analyses of biological macromolecules"[2]. Tanaka had developed a method where the sample is deposited on the surface of a liquid matrix containing glycerol and cobalt powder [19]. The method has a poor sensitivity compared to MALDI where the analyte is mixed with a crystalline matrix. For this reason MALDI was embraced by the scientific community [15].

MALDI-TOF mass spectrometers were commercially available since the early 1990s. The first integrated MALDI-TOF instrument and software solution for routine clinical use was the MALDI Biotyper. In 2012, the MALDI Bioytyper got FDA approval for diagnostics of cultured bacteria from human specimens [20].

Novel applications like MALDI MS imaging and high throughput MALDI MS assays were facilitated by novel mass spectrometers with much increased speed of data acquisition provided, for example, by new lasers such as a Smartbeam 3D 10 kHz frequency-tripled Nd:YAG laser. Early MALDI-TOF instruments required 1-2 minutes / data point, however

[1] Nobelprize.org (1906) The Nobel Prize in Physics 1906. https://www.nobelprize.org/nobel_prizes/physics/laureates/1906/.
[2] Nobelprize.org (2002) The Nobel Prize in Chemistry 2002. https://www.nobelprize.org/nobel_prizes/chemistry/laureates/2002/index.html.

advances in laser technology and data acquisition methodology enable the latest mass spectrometers to have a sampling rate of 50 data points / s [21].

1.1.3 MALDI MS WHOLE CELL ASSAYS

The terms whole cell (WC) or intact cell (IC) measurements refer to methods in which cells are directly subjected to MS analysis without prior fractionation or extraction. Despite the fact that omitting pre-purification steps reduces sensitivity, IC-MALDI MS has been appreciated for its speed, robustness, low cost, and ease of automation early on [3]. The development of whole cell-based MALDI MS assays went hand in hand with advances of the MALDI MS technology (**Fig. 1.1.3**).

The first whole cell measurements were described by Anhalt *et al.* in 1975 [22]. The study team had directly inserted lyophilized bacteria into the heated ion source of a plasma ionization mass spectrometer and observed species-specific pyrolysis products of ubiquinones and phospholipids. The publication had opened the field of species-specific pattern recognition, also referred to as fingerprinting or biotyping, using mass spectrometry.

In 1996 Holland *et al.* were the first to implement MALDI-TOF MS for bacterial biotyping. Since that time MALDI MS biotyping has been established as an important tool in both environmental microbiology and clinical diagnostics of pathogenic bacteria [23].

In more recent years, MALDI biotyping has also been applied to mammalian whole cells. The Lam and the Hopf laboratories were among the first to develop MALDI MS-based biotyping methods for the, compared to bacteria, more complex mammalian cells. In a seminal study Zhang *et al.* generated protein fingerprints that enabled one to distinguish different cell lines [24]. The publication had a strong focus on the identification of the underlying proteins which were mainly abundant proteins like ribosomes and histones. In contrast, Munteanu *et al.* centered method development on the generation of a standardized protein fingerprint from whole mammalian cells [25]. The method was able to reproducibly distinguish cell lines and primary cells in PCA space. Due to its robustness, this method is suited to characterize cells during bioprocesses [26, 27].

The first pharmacological relevant studies using IC-MALDI MS were also protein-based. Dong *et al.* described an IC-MALDI MS assay to detect apoptosis-based on specific features that were reproduced in several different cell lines [28]. The first quantitative drug target engagement study using IC-MALDI MS was reported by Munteanu *et al.* in 2014 [29]. The group was able to derive IC50 values of histone deacetylase inhibitors by quantifying histone

acetylation specific mass shifts. These mass shifts were directly observed in the IC-MALDI fingerprint without any sophisticated enrichment steps.

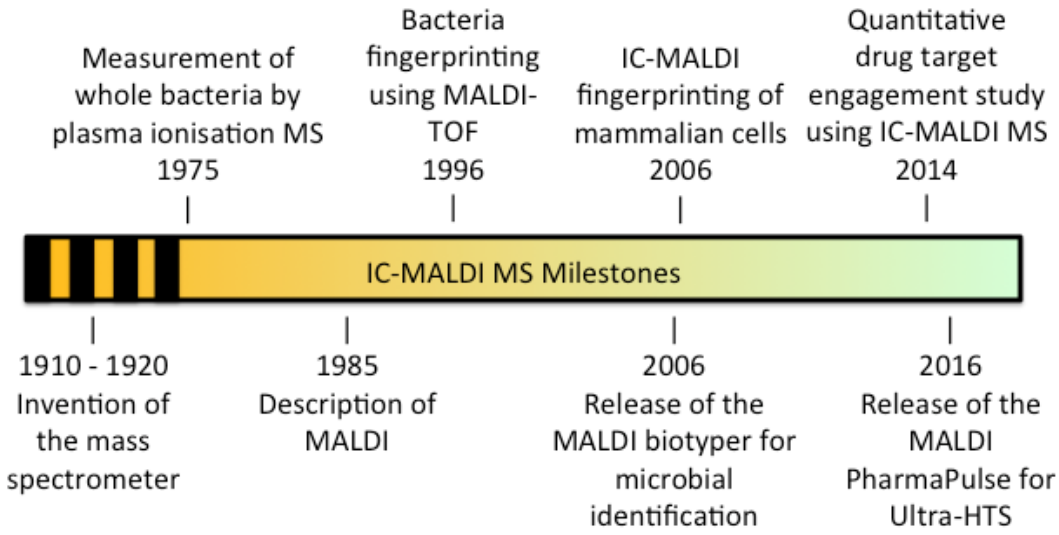

Figure 1.1.3: Technological milestones in the development of IC-MALDI MS. In 1919, Thomson and Aston developed the first mass spectrometer for charged atoms. In 1975, the Fenselau group obtained mass spectra of whole bacteria. Karas and Hillenkamp discovered the MALDI process in 1985. In 1996, MALDI-TOF MS was first used for bacteria fingerprinting. A decade later, the first end-user friendly MALDI biotyper was launched. Around the same time fingerprints of intact mammalian cells were reported in a seminal study. In 2014, histone deacetylase drug target engagement was monitored by IC-MALDI. Two years later the rapifleX MALDI PharmaPulse for ultra-HTS was released.

By now, protein-based IC-MALDI MS assays have been reported for the use of pharmacodynamic characterizations repeatedly [30, 31]. In contrast, metabolite-based IC-MALDI MS assays to determine IC_{50} values have not been described thus far.

Still some notable work has been done in the field already. In 2012 the Corcelli study team used MALDI MS to measure lipids from intact mitochondria [32]. In follow-up work, they were able to generate a cardiolipin fingerprint of whole leukocytes, which worked as a diagnostic tool for Barth syndrome [33]. In 2017, Lobasso *et al.*, found alterations of phospholipids and glycosphingolipids in whole cell MS profiles of *parkin*-mutant human skin primary fibroblasts. These alterations are hypothesized to be due to mitochondrial turnover and autophagy [34].

In a single pharmacology related study, Sakai *et al.* compared lipid patterns of benign prostate hyperplasia to Degarelix treated prostate cancer cells [31]. The authors monitored global changes in the lipid pattern upon treatment with a single concentration of Degarelix. A quantitative pharmacodynamic characterization of drug action has not yet been performed by

metabolite-based IC-MALDI MS and neither automatable phenotypic or mechanistic MALDI MS-based cellular assays exist to date.

1.1.4 Sample preparation and multifactorial method development for small molecule-based MALDI MS

Co-crystallization of matrix molecules and analyte is a prerequisite for MALDI. Particularly for the detection of peptides and metabolites, the incorporation of the analyte into the matrix crystals has substantial impact on the limit of detection [35]. The sample preparation protocol for MALDI has been subjected to research for decades. Plenty of preparatory methods have been described.

Commonly used MALDI matrices, that have been described for lipid and metabolite detection include 1,5-diaminonaphthalene (DAN) [36], 2,5-dihydroxybenzoic acid (DHB) [37], 6-Aza-2-thiothymine (ATT) [38], 9-aminoacridine (9AA) [33] and α-cyano-4-hydroxy cinnamic acid (HCCA) [39].

MALDI matrices are required to form crystals, which enable the incorporation of analyte molecules. At the same time the blessing of a well crystallizing matrix is also a burden. When applying mixtures of analyte and DHB matrix on a target spot, DHB forms large crystals at the periphery of the spot. Best signal intensities are obtained when the UV-laser directly hits these crystals, the so called “sweet spots”. The existence of these sweet spots is a main reason for signal heterogeneity, poor automation and poor reproducibility [40].

The reason for crystals growing from the periphery of the spot is the **coffee stain effect**. Evaporation of solvent causes a periphery driven flux inside the droplet. The outward driven flow compensates for rapidly decreasing droplet-height at its edges. The analyte molecules are pinned at the three phase contact line between solvent, air and steel target [41].

To this day, plenty of matrix application methods have been described, but still the gold standard is missing. In a classic preparation, which is typically referred to as **dried droplet**, the MALDI matrix is directly mixed with the analyte and applied on the MALDI target. A **sandwich** preparation describes the deposition of an analyte and matrix containing droplet on top of a predeposited matrix layer [25]. The predeposited matrix molecules function as anchor-crystals for the applied solution. Ruh *et al.* described the **PrimaDrop** method for lipids where the analyte is prespotted on the target plate and the matrix, dissolved in a highly volatile solvent, is spotted on top [38]. Fast evaporation of the solvent diminishes the formation of

larger crystals while the preparation is aggravated by volatile solvents. In the field of mass spectrometry imaging a standard operation is to **spray** the matrix on top of the specimen using capillary flows [42]. Small applied volumes result in a layer of equally distributed, small crystals. Hankin *et al.* introduced the use of matrix **sublimation** to homogenously coat the sample with matrix [43]. In this solvent free system, the matrix crystals grow with the amount of sublimated matrix. Kudina *et al.* enhanced drying of analyte and matrix solutions by **electrowetting** [41]. In an electric field the applied sample spot is exposed to flow fields that counteract the molecule-flux driven by evaporation. The preparation requires a non-commercially available target plate that enables row wise application of an alternating voltage.

In addition to matrix preparations and deposition methods, several **solvent additives** have been described to increase method performance. Trifluoroacetic acid (TFA), a strong organic acid, increases signal intensities of basic analytes in positive ion mode by decreasing the pKa of the matrix [44]. Addition of (alkali) salts has been described to facilitate spectra interpretation and to improve detectability of certain lipids since analyte signals are shifted from multiple adducts to one forced adduct [45].

A multitude of small molecules to facilitate the detection of metabolites and lipids are proposed in the literature. Also, the number of parameters that require optimization in the course of method development exceeds a dimensionality that can be reduced to visualization and evaluation in 2- or 3D space.

AlMasoud *et al.* performed **fractional factorial design** (FFD) to optimize the detection of 5 lipids [46]. The authors considered 8 different matrices, 11 matrix additives, 5 additive concentrations, 6 matrix preparation methods and 3 deposition methods as important factors. The FFD algorithm selected the lowest number of experiments to sufficiently describe the underlying problem and reduced the possible 8064 experiments to 720 key experiments. This approach is especially helpful if a method is developed from scratch. Despite a reduction of experimental effort by more than 90 %, the 720 remaining experiments are still considerably cost and time consuming.

Erich *et al.* developed an on-tissue digest method for MSI by score-based comparison of four state of the art on tissue digestion protocols and combining parts of the methods to a new method. They also introduced a **method scoring system**, which reflects data scattering in PCA space. The interclass overlap score $\boldsymbol{J_{overlap}}$ is the quotient of data scattering within a coherent group (W_S) divided by data scattering between non-coherent groups (B_S).

$$J_{overlap} = \frac{|W_S|}{|B_S|}$$

Even though the score was intended as a tool to measure reproducibility in multivariate space [47], $J_{overlap}$ enables parallel optimization of reproducibility and information content.

Another valuable score is the **matrix suppression effect** (MSE) [48]. The MSE occurs when sufficient analyte molecules are present in the sample. Ideally all matrix ions are suppressed and the spectrum contains only analyte signals. Fülöp *et al.* published the MSE by lipids score (MSE_{lip}) as the ratio of the amount of lipid signals (Σ lipids) compared to all signals (Σ lipids + Σ matrix) for a given mass range [49]:

$$MSE_{lip} = \frac{\sum lipids}{\sum lipids + \sum matrix}$$

1.1.5 Introduction to principal component analysis

Principal component analysis (PCA) is a widespread tool for dimensionality reduction while maintaining the majority of information of the dataset [50]. The use of PCA for dimensionality reduction of mass spectra has previously been implemented for the analysis of both MALDI MS imaging [51, 52] and fingerprinting [25, 53, 54] data.

The means by which PCA reduces data complexity while maintaining the majority of the data sets' information, i.e. the variance in the data, is briefly described for a simplified set of 20 mass spectra consisting of 3 peaks each (**Fig. 1.1.4 A**)[3]. The mass spectrum is vectorized and projected into a multidimensional space (**Fig. 1.1.4 B**). This is performed for all 20 mass spectra of the sample set, which all display different intensities of the 3 same signals (**Fig. 1.1.4 C**). In general, a set of mass spectra containing n distinct signals can be projected in an n-dimensional space, which features n so called principle components (PC) as the basis for a novel coordinate system (**Fig. 1.1.4 D**). The PCs are placed into the old coordinate system according to the following rules [55]:

- The center of the datapoints is the origin of the new coordinate system
- The first PC is placed in the direction of the highest variance. The second PC is placed in the direction of the second highest variance and so on.
- The coordinates are perpendicular

[3] Example adapted from: BRUKER - MALDI Imaging tutorial PCA intro, © Bruker 2010

The variance plot describes which fraction of the data set's variance is covered by the respective PC (**Fig. 1.1.4 E**). By excluding low variance PCs, the dataset is projected into a lower dimensional space while retaining most of the dataset's variance (**Fig. 1.1.4 F**).

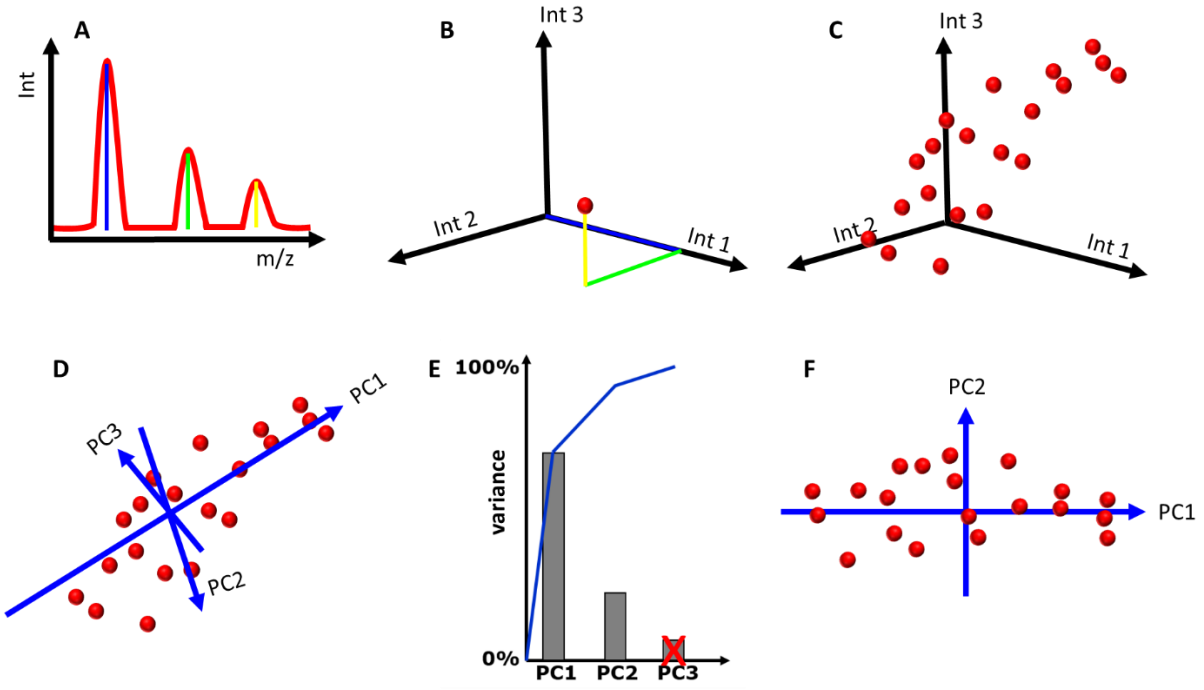

Figure 1.1.4: Dimensionality reduction using PCA. A) Illustration of a mass spectrum consisting of 3 signals. B) Vectorized illustration in 3D space of spectrum displayed in (A). C) Vectorized illustration in 3D space of 20 sample mass spectra. D) Graph displayed in (C) with PCs as novel coordinates. E) Variance plot, displaying the variance covered by the PCs displayed in (D). F) Graph displayed in (D) upon reduction of PC3. (Example adapted with some modifications from: BRUKER - MALDI Imaging tutorial PCA intro, © Bruker 2010)

In the end PCA illustrates how similar spectra are [56]. Groups of spectra that form more condensed "clouds" are more similar, whereas the distance between spectra or groups of spectra is a measure for spectral differences.

Since some signals expose greater variance than others, not all signals contribute equally to the placement of the PCs. Therefore, an additional, interesting piece of information is to which extend a certain signal contributed to the variance covered by a certain PC. In other words: "Which signals contributed most to separate my data along the PC1 axis?" This information is displayed in the loadings plot [56].

1.2 DRUG DISCOVERY

Drug discovery is the process, which aims to find **preclinical candidates** for novel medications. At the end of discovery, preclinical candidate leads are selected and progressed into preclinical development. The output of a successful preclinical development is an **investigational new drug** (IND) application which includes information on animal pharmacology and toxicology studies, manufacturing information and clinical investigator guidance. The IND is required to start clinical trials. The result of successful clinical development is the filing of a **new drug application** (NDA), which requests the food and drug administration to approve the market entry of a new drug in the United States. The NDA includes information for FDA reviewers on the drug's safety, proposed use, appropriate labelling and manufacturing[4]. In contrast to drug discovery, clinical development is highly regulated by requirements like **good clinical practice** (GCP) and **good manufacturing practice** (GMP).

A key process in drug discovery is the identification of **lead compounds**. These are compounds that possess pharmacological activity and could become therapeutically useful upon structural optimization. As a first step, **hit compounds** are identified by **high throughput screening** (HTS) [57]. During a HTS campaign, pharmaceutical companies test **compound libraries,** which contain typically more than 50.000 and up to millions of compounds [58]. HTS is driven by a high degree of automation and has been established in the early 90th. The past three decades were dominated by **target-based drug discovery** (TDD), where a presumably disease relevant molecular target was the starting point of screening campaigns [59]. In recent years, interest in **phenotypic drug discovery** (PDD), in which the molecular drug target is unknown, was revived by studies highlighting PDD's strong contribution to the past discovery of first in class drugs [59, 60].

In vitro assays used for drug discovery can be differentiated between biochemical assays and cell-based assays. For **biochemical assays,** the compounds are tested in a reaction mixture containing the purified protein drug target and all relevant substrates. For **mechanistic cell assays** the drug target is also known and the assay readout is directly linked to the cellular target activity. Mechanistic cell assays are important for drug discovery in pharmaceutical industry. There are numerous examples in the literature of biochemical enzyme assays and mechanistic assays going hand in hand to measure the cellular activity of inhibitors [61, 62]. **Phenotypic cell assays** can be of help when the complexity of a disease is not completely

[4] Investigational New Drug (IND) Application - Drug Development and Review Definitions. Available at: https://www.fda.gov/drugs/developmentapprovalprocess/howdrugsaredevelopedandapproved/approvalapplications/investigationalnewdrugindapplication/ucm176522.htm.

understood or a mechanistic readout is not accessible. In this case, changes of the cellular morphology or molecular signatures are potential assay readouts [59].

Upon their identification, screening hits are confirmed by approaches like counter-screens, orthogonal assays or computational approaches [63]. Confirmed hit compounds are optimized in a process called **hit-to-lead expansion**. Lead compounds are improved by medicinal chemists in a synthetic effort to optimize biologic activity towards one or several candidate compounds for clinical trials. These optimizations may include modifications of lipophilicity, binding efficiency and molecular weight [64]. The **chemical space** is estimated to theoretically harbor 10^{30} – 10^{60} drug like molecules, enabling a vast variety of options to optimize the screening hit. The final clinical candidate often constitutes a compromise between biological activity and ADMET (absorption, distribution, metabolism, excretion and toxicity) properties [65].

Presently, clinical development and approval of a new drug requires extensive resources and can cost up to a billion dollars. Therefore, a thorough characterization of novel compounds in the early discovery stage is vital for the pharmaceutical industry [66]. Over the past 60 years, advances in **combinatorial chemistry** considerably increased the size of compound libraries. Increased speed of DNA sequencing by orders of magnitude facilitated the discovery of novel potential drug targets. Databases with protein structures facilitate structure guided lead improvement. Nevertheless, the number of new drugs brought to the market per billion US dollar spent on R&D has constantly declined over the past 50 years [67]. This trend indicates a **declining efficiency of pharmaceutical R&D** and is presumably not answered by further increasing budgets spend on R&D. In recent years, there is a growing tendency for pharmaceutical companies to outsource the early phase of drug research and discovery to contract research organizations (CROs) [68]. The market-research publisher Kalorama predicted that by 2021 more than one third of drug discovery worldwide will be outsourced to CROs[5].

1.2.1 Rationale for metabolite-based MALDI MS to support cell-based assays in drug discovery

Historically, the most widespread application of cell-based assays was to evaluate cell death. Since *in vitro* cytotoxicity assays have been found to not be very predictive for *in vivo* toxicity

[5] Kalorama Information: Outsourced Drug Discovery Market Boosted by Gap in Pipelines. Available at: https://www.kaloramainformation.com/about/release.asp?id=4326.

[69], cytotoxicity assays are mainly used as controls for other cell-based assays. These assays evaluate biological activity, biochemical mechanisms, and off-target effects [66]. Moreover, cell-based assays are used for HTS due to their complaisance to multiplexing [70] and miniaturization down to the single cell level [71].

Fluorescence-based readouts are most widely used in both biochemical and cellular drug discovery assays [72]. Compared to biochemical screenings, cell-based assays do not require confirmation that the compound is cell-permeable and is still active in its destined compartment in the presence of competing small molecules. For example, GSK performed an *in vitro* screening campaign against the full-length, recombinant fatty acid synthase, purified from insect cells. The hit-compound GSK837149A turned out to have impaired cell penetration [73].

Still fluorescence, as well as other label-dependent cell assays, require extensive validation, due to photonic artefacts including autofluorescence of the compound, spectral overlap of compound and fluorophore as well as quenching of the fluorescence or bleaching of the fluorophore[6]. Transfection of engineered cells and interferences of reporter constructs can lead to a distortion of cellular physiology that diminishes data reliability [74]. The emergence of label-free platforms aspires to overcome these limitations by providing readouts that do not interfere with biological function. Major classes of label-free systems for cell-based investigations besides mass spectrometry include refraction index and cell impedance. Refraction index is employed to monitor binding properties of drug candidates and cell impedance could be used to monitor physiologic events such as cell attachment, migration or apoptosis [74, 75]. MS technologies are especially amenable for targeted investigations of mass changes, like enzyme reactions [75].

Liquid chromatography (LC) MS is a sensitive method that can quantitatively monitor a broad range of drug actions without any labeling reagents. A major limitation of LC-MS is the method's throughput. With durations of ~4h per 96-well plate, LC-MS is suitable for medium throughput screens rather than high-throughput primary screens [58, 76].

Automated MALDI-TOF cell assays, as a fast, sensitive and rather impurity tolerant approach, could be a cost effective alternative to existing label-dependent methods. The label-free MALDI-TOF readout saves expensive detection kits, but purified proteins and antibodies are required for biochemical assays. Additionally, low sample volumes of ≤2µl per measuring spot are compatible with current HTS standards [77].

MALDI-TOF MS has already proven to be a valuable tool to screen inhibitors of pharmacologically relevant targets in biochemical assays. These targets included various

[6] Simeonov A, Davis MI (2004) Interference with Fluorescence and Absorbance. Eli Lilly & Company and the National Center for Advancing Translational Sciences

kinases [77–79], the histone demethylase JMJD2c [80], the tyrosine phosphatase PTP1B [57] and several human deubiquitinases [81].

Also protein-based IC-MALDI MS assays have been suggested as relevant tools to support drug discovery. Especially noteworthy is the aforementioned cell-assay developed by Munteanu *et al.* that enables label-free monitoring of histone deacetylase inhibition [29]. Due to protein modification turnover rates of only seconds, monitoring of protein modifications, as in the Munteanu *et al.* publication, is a sensitive and fast methodology. On the other hand, choosing protein levels as response markers for inhibitor treatment might be unfavorable, since protein turnover in mammalian cells can take up to several hours [82]. In comparison, metabolites, especially metabolites containing reactive phosphate groups, have been described to be turned over within seconds or fractions of a second [83]. Therefore, monitoring of metabolites harbors the expectation to dramatically increase the sensitivity and dynamic range MALDI MS cell assays.

Moreover, establishment of protein-based MALDI-TOF cell assays requires extensive work to identify the response biomarker by top-down proteomics. This is expected to be less tedious for metabolite-based assays where the signal can be validated by structural elucidation using high resolution mass determination and MS/MS fragmentation analysis [84].

Additionally, with its unique strengths MALDI-TOF MS is anticipated to tackle a problem called "**screening the unscreenable**". For example, the dihydroceramide desaturase 1 (DEGS1) is a multiple membrane-spanning protein located in the ER which catalyzes the final step of de novo ceramide synthesis. DEGS1 is a therapeutic target for metabolic diseases since it has been described to regulate ceramide induced lipotoxicity [85] and to simultaneously stimulate anabolic and catabolic signaling [86]. Despite its potential therapeutic relevance DEGS1 is notoriously difficult to screen. As an enzyme that requires its transmembrane domains for catalytic activity, the protein is particular difficult to purify and therefore hardly accessible for cell-free *in vitro* screens. The same holds true for additional transmembrane enzymes like the stearoyl-CoA desaturase SCD1, which catalyzes the formation of monounsaturated fatty acids. Regulation of SCD1 activity has been known to affect susceptibility of several diseases including obesity, insulin resistance and diabetes [87]. These targets require analysis in a more physiological, ideally cellular, context.

Ordóñez-Gutiérrez *et al.* determined DEGS1 activity in cellular lysates by adding a fluorescent substrate. The suspension was analyzed by HPLC coupled to a fluorescence detector [88]. Li *et al.* measured the stearoyl-CoA to oleoyl-CoA ratio in mouse hepatocytes upon knock out of an SCD1 regulating protein by LC-MS [89]. Roemeling *et al.* isolated SCD1 containing

microsomes from murine liver. The *in vitro* biotransformation of $^{13}C_{18}$-stearoyl-CoA to $^{13}C_{18}$-oleoyl-CoA was monitored by LC-MS [90].

To date, no HTS-compatible analysis has been described to analyze the activity of either of these enzymes. Therefore, especially metabolic transmembrane enzymes are a challenging but reasonable target for metabolite-based MALDI MS cell assays. A fundamental step would be to prove that metabolite-based MALDI MS cell assays are feasible.

1.2.2 IMATINIB – THE FIRST FDA-APPROVED TYROSINE KINASE INHIBITOR – AND OTHER BCR-ABL INHIBITORS

Chronic myeloid leukemia (CML) is a leukemia that is characterized by an upregulated proliferation of myeloid cells in the bone marrow. CML accounts for about 15 % of newly diagnosed leukemias in adults [91].

A unique gene translocation known as the Philadelphia chromosome is the most frequent cause of CML. The Philadelphia chromosome is an oncogenic fusion of the breakpoint cluster region (BCR) which is localized on chromosome 22 and the *abl* gene from chromosome 9 (**Fig. 1.2.1**). The resulting gene product is a continuously active tyrosine kinase that promotes cell proliferation and inhibits DNA repair [92].

Due to difficulties to identify molecular components downstream of BCR-Abl, the tyrosine kinase itself is the most relevant target for drug discovery [93]. The first orally available and potent BCR-Abl tyrosine kinase inhibitors were discovered using a targeted approach in the late 1980s by the famous scientist Brian Druker at Ciba Geigy, today part of Novartis [93]. The lead compound was based on a hit from a screen of inhibitors against protein kinase C [94]. Lead optimization resulted in the promising candidate, imatinib mesylate, which entered clinical trials in 1998 [93, 94].

On the 18th month of phase 3 clinical trials, CML patients treated with imatinib showed 76.2 % complete cytogenetic response (0 % BCR-Abl+ cells) compared to 14.5 % in the interferon alpha plus cytarabin-treated group [95]. Due to the dramatic benefit of imatinib between groups, the comparison-clinical trials were aborted and the interferon alpha plus cytarabine-treated group crossed over to the imatinib treated group, shifting the focus to an in-depth understanding of imatinib treatment [95].

The tyrosine kinase inhibitor Imatinib has revolutionized the therapy of not only of CML but also malignancies related to KIT and PDGFRA mutations. Activating mutations of the receptor

tyrosine kinases KIT and PDGFRA are especially associated with gastrointestinal stromal tumors [96]. Moreover, activating KIT mutations are known to cause sporadic adult human mastocytosis [97].

Although survival rates of BCR-Abl+ patients dramatically increase upon imatinib administration, a number of mechanisms by which resistance to imatinib arises have been described. These include mutations in the ABL-kinase domain, amplification of BCR-Abl and the overexpression of the multidrug-resistance transporter, P-glycoprotein [98].

The limitations of imatinib inspired the development of more potent second generation tyrosine kinase inhibitors like nilotinib and dasatinib [99]. Imatinib, as well as its FDA approved second generation inhibitors, are ATP competitive, catalytic-side ABL1 inhibitors. Discovery of novel pharmaceuticals for dual inhibition of BCR-Abl has become increasingly interesting in recent years [100]. One fascinating strategy is to target the myristate-pocket of BCR-Abl. The intact Abl kinase contains a myristoylated cap region that induces an autoinhibitory conformational change [101]. Even though the myristoylated cap region has been replaced by the truncated BCR protein, the myristate-pocket remained in the BCR-Abl fusion protein. The non-ATP competitive inhibitor ABL001 mimics myristate binding and was shown to be antiproliferative at submicromolar concentrations in preclinical studies, using BCR-Abl+ cell lines [100]. ABL001 is currently being tested in a phase I, multicenter, open-label study.

In 2015, Breitkopf *et al.* published a study on the effect of imatinib treatment on BCR-Abl+ H929 multiple myeloma cells, which were analyzed by a combination of metabolomics, lipidomics, and phosphoproteomics approaches [102]. The triomics study presents evidence that imatinib globally induces lipidome changes which is primarily mediated through signaling of the BCR-Abl-ERK pathway [102].

Due to the multitude of reported lipidomic changes, monitoring of BCR-Abl inhibition is expected to be a relevant example for the application of a small molecule-based MALDI MS biotyping workflow.

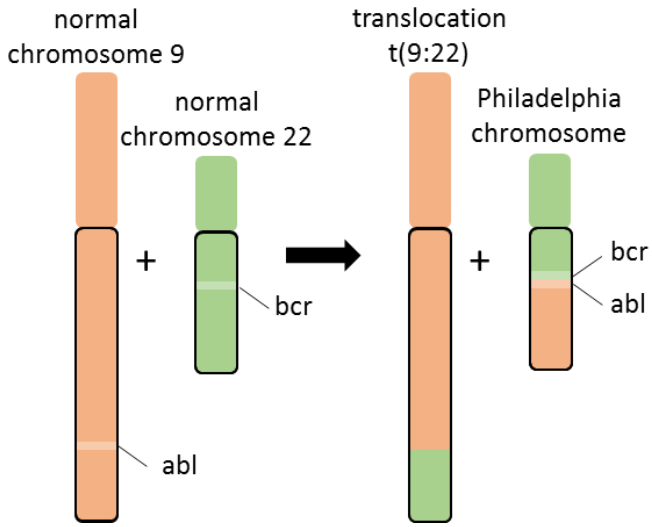

Figure 1.2.1: Formation of the Philadelphia chromosome by reciprocal translocation.

1.2.3 FATTY ACID SYNTHASE AS A DRUG TARGET

Fatty acid synthase (FASN) is a multi-enzyme protein that catalyzes the formation of the fatty acid palmitate, which is formed in an NADPH dependent condensation of acetyl-CoA and malonyl-CoA:

$$\text{Acetyl-CoA} + 7\ \text{Malonyl-CoA} + 14\ \text{NADPH} \rightarrow$$

$$\text{Palmitate} + 14\ \text{NADP}^{+} + 7\ \text{CO}_2 + 8\ \text{CoA}$$

The growing fatty acid chain is formed by an iterative action of a ketoreductase (KR), a dehydratase (DH) and enoyl reductase (ER) (**Fig. 1.2.2**).

FASN is a key enzyme in the lipid metabolism, which has been associated with a variety of diseases including cancer [103], diabetes [104], cardiovascular [105] and neurodegenerative diseases [106].

FASN overexpression has been described in many hematopoietic and solid tumors, including lung, colon, prostate and breast cancer. Moreover, overexpression of FASN in human carcinomas is associated with a poor prognosis and resistance to cancer therapy [107].

Ventura *et al.* showed anti-tumor activity of FASN inhibition using *in vitro* and *in vivo* models of human cancer [107]. FASN inhibition causes tumor apoptosis by multiple mechanisms, including reprogramming of gene expression, inhibition of signaling pathways, and remodeling of cell membranes.

A HTS strategy, using the full length recombinant, human FASN in a biochemical assay, to identify FASN inhibitors has been published by GSK [73, 108]. Vazquez *et al.* performed a biochemical NADPH consumption assay with a resorufin-based fluorescence readout. NADPH itself is UV absorbent. Yet, measuring its absorbance is poorly sensitive and interferes with too many compounds. Resorufin is sensitive to quenching by the nucleotides NADH and NADPH. In batches containing potent FASN inhibitors, little NADPH is consumed by the enzymatic reaction. Due to quenching of resorufin a weak fluorescent signal is obtained for hit compounds.

One screening hit was the aforementioned GSK837149A, an inhibitor of the 3-ketoacyl reductase domain of the FASN, which is apparently not cell-permeable [73]. Another hit compound was GSK2194069, a potent (pIC50 = 7.7 nM, biochemical assay), cell-permeable inhibitor which also targets the 3-ketoacyl reductase domain of the FASN [109]. Fasnall is a potent FASN inhibitor (pIC50 = 147 nM, cellular assay) discovered at Duke University School of Medicine in a chemoproteomics screen where compounds were tested for the release of protein extracts bound to cibacron blue sepharose beads upon exposure to a compound library. The used protein extracts were obtained from porcine lactating mammary glands, which are a rich source of FASN [110]. It is worth mentioning that the authors provided no information on cofactor competition or the inhibited target domain. A summary of latest generation, preclinical FASN inhibitors, all displaying at least a nanomolar IC50 in a biochemical or cellular FASN assay, is provided in **table 1.2.1**. The majority of FASN inhibitors have failed to advance into development. Presently, the only FASN inhibitor that has advanced to a clinical trial is 3V Biosciences' TVB-2640, which is currently not commercially available. TVB-2640 is tested for treatment of solid tumors [110, 111]. This chapter elaborates that presently available FASN assays are indirect, unprecise and time consuming, which highlights the need for the development of advanced assays.

Table 1.2.1: Selected, preclinical FASN inhibitors.

Compound, Sponsor	assay for hit identification	IC50 [nM]	assay for IC50 determination	Ref.
TVB-3166, 3-V Biosciences	undisclosed	60	Cell assay of palmitate generation from ^{13}C-acetate using human cervical cancer HeLa cells; saponified extracts analyzed by triple quad LC-MS.	[107]
BI 99179, Boehringer Ingelheim	undisclosed	600	Cell assay: Mouse hypothalamic N-42 cells incubated with compound for 1h, ^{14}C-acetate in Krebs-Ringer-buffer incubation for 4h, methanol/chloroform (1/1) extraction, measurement in ß-counter.	[112]
		79	Biochemical assay: NADPH consumption using FASN isolated from Hela cells (undisclosed purification strategy), photometric detection of NADPH at 340 nm.	
Fasnall, Duke University	Chemoproteomic screen: Release of proteins bound to cibacron blue sepharose upon exposure to compound library.	147	Cellular assay: Human liver cancer HepG2 cells incubated in ^{3}H-acetate medium and compound for 1 h, lysates were subjected to liquid scintillation counting.	[110]
		3710	Biochemical assay: human FASN (undisclosed source and purification strategy) was pre-incubated with Fasnall, addition of substrates acetyl-CoA, NADPH and malonyl-CoA spiked with 2-[^{14}C]malonyl- CoA for 30 min, chloroform/methanol (2/1) extraction, measurement by liquid scintillation counting.	
GSK2194069, GlaxoSmith-Kline	Biochemical FASN assay: Monitoring of NADPH consumption using full length recombinant hFASN, photometric detection of NADPH induced quenching of resorufin.	7.7	Biochemical assay using full length recombinant, human FASN expressed in Sf9 insect cells: Detection of CoA production using thio-reactive coumarin dye CPM, fluorescent readout using 380 nm excitation wavelength filter, and 486 nm emission filter.	[109]
		15	Cellular phospholipid assay: A549 cells treated for 48 h, phospholipids were measured in an enzyme-coupled reaction using PC-specific phospholipase D and choline-oxidase. Reaction product H_2O_2 was detected using Amplex Red fluorogenic substrate reactoin, fluorescent readout at 560 nm.	
JNJ-54302833, Johnson & Johnson	undisclosed	28	Biochemical assay using full length recombinant, human FASN expressed in insect cells: ^{3}H-acetyl-CoA and malonyl-CoA were used as substrates. Product ^{3}H-palmitate binds to hydrophobic scintillation proximity assay imaging beads. Emitted light is measured using a 610 nm pass filter.	[113]
Platensimycin, Merck	Same principle as for IC50 determination.	300	Biochemical assay using human FASN purified by ammonium sulfate fractionation and ion-exchange chromatography from human cell lines (SKBr3 and HepG2): Detection of CoA production using thio-reactive coumarin dye CPM, fluorescent readout using 380 nm excitation wavelength filter, and 486 nm emission filter.	[114]

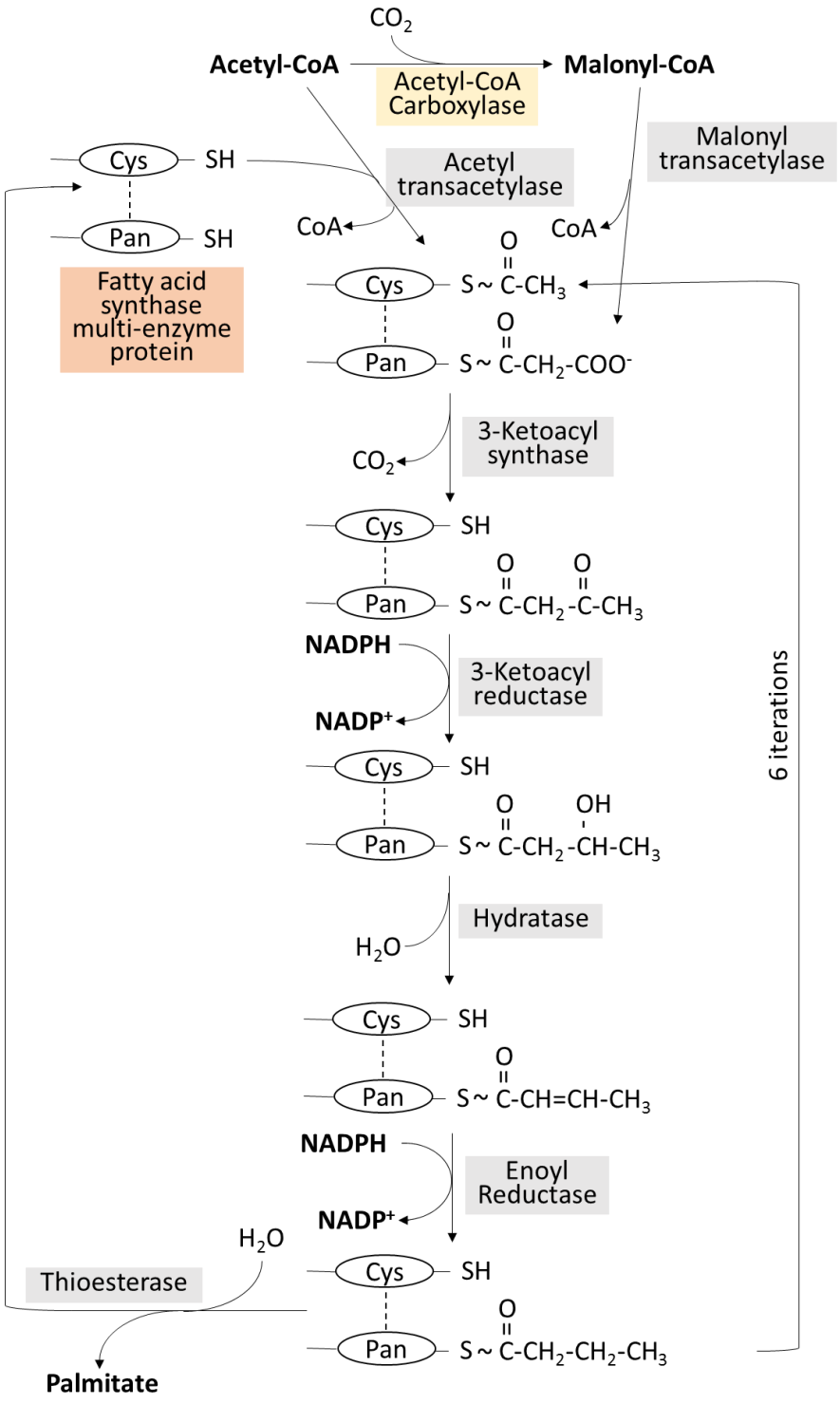

Figure 1.2.2: The enzymatic reactions of the fatty acid synthase. Malonyl-CoA is composed from acetyl-CoA and CO_2 by the enzyme acetyl-CoA carboxylase. 6 distinct enzymatic domains, highlighted in grey, of the FASN are involved in the formation of palmitate. The growing fatty acid chain is linked to and shuttled between the enzymatic domains by a phosphopantetheine prosthetic group, "Pan", of an acyl carrier protein. The enzymatic reaction is initiated by the acetyl transacetylase. Palmitate is formed in 7 consecutive cycles of 3-ketoacyl synthase, 3-ketoacyl synthase, hydratase and enoyl reductase which is released by the thioesterase domain.

2 AIMS

MALDI MS is a sensitive and a rather impurity tolerant method. Technological advances increased measurement speed to less than a second per data point. The implementation of MALDI MS *in vitro* assays has advanced the repertoire of targets that can be screened by label free, high throughput technology. The limitations of MALDI MS *in vitro* biochemical assays are the restricted availability of purified drug targets, as well as the poor predictability of a screening hit's action in a more physiologic, cellular environment. Moreover, established protein-based MALDI MS cell assays are limited by a complicated identification of the underlying protein marker molecules, and a small dynamic range of the assay readout. Cellular metabolites harbor the potential to display a greater dynamic range compared to proteins. Additionally, identification and validation of metabolite marker molecules is potentially much easier with FTMS technology. In conclusion, metabolite-based MALDI MS cell assays might open up a completely new avenue for drug discovery.

Therefore, this thesis is focused on the following objectives:

- Development of a MALDI MS workflow that enables sensitive and reproducible acquisition of metabolite spectra from whole cells.

- Incorporation of the developed MALDI MS workflow into pharmacologically relevant assays.

- Discovery of metabolite drug response markers by MALDI-TOF MS and their identification/validation by MALDI-FTICR MS/MS.

- Evaluation of the utility of these workflows for standardized metabolite-based MALDI MS cell drug assays. It was intended to evaluate examples for MALDI MS-based phenotypic as well as mechanistic cell assays.

- Automation of the established assays by evaluating and developing both novel technologies and software solutions.

3 Materials and Methods

3.1 Materials

3.1.1 Chemicals

3.1.1.1 General Chemicals

Chemical	Company (Headquarter)	Catalogue number
Acetone	VWR International (Darmstadt, GER)	1.00012
Acetonitrile	VWR International (Darmstadt, GER)	1.00030
Benzoic acid	Sigma Aldrich (Munich, GER)	242381
Bovine serum albumin	Applichem (Darmstadt, GER)	A1391
5x Bradford reagent	Bio-Rad (München, GER)	5000006
Ethanol absolute	VWR International (Darmstadt, GER)	20825
Glycerol	Sigma Aldrich (Munich, GER)	G9012
Hexane	VWR International (Darmstadt, GER)	83992.320
Methanol	VWR International (Darmstadt, GER)	83638.320
Milli-Q water	Prepared in-house	
Nitrocellulose	Sigma Aldrich (Munich, GER)	88018
Peptide Calibration Standard II	Bruker Daltonics (Bremen, GER)	8222570

Propan-2-ol	VWR International (Darmstadt, GER)	1.09634

3.1.1.2 CHEMICALS FOR CELL CULTURE

Chemical	**Company (Headquarter)**	**Catalogue number**
D(+)Glucose	Applichem (Darmstadt, GER)	A1422
DMSO	VWR International (Darmstadt, GER)	A3672
FCS	Life Technologies (Darmstadt, GER)	10270
FCS, charcoal stripped	Life Technologies (Darmstadt, GER)	F6765
HEPES	Applichem (Darmstadt, GER)	A1069
IMDM	VWR International (Darmstadt, GER)	L0190
L-Glutamine	Sigma Aldrich (Munich, GER)	G7513
PBS	Sigma Aldrich (Munich, GER)	P3744
PEN/STREP	Life Technologies (Darmstadt, GER)	15140122
RPMI	VWR International (Darmstadt, GER)	L0498-500P
Sodium pyruvate	Sigma Aldrich (Munich, GER)	S8636
Trypan blue	Sigma Aldrich (Munich, GER)	T8154
Trypsin/EDTA	Sigma Aldrich (Munich, GER)	T4049

3.1.1.3 COMPOUNDS FOR CELL CULTURE TREATMENT

Compound	Company (Headquarter)	Catalogue number
BI 99179	Boehringer Ingelheim (Ingelheim, GER)	not commercially available[7]
BI 99990	Boehringer Ingelheim (Ingelheim, GER)	
Chloroquine diphosphate salt	Sigma Aldrich (Munich, GER)	C6628
Dasatinib	LC Laboratories (Woburn, USA)	D-3307
Imatinib	LC Laboratories (Woburn, USA)	I-5577
GSK2194069	Sigma Aldrich (Munich, GER)	SML1259
GSK837149A	Sigma Aldrich (Munich, GER)	G5547
Nilotinib	LC Laboratories (Woburn, USA)	N-8207
Orlistat	Sigma Aldrich (Munich, GER)	O4139
Sunitinib malate salt	LC Laboratories (Woburn, USA)	S-8803
Triclosan	VWR International (Darmstadt, GER)	L18655
TOFA	VWR International (Darmstadt, GER)	10005263
Vandetanib	LC Laboratories (Woburn, USA)	V-9402

[7] Compounds were kindly shared by Boehringer Ingelheim's platform to access preclinical molecules for research (www.opnMe.com).

3.1.1.4 CHEMICALS FOR MATRIX PREPARATION

Chemical	Company (Headquarter)	Catalogue number
ATT (6-aza-2-thiothymine)	Sigma Aldrich (Munich, GER)	275514
DHB (2,5-Dihydroxybenzoic acid)	Bruker Daltonics (Bremen, GER)	8201346
Trifluoroacetic acid	Merck (Darmstadt, Germany)	1082620025

3.1.1.5 CALIBRATION COMPOUNDS AND STANDARDS

Calibrant / Standard	Company (Headquarter)	Catalogue number
Malonyl-CoA	Sigma Aldrich (Munich, GER)	M4263
Malonyl-$^{13}C_3$-CoA	Sigma Aldrich (Munich, GER)	655759
Olanzapine	SelleckChem (Houston, USA)	S2493
Peptide calibration standard II	Bruker Daltonics (Bremen, GER)	8222570
Romidepsin	SelleckChem (Houston, USA)	S3020
Sorafinib Free Base	LC Laboratories (Woburn, USA)	S-8599

3.1.2 CONSUMABLES

Consumable	Company (Headquarter)	Catalogue number
Cell culture plates with 6 / 24 / 96-wells	Greiner bio-one (Solingen, GER)	M8562 / M8812 / M0812
Centrifuge tubes 0.5 / 1.5 / 2 ml	Eppendorf (Hamburg, GER)	0030121023 / 0030120086 / 0030120094
Centrifuge Tubes 15 / 50 ml	VWR International (Darmstadt, GER)	525-0150 / 525-0155
MALDI 384 ground steel target	Bruker Daltonics (Bremen, GER)	8280784
Neubauer Improver	VWR International (Darmstadt, GER)	631-0696
Nitrile examination gloves	VWR International (Darmstadt, GER)	112-4513
Pipet Tips 10/200/1000 µl	VWR International (Darmstadt, GER)	613-0576 / 613-0579 / 613-0582
Serological pipettes 10 / 25 ml	VWR International (Darmstadt, GER)	612-3700DE / 612-3698DE
T75 cell culture flasks for adherent / suspension culture	Greiner bio-one Solingen, GER	C7231-120EA / C6731-200EA
CyBio® RoboTipTray 96/60 µl	Analytik Jena (Jena, GER)	OL3810-25-441

3.1.3 EQUIPMENT AND INSTRUMENTS

Equipment / Instrument	Model, Company (Headquarter)
Centrifuges	Heraeus Fresco 21, Thermo Fisher Scientific (Schwerte, GER)
	SIGMA 6K15, Sigma Laborzentrifugen GmbH (Osterode, GER)
Balances	Analytical Balance Sartorius Research R200D, Sartorius (Göttingen, GER)
Clean Bench	AireGard ES NU-140 Vertical Laminar Airflow Workstation, Nuaire (Caerphilly, UK)
Cell Culture Incubator	Heracell 150, Thermo Fisher Scientific (Schwerte, GER)
Mass spectrometers	autoflex speed MALDI-TOF/TOF, Bruker Daltonics (Bremen, GER)
	solariX 7T XR FTICR, Bruker Daltonics (Bremen, GER)
	ultrafleXtreme MALDI-TOF/TOF, Bruker Daltonics (Bremen, GER)
	rapifleX MALDI-TOF, Bruker Daltonics (Bremen, GER)
Matrix spray device	Sun Collect Sprayer, SunChrom (Friedrichsdorf. GER)
	HTX TM-Sprayer, HTX Technologies (Chapel Hill, North Carolina, USA)
Microscope	Invert light microscope AE 31, Motic (Wetzlar, GER)
Pipettes 10/100/1000 µl	Eppendorf Research plus, Eppendorf (Hamburg, GER)
Pipetting Platform	CyBio FeliX, Head R 96/60 µl, Analytik Jena (Jena, GER)
Plate reader	Multiscan Spectrum, Thermo Fisher Scientific (Schwerte, GER)

Sonic bath	VWR International
Vacuum Aspirator	Vacusafe, Integra (Zizwers, CH)
Water purification system	EMD Millipore™ Milli-Q™ Reference Ultrapure Water Purification System, Thermo Fisher Scientific (Schwerte, GER)

3.1.4 HUMAN CELL LINES

Cell Line	**Origin**	**Culture Properties**	**Provider**
A549	Lung carcinoma	Adherent	Merck (Darmstadt, GER)
GIST-T1	GIST	Adherent	EU-MITIGATE consortium
HL-60	ALL	Suspension	ATCC (Manassas, USA)
K562	CML	Suspension	CLS (Eppelheim, GER)

3.1.5 SOFTWARE FOR DATA ACQUISITION

Name	**Instrument**	**Company**
flexControl 3.4	autoflex speed and ultrafleXtreme MALDI-TOF/TOF	Bruker (Bremen, GER)
flexControl 4.0	rapifleX MALDI-TOF	Bruker (Bremen, GER)
ftmsControl 2.1.0	solariX 7T XR FTICR	Bruker (Bremen, GER)

3.1.6 SOFTWARE FOR DATA ANALYSIS, VISUALIZATION AND CHEMICAL DRAWING

Name	**Company (Headquarter)**
ChemSketch	ACD Systems (Toronto, CAN)
ClinProTools 3.0	Bruker (Bremen, GER)
DataAnalysis 4.4	Bruker (Bremen, GER)
flexAnalysis 3.4	Bruker (Bremen, GER)
Microsoft Visio	Microsoft (Redmond, USA)
Microsoft Powerpoint	Microsoft (Redmond, USA)
R Studio	RStudio Team (Boston, USA)
R 3.3.1	R Foundation for Statistical Computing (Vienna, AUT)
Prism 5	GraphPad Software (California, USA)

3.2 METHODS

3.2.1 CULTIVATION OF HUMAN CELL LINES

3.2.1.1 CULTIVATION OF A549 AND GIST-T1 ADHERENT CELL LINES

A549 and GIST-T1 cells were cultured at 37 °C, 5 % CO_2 and 95 % humidity in supplemented RPMI-1640 or IMDM respectively. Cells were grown to 70 % confluency in T75 flasks. To split, a T75 flask was washed with 2 ml trypsin buffer prior to incubation with 2 ml trypsin buffer for 5 mins. Cells were resuspended in 8 ml of fresh medium and split into a new maintaining flask. A maintaining flask was seeded at 10 - 20 % confluency.

Supplements added to RPMI-1640 for A549 cultivation

10 %	FBS
2 mM	Glutamine
120 µg	Penicillin / Streptomycin

Supplements added to IMDM for GIST-T1 cultivation

15 %	FBS
2 mM	Glutamine
120 µg	Penicillin / Streptomycin

3.2.1.2 CULTIVATION OF HL60 AND K562 SUSPENSION CELL LINES

HL60 and K562 cells were cultured at 37 °C, 5 % CO_2 and 95 % humidity in supplemented IMDM or RPMI-1640, respectively. The cell density was determined by applying 10 µl of suspension to a Neubauer counting chamber (hemocytometer). The cultures were split when cultures reached a density of 1 - 2 · 10^6 cells / ml. A new maintaining flask was seeded at 0.1 - 0.2 · 10^6 cells / ml, by transferring the needed amount of culture to a new flask and adding fresh media.

Supplements added to IMDM for HL60 cultivation

20 %	FBS
4 mM	Glutamine
120 µg	Penicillin / Streptomycin

Supplements added to RPMI-1640 for K562 cultivation

10 %	FBS
2 mM	Glutamine
1 mM	Sodium pyruvate
10 mM	HEPES
1.25 g	Glucose
120 µg	Penicillin / Streptomycin

3.2.1.3 CELL HARVEST FOR MALDI METHOD DEVELOPMENT

Trypsinized, adherent cells or suspension culture cells were pelleted by centrifugation for 5 min at 800 rpm and 4 °C. The pellet was resuspended in ice cold PBS and pelleted again. The pellet was resuspended in PBS a second time. A 10 µl aliquot was mixed with Trypan Blue and applied to a Neubauer counting chamber to determine the cell density and viability.

Cell aliquots containing 10^6 cells each were transferred to Eppendorf cups and centrifuged at 2,000 rpm for 5 min at 4 °C on a benchtop centrifuge. Supernatants were removed using a vacuum aspirator. The pellets were snap-frozen and stored at -80 °C until further use.

3.2.1.4 CELL PELLET GENERATION FOR CELL DRUG ASSAYS

1 day prior to inhibitor treatment K562 cells were resuspended at 0.25 x 10^6 cells / ml in assay medium. 1 ml of the suspension was added to each well of a 24-well plate. Except for chloroquine, all inhibitors were dissolved in DMSO to a final concentration of 30 mM. Chloroquine was dissolved in H_2O to a final concentration of 30 mM. On the day of inhibitor treatment, dilution series of the inhibitors were prepared in a 12-step dilution series and 1 µl inhibitor was added to 1 ml culture. After 6, 12, 24 or 48 h, cells were transferred to Eppendorf tubes and pelleted at 2,000 rpm for 5 min at 4 °C using a benchtop centrifuge. Supernatants were removed using a multi-channel vacuum aspirator. The pellets were snap-frozen and stored at -80 °C until further use.

Tyrosine-kinase inhibitor assay medium

500 ml	RPMI-1640
10 %	FBS
2 mM	Glutamine
1 mM	Sodium pyruvate
10 mM	HEPES
1.25 g	Glucose
120 µg	Penicillin / Streptomycin

FASN assay medium

500 ml	RPMI-1640
2 mM	L-Glutamine
10 %	FCS, charcoal stripped

3.2.1.5 CELL PELLET GENERATION FOR AUTOMATED CELL DRUG ASSAYS

1 day prior to inhibitor treatment, cells were resuspended at 0.25 x 10^6 cells / ml (K562 cells) or 0.1 x 10^6 cells / ml (A549 cells) in FASN assay medium. 200 µl of the suspension were added to each well of a 96-well "culture-plate". All inhibitors were dissolved in 40 µl DMSO and transferred to a new 96-well "compound-plate". On the day of inhibitor treatment, 1 µl inhibitor were transferred from the 96-well compound plate to the 96-well cell culture plate using the CyBio FeliX pipetting platform. For that purpose, the pipetting platform was equipped with a 96-well 60 µl tip tray, aspirated 10 µl from the cavities of the compound plate and released 1 µl in the cavities of the culture plate. The remaining liquid was disposed into a waste bucket. After 24 h, whole 96-well culture plates were centrifuged at 800 rpm for 5 min using a SIGMA 6K15 centrifuge. Supernatants were removed using a vacuum aspirator. The plates were snap-frozen and stored at -80 °C until further use.

3.2.2 MALDI MS WHOLE CELL MEASUREMENTS

3.2.2.1 SAMPLE PREPARATION

In general, samples were prepared on a 384-well ground steel MALDI target plate (MTP). Prior to a new preparation, the MTP was placed into a beaker filled with MTP-cleaning solution and exposed to an ultrasonic bath for 15 mins.

Cell aliquots were resuspended at 5,000 cells/µl in 50 % acetonitrile (v/v) in H_2O which was supplemented with 5 µM malonyl-$^{13}C_3$ CoA for the FASN assay. 1 µl of the suspension was applied on the ground steel target in eight technical replicates. Samples from the same batch that were prepared on different days to evaluate intra-assay reproducibility are also referred to

as technical replicates with an indication of the time between the preparations. Cells that originate from different passage numbers are referred to as biological replicates.

MTP-cleaning solution

50 %	Methanol
45 %	H_2O
5 %	Acetic acid

3.2.2.2 AUTOMATED SAMPLE PREPARATION FOR THE FASN ASSAY

The CyBio FeliX pipetting platform was used for automated sample preparation. Frozen 96-well plates containing harvested cell pellets were placed on the instrument's thermal mixer, BioShake, and warmed to room temperature. Cell pellets were resuspended in 40 µl 50 % acetonitrile (K562 cells) or pure H_2O (A549 cells) supplemented with 5 µM malonyl-$^{13}C_3$ CoA using the CyBio 96-well 60 µl tip tray. The plate was shaken for 3 s at 2,000 rpm using the BioShake. The suspension was aspirated using the CyBio 96-well 60 µl tip tray. The instrument was paused for 5 s upon sample aspiration to saturate the gas phase above the liquids phase in the pipetting tip. 1 µl (K562 cells) or 2 µl (A549 cells) of the suspension were applied in 4-fold technical replicates to a 384-well ground steel MALDI target plate.

3.2.2.3 MATRIX APPLICATION

Upon analyte application, the MALDI target was coated with matrix using a Sun Collect Sprayer. To avoid clogging of the sprayer with matrix crystals, each matrix preparation was exposed to an ultrasonic bath for 5 min. Additionally, the sprayer was thoroughly rinsed with 50 % acetonitrile (v/v) in H_2O before and after use. As a rule of thumb, 3 ml of matrix preparation are sufficient to coat a whole MTP with matrix. Matrix preparations and the matrix spray protocol are listed in the table below. The SunCollect sprayer was used throughout the whole thesis. A HTX sprayer was only used in combination with automated assays. The use of the HTX sprayer was implemented for the automated FASN assay, since it proved as a reliable and fast tool to spray-coat whole MALDI target plates.

Matrix preparation for standard fingerprinting and the tyrosine-kinase inhibitor assay

20 mg/ml	DHB
50 %	Acetonitrile
50 %	H_2O
0.5 %	Trifluoroacetic acid

Matrix preparation for the FASN assay

20 mg/ml	DHB
50 %	Acetonitrile
50 %	H_2O
2.5 %	Trifluoroacetic acid

Matrix spray protocol SunCollect sprayer

Spray-head velocity	900 mm/min
Spray-head height	2.8 cm
Distance between sprayed lines	2 mm
Matrix flow rate	30 µl/min
Sprayed layers	10

Matrix spray protocol HTX sprayer

Spray-head velocity	1000 mm/min
Spray-head height	4 cm
Distance between sprayed lines	2 mm
Matrix flow rate	60 µl/min
Sprayed layers	4
Spray nozzle temperature	50 °C

3.2.2.4 MALDI-TOF MS DATA ACQUISITION

Early method development was performed on an autoflex speed MALDI-TOF/TOF mass spectrometer. Later on an ultrafleXtreme MALDI-TOF/TOF MS was used for this purpose due to its enhanced mass resolution. Both instruments were equipped with a 2 kHz smartbeam II laser. Automated data acquisition in the *m/z* range from 200 – 2,000 on both instruments was controlled by the AutoXecute function of the flexControl 3.4 software. 4,000 laser shots were accumulated per measuring spot in random walk mode. The laser focus was set to large on the autoflex or medium on the ultrafleXtreme. Laser intensity was adjusted to obtain signal intensities in the range of 10^3 and 10^4 AU. The sampling rate was adjusted to 4 giga samples / s on the autoflex and to 5 giga samples / s on the ultrafleXtreme.

Calibration of the instruments was performed using an in-house prepared mixture of the peptide calibration standard II (Bruker Daltonics) and the low molecular mass compounds sorafenib ($[M+H]^+$ - 465.0935), romidepsin ($[M+H]^+$ - 541.2149), sunitinib ($[M+H]^+$ - 399.219), and olanzapine ($[M+H]^+$ - 313.1481).

Data acquisition for the FASN assay was performed on the rapifleX MALDI-TOF mass spectrometer. The instrument was equipped with a 10 kHz smartbeam 3D laser. Automated data acquisition was controlled by the AutoXecute function of the flexControl 4.0 software. Spectra were acquired in the *m/z* range from 500 – 1,000. 4,000 laser shots were accumulated per measuring spot in random walk mode. The laser focus was adjusted to “MS thin layer”.

Calibration of the rapifleX was performed internally using the lysophosphatidylcholine LPC(18:1) ($[M+H]^+$ - 522.355), the phosphatidylcholine, PC(34:1) ($[M+H]^+$ - 760.585 and $[M+K]^+$ - 798.541) and malonyl-$^{13}C_3$-CoA ($[M+H]^+$ - 857.126).

3.2.2.5 MALDI-FTICR INSTRUMENT SETTINGS

For structural elucidation of concentration-response marker molecules, sample spots exposing highest feature-of-interest intensity, were remeasured using an ultra-high resolution solariX 7T XR FTICR. The mass spectrometer was controlled by ftmsControl 2.1.0 software. In the first step, a full spectrum was acquired in the low molecular mass range (*m/z* 150 to 5,000) using a 4 M AMP transient. Laser intensity and shot per spot number were adjusted to obtain signal intensities between 10^8 and 10^9 AU. These settings enabled a typical resolving power of 800,000 at *m/z* 400. Calibration was again performed externally using the calibration mixture described above. In addition, an abundant phosphatidyl choline at *m/z* 760.5851 ((PC(34:1)+H^+) was used for internal, single point on-line calibration with a mass tolerance of 6 ppm.

The accurate mass of the marker molecule was determined from the full scan spectrum. For structural elucidation the marker molecule was fragmented. The instrument was set to tune mode to continuously acquire spectra. Quadrupole isolation was checked in the "Source MS/MS" tab. The isolation window was set to 1 *m/z*. RF frequency was set to 5. Collision cell RF amplitude was 2,000 V. The voltage for collision induced fragmentation was adjusted so that the intensity of the parent mass decreased to half of its initial intensity.

Additional instrument settings solariX

Ion transfer	
Voltage Funnel 1	150 V
Voltage Skimmer 1	15 V
Funnel RFamplitude	150 Vpp
Octopole RF amplitude	350 Vpp
RF frequency	5 MHz

Transfer optics	
Time off light	1.2 ms
ICR Hexapole rod frequency	4 MHz
Excitation mode	Sweep mode
Sweep step time	15 µs
Ramped power exitation	Continous (14-28 %)
ICR Paracell	
Exit lens voltage	-20 V
Entrance voltage	-10
Front and back plate voltages	1.5 V
Side-kick offset	-1.5 V

3.2.3 DATA ANALYSIS AND -VISUALIZATION USING COMMERCIAL SOFTWARE

Gelview illustrations of MALDI-TOF spectra were generated using ClinProTools 3.0 software. MALDI-FTICR spectra were visualized using DataAnalysis 4.4 software. Sum formulae were calculated from MALDI-FTICR measurements using the SmartFormula function of DataAnalysis.

3.2.4 DATA PROCESSING PIPELINE FOR MALDI-TOF DATA WRITTEN IN R

MALDI-TOF data acquired on the autoflex, ultrafleXtreme or rapifleX were exported as text-files using a flexAnalysis batch process. Data processing, analysis and visualization was performed in R programming language using RStudio [115].

3.2.4.1 DATA PREPROCESSING

Data were imported as text-files into R using the *MALDIquantForeign* package[8]. Preprocessing was performed using functions of the *MALDIquant* package [116]. The data processing workflow was adapted from Erich *et al.* [47] with the help of Denis Abu Sammour. The adapted workflow included TIC normalization of the spectra, “Tophat“ baseline subtraction, spectra alignment (tolerance = 0.002), peak picking of all signals with S/N > 5 (method = "SuperSmoother", halfWindowSize = 20, SNR > 5), peak binning (tolerance = 0.002) and calculation of a matrix containing all features (features matrix). The data preprocessing pipeline was implemented with the help of Denis Abu-Sammour.

3.2.4.2 MULTIVARIATE DATA ANALYSIS USING PCA

During the course of this thesis, principle component analysis (PCA) was employed to reduce spectral complexity and to obtain a simplified view on spectral similarities. Additionally, PCA scores were used as the basis for the calculation of $J_{overlap}$ scores described below. For the work of this thesis, PCA was calculated based on the features matrix using the prcomp function of the R statistics package.

3.2.4.3 MSEMOD-BASED METHOD SCORING

The MSE_{mod} –score is a modification of the previously published matrix suppression effect by lipids MSE_{lip} [49]. For MSE_{mod} calculation all ions that were observed (S/N > 5) in the pure matrix spectrum were matched with the analyte spectrum (mass tolerance: 0.1 Da). The sum of ions in the analyte spectrum that did not occur in the matrix spectrum was divided by the sum of all ions observed in the analyte spectrum:

$$MSE_{mod} = \frac{\sum non\ matrix\ ions}{\sum all\ ions}$$

[8] Gibb S (2015) MALDIquantForeign: Import/Export Routines for MALDIquant.

3.2.4.4 $J_{OVERLAP}$-BASED METHOD SCORING

The interclass overlap, $J_{overlap}$, is a score that compares different sets of experiments in the same PCA space and was determined as published by Erich *et al.* [47]. The score is described by the quotient of within-class scattering (*WS*) and between-classes scattering (*BS*):

$$J_{overlap} = \frac{|W_S|}{|B_S|}$$

PCA was calculated based on the features matrix using the R statistics package. The *DiscriMiner* package[9] was used to calculate *WS* and *BS* based on the coordinates of the datapoints in PCA space. The *rgl* package [117] was used for 3D-plotting of the PCA, as well as drawing of ellipsoids around each group and drawing distance lines between groups.

3.2.4.5 EXTRACTION OF DRUG SENSITIVE *M/Z* FEATURES

Drug sensitive *m/z* features were extracted using a two-step filtration strategy consisting of the exclusion of non-significant features in the first step and, in the second step, evaluation of how well the remaining features fit to a concentration response curve. Theresia Salonikios, a former PhD candidate in our laboratory, worked on MATLAB scripts for the extraction of protein response markers [118]. The idea to extract marker molecules by their fit to a concentration response curve originated from her work. Protein fingerprints and data analysis is based on broad linear mode peaks, whereas metabolites are measured in reflector mode. The feature extraction pipeline for metabolites was implemented in R programming language in collaboration with Timon Ulrich, a student of information technology.

In the first step low variance features were excluded to omit non-significant masses that, by chance, might fit well to the concentration-response curve shape. Feature-wise variances across all datasets were calculated. The mean of all variances was used as a threshold to select masses of interest. Since the variance of most features was close to zero, the variances-histogram was clearly right-skewed (**Fig. 3.2.1**).

[9] Sanchez G (2013) DiscriMiner: Tools of the Trade for Discriminant Analysis.

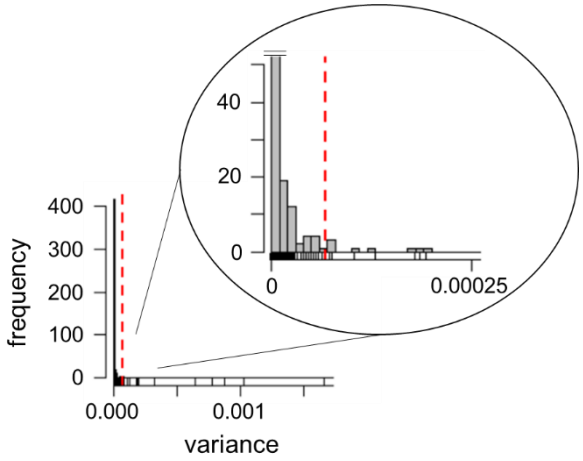

Figure 3.2.1: Variances-histogram of a concentration-response study. K562 cells were treated with 12 different concentrations of imatinib for 48 h. Samples were analyzed by MALDI MS whole cell fingerprinting. Feature wise variances across all 12 concentrations were calculated and illustrated as variances-histogram. The red dashed line indicates the mean overall variance. All features falling to the right of this right-skewed histogram were of interest.

In the second step all significant masses were fitted to concentration response curves using the *nls* function from R's statistics package. Features exposing a descending concentration response were fitted to the equation:

$$f(x) = top + \frac{bottom - top}{1 + 10^{(LogIC50 - x) \cdot HillSlope}}$$

where *f(x)* is the signal intensity, *x* is the decadal logarithm of the drug concentration, top is the f(x) value at the top plateau, bottom is the f(x) value at the bottom plateau.

For ascending concentration responses, the effect of hormesis needed to be taken into consideration. Mattson (2008) defined hormesis of cells as a stress response phenomenon charactericed by a low concentration induction and a high concentration inhibition [119]. To account for the occurrence of these biphasic responses, ascending concentration responses were only fitted up to the highest intensity value. Putative "toxic" concentrations following this global maximum were excluded. The remaining data points were fitted to the equation:

$$f(x) = bottom + \frac{top - bottom}{1 + 10^{(LogIC50 - x) \cdot HillSlope}}$$

R^2 value was used to rate how well a concentration response curve explains the variation of the data. Features with R^2 values below 0.9 were excluded. The remaining features were stored in lists. Concentration response curve fits were plotted using the *ggplot2* package[10].

[10] Wickham H (2009) ggplot2. Springer New York, New York, NY

4 RESULTS

The results of this thesis are presented in three parts:

- The first section presents the development of a broadly applicable IC-MALDI MS fingerprinting workflow. The section has a strong focus on method development which includes testing of parameters for sample preparation as well as various instrument settings. Moreover, the implementation of scores is presented to evaluate method performance by design of experiment principles.

- The second section presents the application of the workflow, introduced in the first section, as a phenotypic assay to monitor BCR-Abl tyrosine kinase inhibition. The section also describes the development of an R software tool that enables automated data processing and extraction of concentration response markers. The identification of concentration response markers by MALDI-FTICR MS is demonstrated as well as how these markers can be used to compare drug potencies.

- The third section presents the development of a mechanistic cell-based assay monitor inhibition of the fatty acid synthase. This section describes the discovery of CDP-choline as a marker for lipid synthesis inhibition as well as methods development of a standardized malonyl-CoA-based assay readout. Moreover, the section describes the automation and parallelization of several liquid handling steps of the developed FASN assay to further direct MALDI MS cell assays towards routine use in compound profiling.

4.1 METHOD DEVELOPMENT METABOLITE-BASED IC-MALDI MS FINGERPRINTING

Munteanu *et al*. developed a standardized IC-MALDI-TOF biotyping workflow based on protein fingerprints, which enables monitoring of drug action directly in whole cells [25, 29]. The aim was to develop an analogous workflow applicable for the detection of lipids and metabolites, which can be used to address medical, pharmaceutical and biotechnological issues. Metabolites detected in the low molecular *m/z* range interfere with the detection of small molecules used to facilitate the MALDI process like matrix and solvent additives. Therefore, the development of a metabolite-based workflow requires thorough optimization and evaluation.

4.1.1 APPLICATION OF A SCORE-BASED METHOD DEVELOPMENT APPROACH

When developing a MALDI-TOF fingerprinting method of whole cells, the identity of the detected molecules is not necessarily known. Guided by design of experiment principles, two score-based approaches were adapted from the literature to evaluate method performance. To compare different preparation protocols three cancer cell lines were cultured. These cell lines included one gastrointestinal stromal tumor cell line T1 (GIST) as well as the two leukemia cell lines, HL60 and K562. Data acquired using a well-performing preparation protocol are expected to expose striking, biological differences among the three cell lines and to therefore enable clear data separation in PCA space. $J_{overlap}$ is a score to quantitatively compare separation efficiency as well as data scattering in PCA space between datasets (here: cell lines) [47]. Another score that enables to approximate the information content of a mass spectrum is the matrix suppression effect (*MSE)* by lipids [49]. A modification of this score, MSE_{mod}, was used to compare the ratio of matrix signals to analyte signals among different preparation protocols.

The lack of any commercially available software to calculate these scores required the in-house development of a data processing pipeline. The Strimmer group laid an excellent foundation with the publication of the MALDIquant software package written in R [116].

The package contained the most comprehensive tools for MALDI-TOF data preprocessing among the open source programming languages. Spectra acquired on an ultrafleXtreme MALDI-TOF MS were exported as text-files using a flexAnalysis batch process. Import of text-files into R using the MALDIquant foreign package proofed as a reliable strategy. This strategy was especially preferred over the direct import of Bruker fid-files, which led to a loss of spectral

calibration information. Several preprocessing functions were successfully adapted from the MALDIquant package as described by Erich *et al.* [47] including spectra normalization to the total ion current, alignment, peak picking and binning. Processing of spectra in R enabled sensitive and robust detection of signals (**Fig. 4.1.1 A,B**). The detected signals are stored in a feature matrix, which is used for further investigations, such as score-based method development.

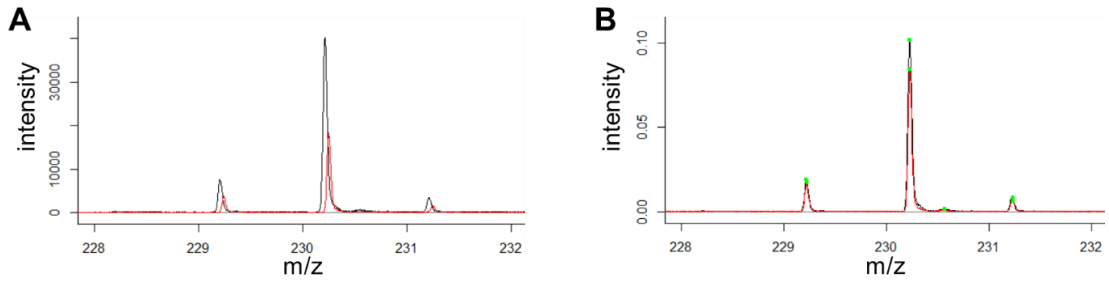

Figure 4.1.1: Data processing pipeline. Spectra acquired on an ultrafleXtreme were exported as text-files and loaded into R-programming environment. A,B) Zoom in of two mass spectra of K562 cells treated with different Imatinib concentrations before (A) and after (B) preprocessing. Detected signals are illustrated as green dots.

Starting method development with 5,000 cells/spot, a cell number compatible with the previously published protein-based IC-MALDI MS workflow, the matrices 6-aza-2-thiothymine (ATT) and 2,5-dihydroxybenzoic acid (DHB) were compared (**Fig. 4.1.2**). Both matrices were previously reported for the analysis of multiple lipid classes [38, 120]. To avoid formation of large matrix crystals, MALDI targets were spray-coated with a SunCollect device utilizing a rather dry spray protocol. A smaller $J_{overlap}$ value suggested a preference for DHB ($J_{overlap}$ = 0.14) over ATT ($J_{overlap}$ = 0.39) in this experimental setting. Reevaluation of both biological replicates in separate PCA spaces confirmed the lower $J_{overlap}$ score for DHB ($J_{overlap}$ = 0.14 ± 0.05) compared to ATT ($J_{overlap}$ = 0.32 ± 0.01).

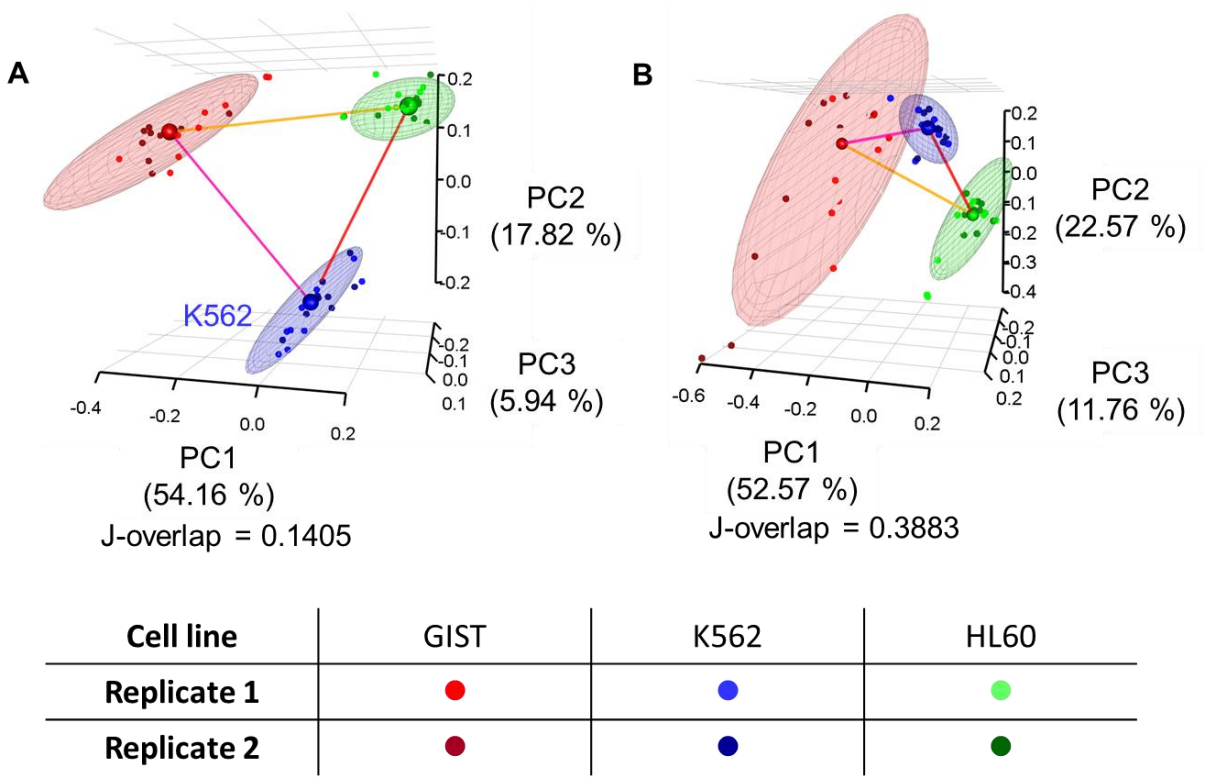

Figure 4.1.2: Using DHB as matrix leads to better separation in PCA space compared to ATT matrix. Cell pellets of three different cell lines (GIST, K562 and HL60) were resuspended at 5,000 cells/µl in acetonitrile/H_2O. One microliter of the suspension was applied on a MALDI target plate, which was spray-coated with either DHB (A; 20 mg/ml in acetonitrile/H_2O/TFA (60/40/0.5)) or ATT (B; 10 mg/ml in the same solvent). Samples were measured using an autoflex Speed MS. PCAs and variances were calculated in R. Biological replicates are colored in different shades of the same color (*m/z* 200-2000, S/N > 5, n = 2 biological replicates, each with ≥ 8 technical replicates measured on the same day).

None of the SunCollect sprayer-compatible solvent mixtures tested for resuspension of cell pellets increased the number of features detected with S/N >10 (**Fig. 4.1.3**). Also the implementation of an additional hexane extraction step did not improve separation efficiency for three different cell lines, as assessed by $J_{overlap}$ value (**Fig. 4.1.4**). Results obtained from $J_{overlap}$ analysis were supported by MSE_{mod} analysis (**Fig. 4.1.5**). Combination of the solvent 50 % acetonitrile in water and the matrix DHB led to an improved matrix suppression.

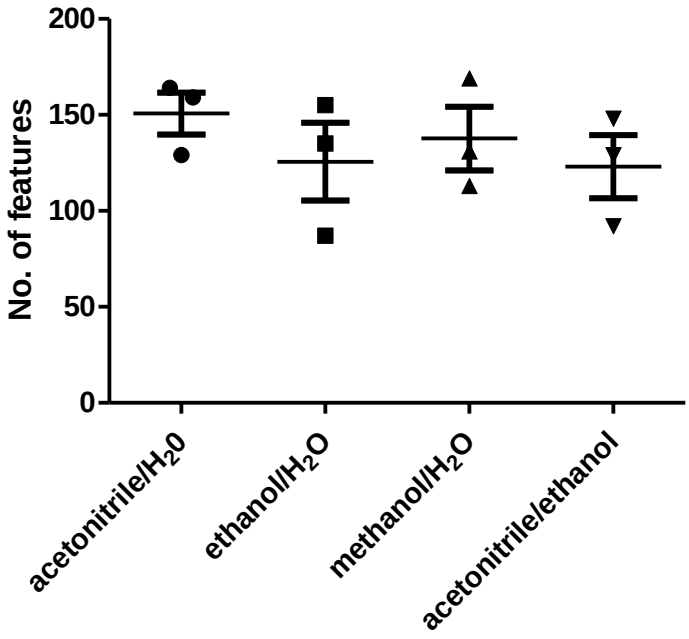

Figure 4.1.3: Tested solvents for sample resuspension. The number of features (S/N > 10, *m/z* 500-2000) does not significantly depend on the solvent mixture used for resuspension of cells. Number of features is plotted against the solvent used for sample resuspension and matrix application (5,000 cells/spot, mean ± standard deviation for n = 3 technical replicates prepared in 8-fold replicates on different days).

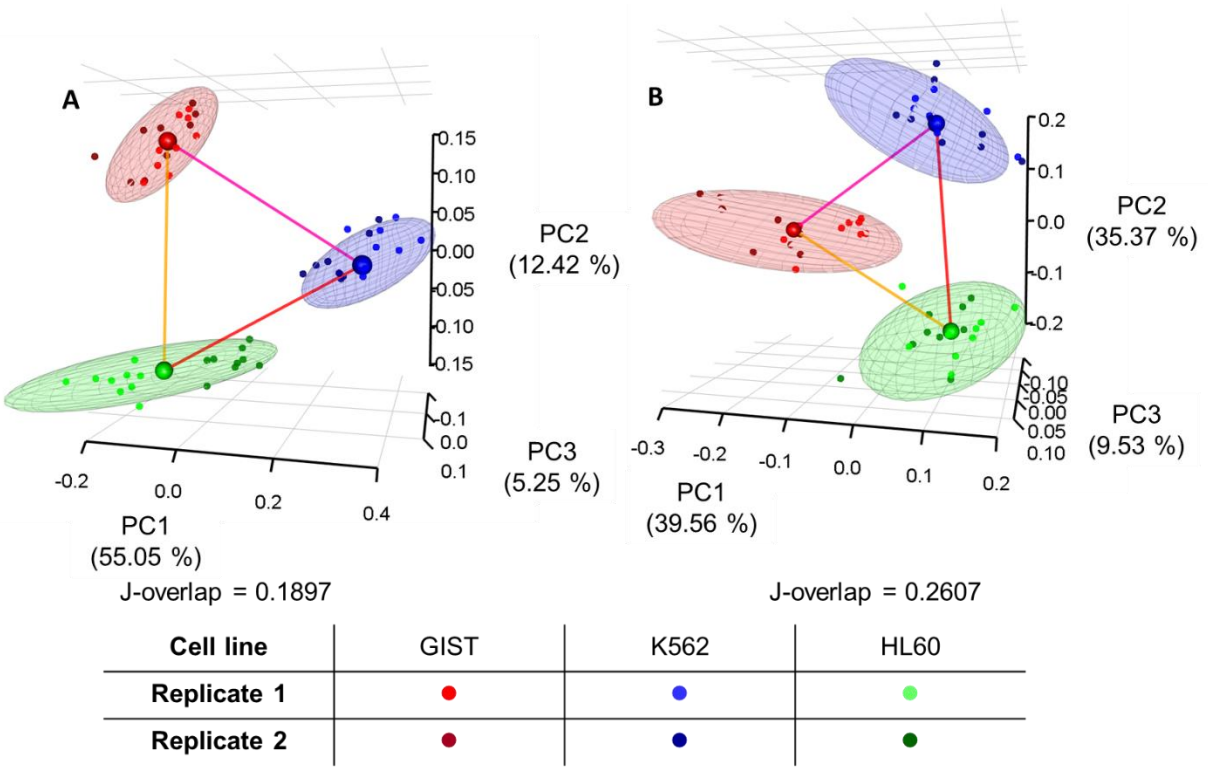

Figure 4.1.4: Direct sample resuspension in acetonitrile/H_2O is more advisable than hexane extraction. (A) Cell pellets of three different cell lines (GIST, HL60 and K562) were suspended at 5,000 cells/µl in acetonitrile/H_2O (1/1). 1 µl of the suspension was applied on the MTP (5,000 cells/spot). (B) Hexane was added (1/1) to the acetonitrile/H_2O suspension. Samples were vortexed and centrifuged for 30 s at 14,000 rpm for phase separation. 1 µl of the hexane extract was applied on the MTP. Cells were spray-coated with DHB matrix (20 mg/ml in acetonitrile/H_2O/TFA (60/40/0.5)). Samples were measured using an autoflex MS. The illustrated PCAs and variances were calculated in R. Biological replicates were colored in different shade of the same color (*m/z* 200-2000, S/N > 5, n = 2 biological replicates with ≥ 8 technical replicates measured on the same day, the figure was adapted with slight modifications from Weigt *et al.*, 2018 [121]).

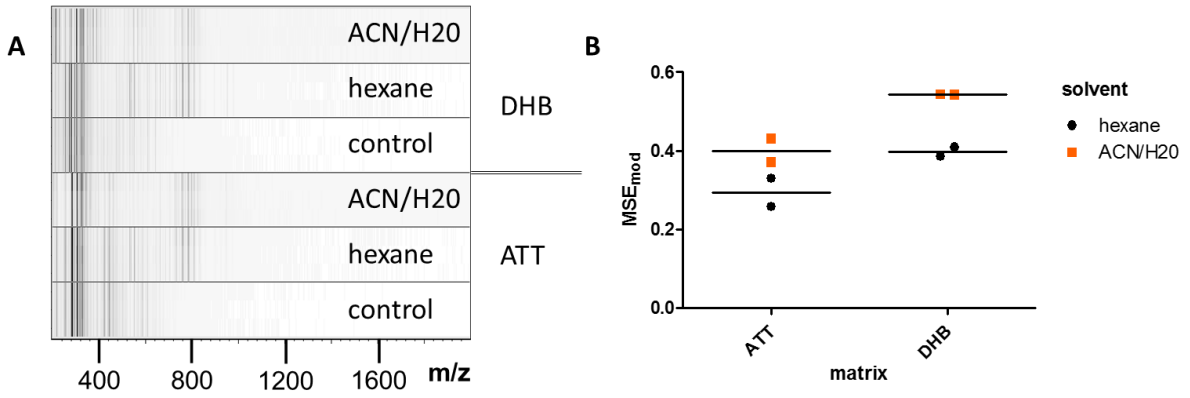

Figure 4.1.5: Validation of $J_{overlap}$ scores. K562 cell pellets were resuspended at 5,000 cells/µl in acetonitrile/H_2O (1/1). 1 µl of the suspension was applied on the MTP (5,000 cells/spot). Hexane was added (1/1) to the acetonitrile/H_2O suspension. Samples were vortexed for 30 s. For phase separation, samples were centrifuged for 30 s at 14,000 rpm. 1 µl of the hexane extract was applied on the MTP. Cells were spray-coated with DHB matrix: 20 mg/ml in acetonitrile/H_2O/TFA (60/40/0.5) or ATT matrix: 10 mg/ml in the same solvent. Samples were measured using an autoflex MS. (A) Spectra are illustrated as gel view generated by ClinProTools software. Pure matrix spectra are illustrated as control. (B) The MSE_{mod} score was plotted for the different solvent and matrix combinations (*m/z* 200-2000, S/N > 5, n = 2 biological replicates with ≥ 8 technical replicates measured on the same day).

The initial, rather "dry" matrix application protocol (15 µl/min flow of matrix solution) was investigated in more detail. $J_{overlap}$ scores suggested that slightly better separation of data sets in PCA space was obtained when a "wet" (30 µl/min flow of matrix solution) matrix application protocol was used instead (**Fig. 4.1.6**).

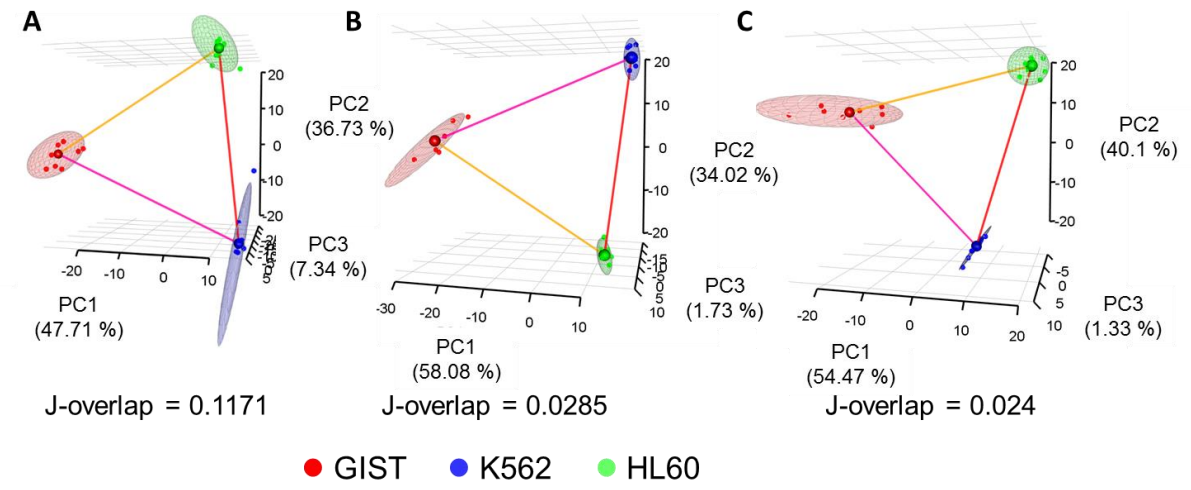

Figure 4.1.6: Preference for a wet matrix application protocol. Cell pellets of three different cell lines (GIST, HL60 and K562) were suspended at 5,000 cells/µl in acetonitrile/H_2O (1/1). 1 µl of the suspension was applied on the target plate (5,000 cells/spot). Matrix (20 mg/ml DHB in 50% acetonitrile, 0.2% TFA) was applied following different spray-protocols using the SunCollect sprayer. The spray head was either moved fast (1250 mm/min) or slow (900 mm/min). Matrix flow rate was either adjusted to "dry" (15 µl/min) or to "wet" (30 µl/min). Samples were measured on an ultraflex. The illustrated PCAs of samples prepared following a fast-dry (A), a fast-wet (B), and a slow-wet (C) spray protocol were calculated in R (*m/z*: 200-2000, n ≥ 8 technical replicates).

Munteanu *et al*. as well as Smolira *et al*. described in previous studies the importance of the analyte-to-matrix ratio for an optimized signal readout and to reproducibly acquire mass spectra [25, 122]. Therefore, it was aimed to fine-tune the amount of cells per measuring spot as the final step of workflow development. A cell dilution series was performed and the ideal amount of analyte again was determined by the matrix suppression effect, MSE_{mod} score. A "by eye" analysis of the gel view revealed increased suppression of matrix ions with increased cell numbers applied per measuring spot **(Fig. 4.1.7 A)**. The majority of remaining matrix signals was observed below *m/z* 500. A plot of the cell number against the MSE_{mod} revealed that the MSE_{mod} did not significantly increase with cell numbers greater than 5,000 cells/spot. Since the amount of detected analyte molecules seemed to plateau at 5,000 cells/spot, this amount was chosen for the final workflow (**Fig. 4.1.7 B)**.

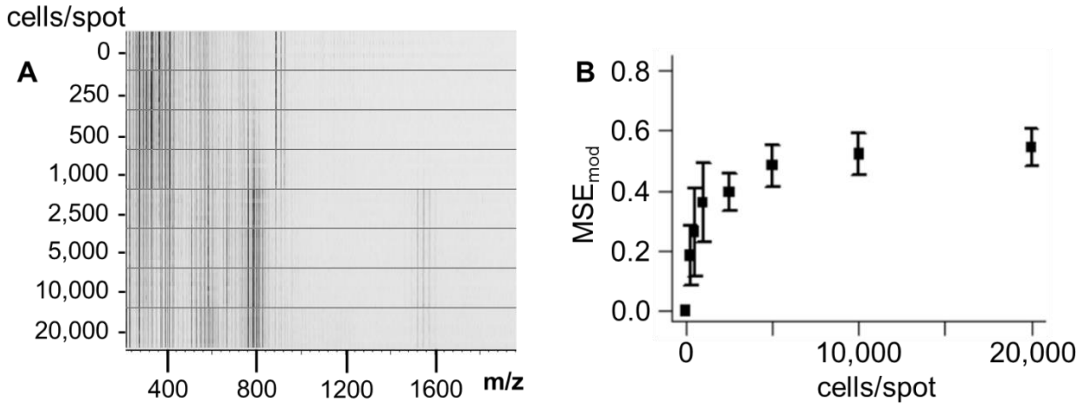

Figure 4.1.7: Effective suppression of matrix ions at 5,000 cells per measuring spot. A dilution series of K562 cells was prepared in acetonitrile/H_2O (1/1) and applied to an MTP. The plate was spray coated with 20 mg/ml DHB matrix resuspended in acetonitrile/H_2O/TFA (50/50/0.5) and measured by an ultrafleXtreme. 4,000 shots per measuring spot were acquired in reflector positive ion mode. (A) Spectra were illustrated as a gel view using ClinProTools software. (B) The cell number per measuring spot was plotted against the MSE_{mod} score calculated in R (mean ± standard deviation for n = 3 technical replicates prepared on different days).

The use of a matrix sprayer resulted in homogenously distributed matrix crystals (**Fig. 4.1.8 A**), which was critical for the automated acquisition of mass spectra. However, matrix application via spray coating requires the use of an additional instrument which increases sample preparation time as well as the cost of equipment. Therefore, several substituting methods to enable a homogenous DHB matrix application were tested. Even though none of the evaluated methods led to a successful replacement of the matrix spray application, the tested approaches are presented as incentives for future developments. Resuspension of cell pellets in aqueous DHB matrix and direct application to a MALDI target plate is not advisable due to the formation of large matrix crystals at the outer ring of the sample spot (**Fig. 4.1.8 B**). Addition of the humectants glycerol and DMSO was tested to delay the crystallization of DHB matrix. Upon desiccation of the samples at less than 1 millibar for 1 h homogenously distributed matrix crystals were observed (**Fig. 4.1.8 C,D**). Due to the available vacuum apparatus the drying was tedious and often incomplete (**Fig. 4.1.8 E**). Munteanu *et al.* described the use of sinapinic acid precoated MALDI target, to provide anchor crystals for the sample and matrix mixture [25]. In contrast to sinapinic acid, DHB precoated on MALDI target plates (**Fig. 4.1.8 F**) is easily dissolved upon application of aqueous or polar solvents (**Fig. 4.1.8 G**). Application of non-polar solvents on the polar surface led to widely dispersed sample spots. Nitrocellulose has been described to form homogenous thin layers that are resistant to most solvents, suppress matrix ions and do not generate endogenous signals [123]. The formation of a nitrocellulose thin layer that enables homogenous sample application was observed (**Fig. 4.1.8**

H). Unfortunately, a standardized reproduction of the result was not achieved. The use of benzoic acid was tested for the interference with DHB crystallization. Addition of benzoic acid resulted in a crystalline layer on the sample spot (**Fig. 4.1.8 I**). The addition of benzoic acid was not pursued further, since benzoic acid is not stable in ultra-high vacuum ion sources.

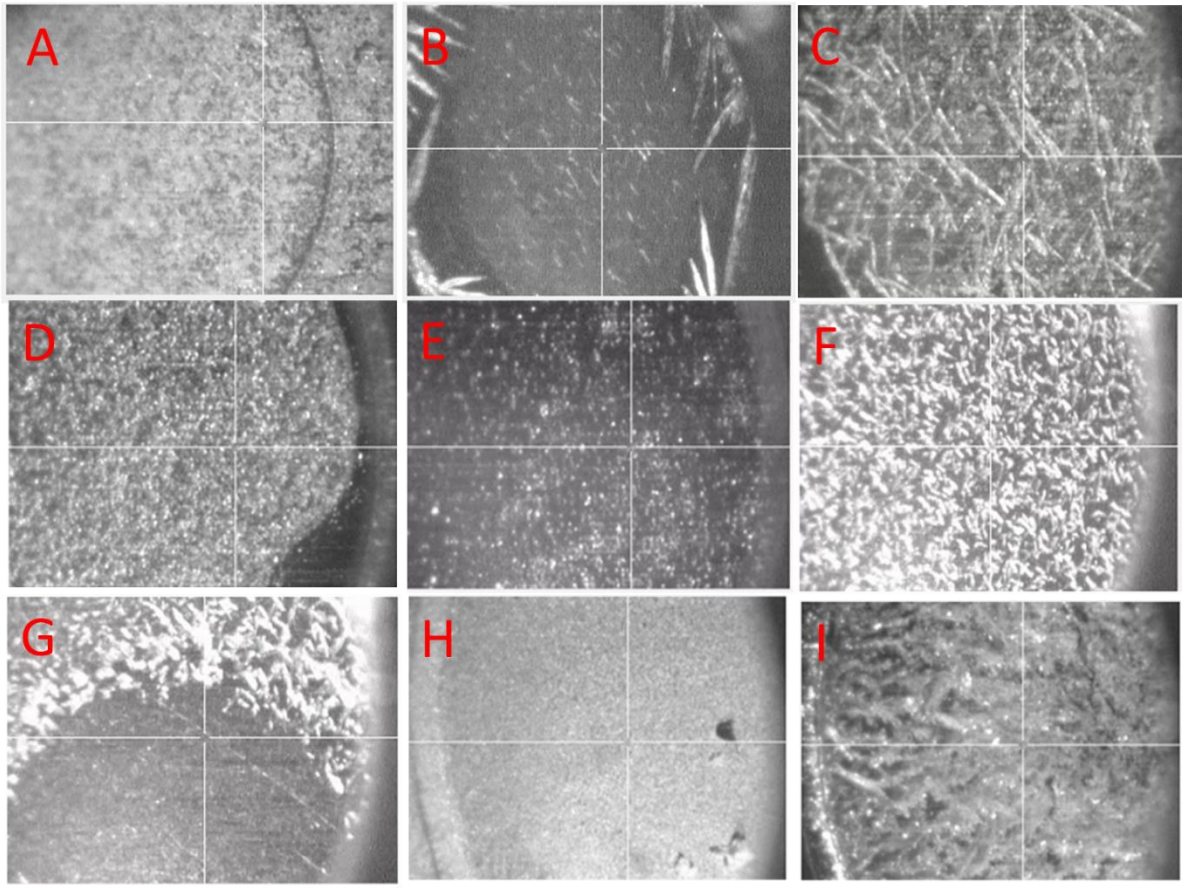

Figure 4.1.8: Evaluation of DHB matrix application protocols. MALDI ultrafleXtreme or autoflex camera images of sample spots prepared according to the following protocols: A) K562 cells were resuspended at 5,000 cells/µl in acetonitrile/H_2O. One microliter of the suspension was applied on a MALDI target plate, which was spray-coated with DHB matrix (20 mg/ml in acetonitrile/H_2O/TFA (50/50/0.5)). B) K562 cells were resuspended at 5,000 cells/µl in DHB matrix (20 mg/ml in acetonitrile/H_2O/TFA (50/50/0.5)). One microliter of the suspension was applied on a MALDI target plate. C) K562 cells were resuspended at 5,000 cells/µl in DHB matrix (10 mg/ml in H_2O) supplemented with 0.1 % TFA and 8 % glycerol/methanol (2/1). Samples were dried in desiccator for 60 min. One microliter of the suspension was applied on a MALDI target plate. D, E) K562 cells were resuspended at 5,000 cells/µl in 10 mg/ml DHB matrix (10 mg/ml in H_2O) supplemented with 0.1 % TFA and 2.5 % DMSO. Samples were dried in a desiccator for 60 min. One microliter of the suspension was applied on a MALDI target plate. D) Completely dried sample. E) Incompletely dried sample. F,G) DHB matrix (60 mg/ml in ethanol) was equally spread on a MALDI target plate (F). One microliter H_2O was applied onto the DHB thin-layer (G). H) Nitrocellulose-solution (20 mg/ml in acetone/propan-2-ol (1/1)) was equally spread on a MALDI target plate. K562 cells were resuspended at 5,000 cells/µl in DHB matrix (10 mg/ml in acetonitrile/H_2O/TFA (50/50/0.1)) and one microliter of the suspension was applied on the nitrocellulose thin layer. I) K562 cells were resuspended at 2,500 cells/µl in DHB matrix (20 mg/ml in acetonitrile/H_2O/TFA (60/40/0.2)) supplemented with 20 mg/ml benzoic acid.

4.1.2 Evaluation of the developed MALDI MS small molecule fingerprinting approach

The final workflow was tested for its ability to separate three cancer cell lines in replicate measurements performed weeks apart from each other (**Fig. 4.1.9 A**). The workflow enabled separation in PCA space, indicating that the detected biological variances outweigh variances caused by technical divergences. It is also noteworthy that these cell lines were all cultivated under similar conditions in culture medium mainly supplemented with FCS. This has been described to cause metabolic adaptations along with the suppression of physiologic pathways [124]. Application of the developed workflow for studies on primary cells likely harbors even more prominent biologic characteristics.

Correlation analysis of K562 cell pellets prepared on different days was chosen as a second approach to assess technical repeatability (**Fig. 4.1.9 B-D**). The analysis was focused on intensities in the lower 95th percentile to avoid a distortion of the correlation by prominent signals. A correlation coefficient, R^2, of 0.77 ± 0.07 suggests adequate repeatability of the workflow.

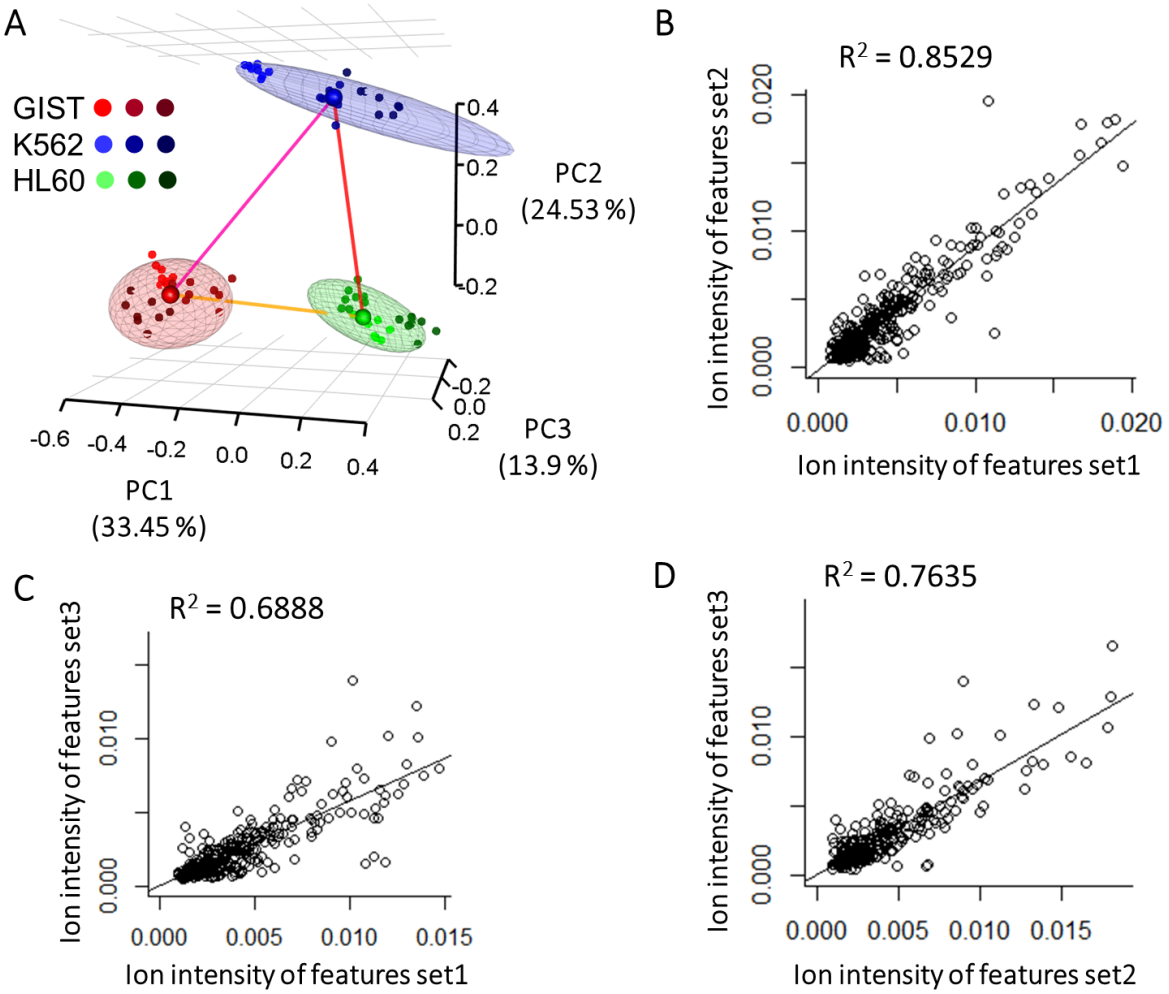

Figure 4.1.9: Evaluation of IC-MALDI MS lipid/metabolite fingerprints repeatability. Cell pellets of three different cell lines (GIST, HL60 and K562) were resuspended at 5,000 cells/µl in acetonitrile/H_2O (1/1). 1 µl of the suspension was applied on the MTP (5,000 cells/spot). Cells were spray-coated with DHB matrix (20 mg/ml in acetonitrile/H_2O/TFA (60/40/0.5)). Samples were prepared separately for measurement on an ultrafleXtreme. (A) PCA and variances were calculated in R (S/N > 5, *m/z* 200-2000, n = 3 biological replicates with respectively ≥ 8 technical replicates measured on different months). (B-D) Mean intensities of all peaks (S/N > 5, *m/z* 200-2000) corresponding to K562 cells independently prepared and measured on different days. Peaks with intensities above the 95th percentile were excluded.

A prerequisite for the detection of metabolites is the co-crystallization of matrix and analyte. Reproducible application of MALDI matrix therefore is of central importance for a standardized workflow. A proposed quality assurance measure is to weigh the sample mounted on a microscope slide prior to measurement before and after matrix coating [125]. Yet, this measure is not applicable to samples applied on a 230 g ground steel MALDI target, which is coated with ~20 mg of DHB matrix. The proposed more practical solution is a by eye evaluation of matrix crystal size and distribution (**Fig. 4.1.10**). Crystals forming in areas where no sample is applied, typically are shorter than 100 µm and not further apart than 20 µm. Matrix crystals are

more densely dispersed on spots containing sample due to co-crystallization of analyte and matrix.

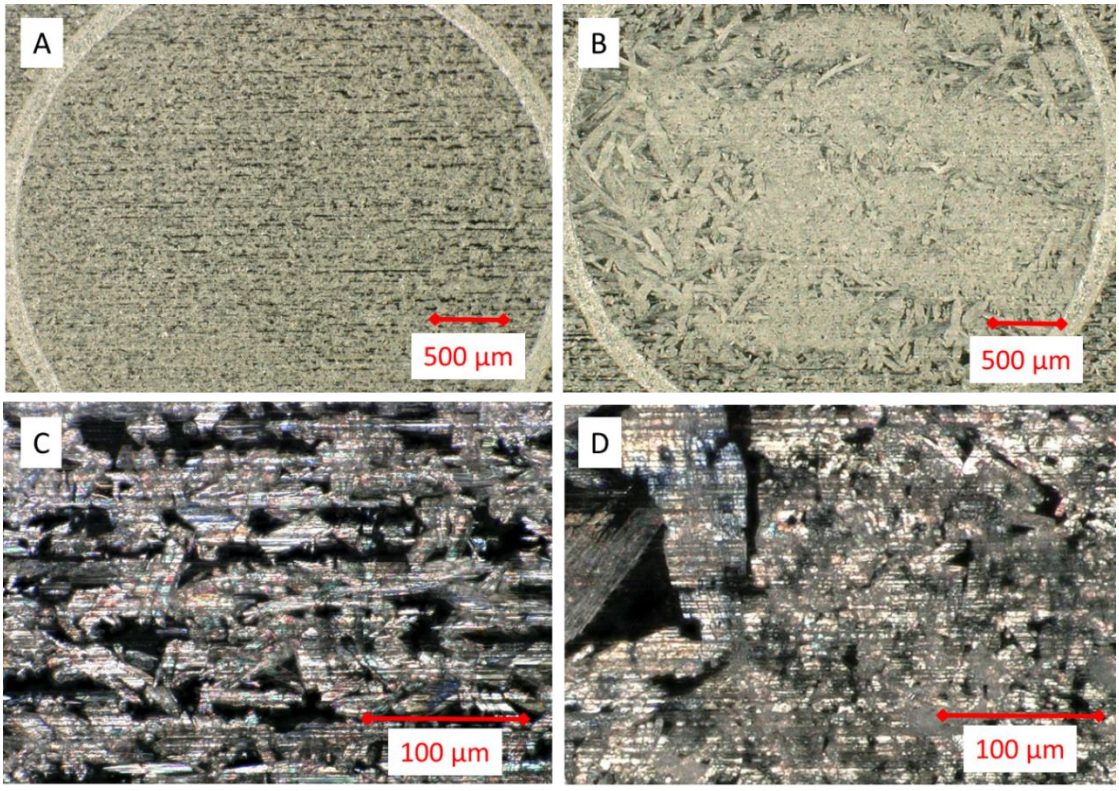

Figure 4.1.10: Monitoring of matrix application performance. K562 cells were resuspended at 5,000 cells/µl in acetonitrile/H_2O (1/1). 1 µl of the suspension was applied on the MALDI target plate (5,000 cells/spot). The target plate was coated with DHB matrix (20 mg/ml in acetonitrile/H_2O/TFA (60/40/0.5)). Optical images of blank spots (A,C) or sample coated spots (B,D) were acquired at different magnifications using a Keyence digital microscope.

To investigate if the final workflow could also be used for analysis and classification of tissue homogenates, five different tissue homogenates (brain, liver, pancreas, spleen, skeletal muscle) were measured, which were independently prepared for measurement on three different days (**Fig. 4.1.11**). All homogenates were separated in PCA space suggesting wider applicability of the developed method.

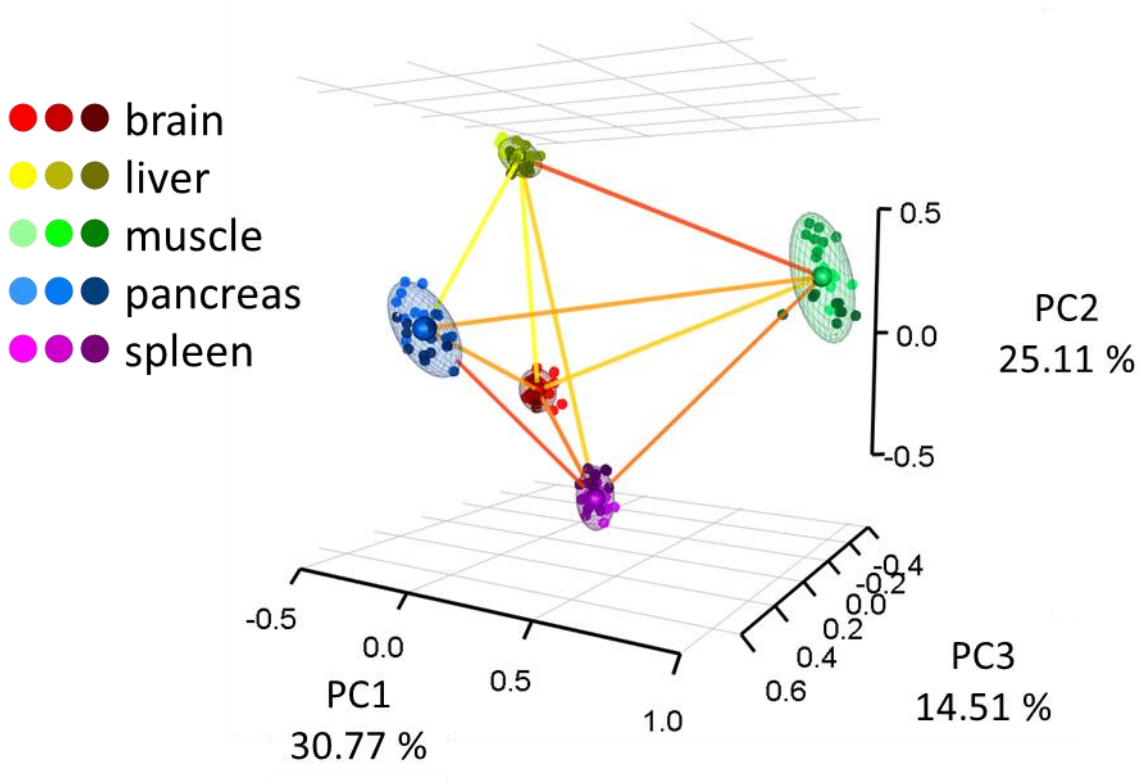

Figure 4.1.11: Small molecule fingerprinting workflow can be applied to fingerprinting analysis of cell-free tissue extracts with high technical reproducibility. Five snap-frozen bovine tissues were cut into small cubes (1 mm^3). Cubes were transferred to 15 ml conical tubes and resuspended at 50 mg/ml in H_2O containing complete protease inhibitor cocktail. The tissue cubes were homogenized for 40 sec using a polytron manual dispenser. Snap-frozen homogenates were thawed on three different days and further processed for MALDI-TOF MS measurement. Homogenates were diluted in acetonitrile/H_2O (1/1) to a final concentration of 10 µg wet weight tissue per µl. 1 µl of the solution was applied to the target plate. Dried sample spots were spray-coated with DHB matrix (20 mg/ml in acetonitrile/H_2O (1/1)). The target was measured using an ultrafleXtreme in reflector positive ion mode. Feature extraction and PCA calculation was performed in R. PCA of all five homogenates demonstrates robust discrimination of small molecular fingerprints. Technical replicates measured on different days are colored in different shades of the same color (n = 3 technical replicates prepared in 8-fold replicates on different days).

Workflow optimization aimed at increasing the information of cell fingerprints (by increasing MSE_{mod}) without being aware of the underlying metabolites and lipids. This was mainly due to the low mass resolving power of the ultrafleXtreme MALDI-TOF MS that was available for method development. A list of putative identities of detected metabolites and lipids that was supported by MALDI-FTICR remeasurements and database search is provided in **table 4.1.1**. It is worth mentioning that the list is not exhaustive, since only a minor fraction of the detected signals was subjected to data-base search.

Table 4.1.1: Candidate cellular metabolites and lipids detected by the developed MALDI-TOF MS fingerprinting workflow. *m/z* values of singly charged molecules or their detected proton adducts are presented. The identity hypothesis was supported by MALDI-FTICR accurate mass remeasurements.

LPE – lysophatidylethanoylamine

CDP – cytidine diphosphate

LPC – lysophatidylcholine

NAD(P) – nicotinamide adenine dinucleotide (phosphate)

SM – Sphingomyeline

PC – phosphatidyl choline

Lipids marked with asterisks were only observed in brain homogenates. The list is not exclusive and does not include measurements of pure or spiked standards.

metabolite/lipid	***m/z***
LPE(18:1)+H$^+$	480.3085
CDP-choline+H$^+$	489.1146
LPC(16_0)+H$^+$	496.3398
LPC(18_1)+H$^+$	522.3554
Heme B$^+$	616.1924
NAD$^+$	664.1164
SM(36_1)+H$^+$ *	731.6061
PC(32_0)+H$^+$	734.5694
NADP$^+$	774.0827
PC(34_1)+H$^+$	760.5851
PC(36_4)+H$^+$	782.5694
PC(36_1)+H$^+$	788.6164
PC(38_4)+H$^+$	810.6007
SM(42_2)+H$^+$ *	813.6844
Malonyl-CoA+H$^+$	854.1229

4.2 DEVELOPMENT OF A PHENOTYPIC ASSAY FOR BCR-ABL TYROSINE KINASE INHIBITORS

BCR-Abl is a well characterized, clinical relevant drug target [100]. Breitkopf *et al.* showed that tyrosine kinase inhibitor treatment affects the metabolome and lipidome of cultured cells [102]. Therefore, tyrosine kinase inhibition of the BCR-Abl positive K562 cell line was chosen as an example to integrate the developed metabolite-based IC-MALDI MS workflow into a cell-based assay for drug discovery. The developed workflow aims at supporting drug discovery in two conceivable ways (**Fig. 4.2.1**).

The first application deals with the identification of candidate pharmacodynamics biomarkers, i.e. of drug-sensitive *m/z* features. Cultivated cell lines are treated with various concentrations of well-characterized inhibitors. Upon incubation, the cells are harvested and applied on a ground steel MALDI MS target plate. The plate is spray-coated with DHB matrix and automatically analyzed by an ultrafleXtreme MALDI-TOF MS. The acquired data are imported into R. Drug-sensitive *m/z* features are extracted in a two-step filtration strategy (chapter 4.2.1.). In short, first features are filtered by their variance spanning all datasets. Then features are filtered by their fit to a concentration-response curve. Extracted features exposing the best curve-fit, candidates for so called concentration-response or pharmacodynamic markers, are structurally elucidated by MALDI-FTICR MS/MS.

In the second scenario, a previously identified concentration-response marker is employed for the discovery of novel inhibitors. Cell cultures are treated with compounds of unknown activity. The activity of compounds is evaluated based on the response of a defined marker molecule. This second, throughput-oriented workflow relies only on the use of the fast MALDI-TOF mass spectrometer.

The first workflow was developed by treating K562 cells with the well-characterized tyrosine kinase inhibitor imatinib. An initial single replicate experiment revealed that distinctness among treated and control cells increased with the inhibitor incubation time (**Fig. 4.2.2 A**). Most striking differences among treated and control group were observed after 72 h, which was confirmed by $J_{overlap}$ analysis (**Fig. 4.2.2 B**). However, assessment of cellular viability by trypan blue staining gave evidence for widespread cell death at that time point. 48 h inhibitor incubation was chosen instead, because it enabled clear separation in PCA-space at >80 % viability of the control.

The next sections focus on the development of an automated data processing pipeline, the identification of marker molecules by FTICR-MS/MS (workflow 1) and application of the concentration-response markers for potency evaluation of drugs (workflow 2).

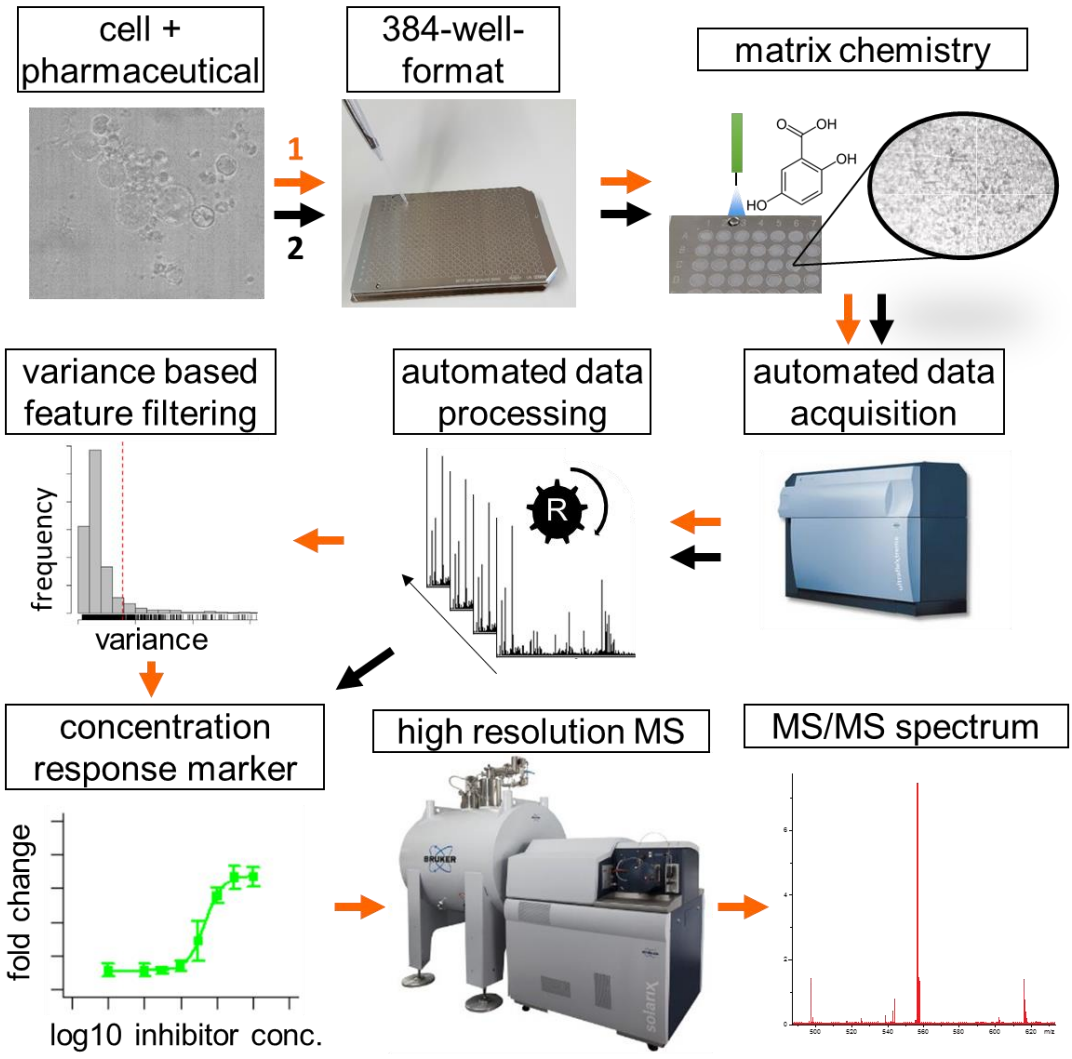

Figure 4.2.1: Concentration-response marker workflows. Cell lines are cultured in 6- or 24-well plates and treated with various concentrations of (**1**) well-characterized or (**2**) novel inhibitors. Upon inhibitor incubation, cells are harvested and snap-frozen. Cell pellets are resuspended in acetonitrile/H_2O (1/1). 1 µl is applied on a 384-well MTP (5,000 cells/spot). The target is coated with DHB (20 mg/ml in acetonitrile/H_2O/TFA (50/50/0.5)). Data are automatically acquired by an ultrafleXtreme MALDI-TOF mass spectrometer. Data are loaded into R programming language for preprocessing. (**1**) Drug sensitive *m/z* features are filtered by their variance and their fit to a concentration response curve. Extracted features are structurally elucidated by MALDI-FTICR MS/MS. (**2**) Compounds that induce a response of the marker molecule are identified as promising drug candidates (This image was adapted with some modifications from Weigt *et al.*, 2018 [121]).

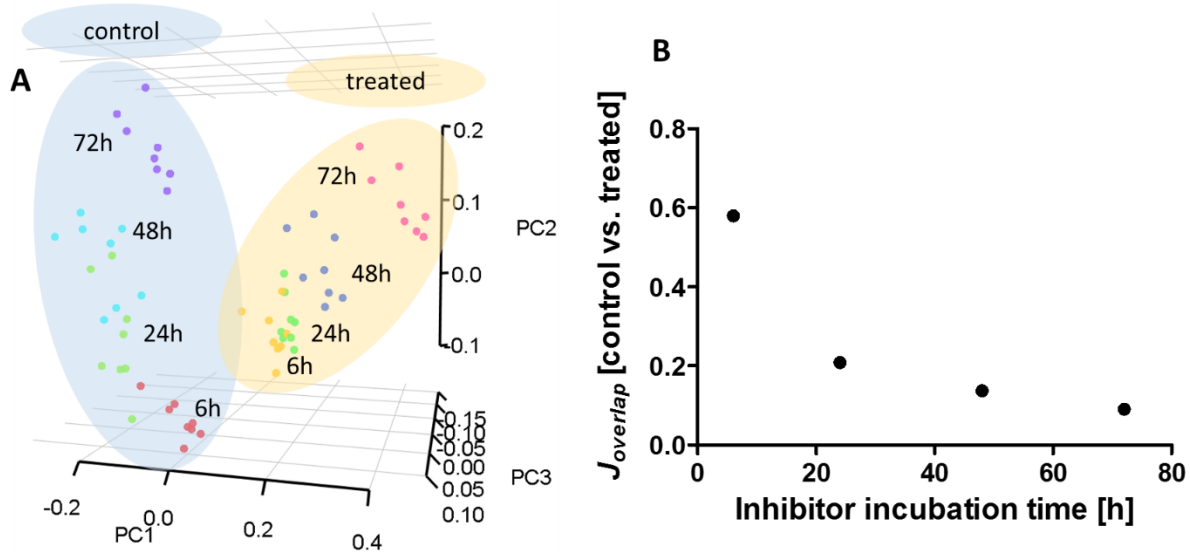

Figure 4.2.2: Increased incubation time favors separation of control and Imatinib treated cells in PCA space. K562 cells were treated with 1 µM imatinib in a time course. Imatinib treatment was stopped by cell harvest after 6, 24, 48 and 72 h. Samples were measured by an ultrafleXtreme in reflector positive ion mode. Feature extraction, PCA calculation (A) and $J_{overlap}$ analysis (B) was performed in R. (n = 8 technical replicates measured on the same day).

4.2.1 Automated extraction of concentration response markers

A whole cell spectrum acquired by the developed MS fingerprinting workflow typically contains > 500 signals (S/N > 5, *m/z* 200-2000). This number of features and the lack of any commercially available software required the in-house development of a pipeline to automatically extract drug sensitive *m/z* values.

The fundamental idea of the developed pipeline is that drug-sensitive *m/z* features show unique curve shapes in a concentration-response plot. For this reason, every relevant *m/z* feature was fitted to its specific concentration-response curve. Since hundreds of features were extracted during data preprocessing, several signals fitted a concentration-response curve-fit due to noise fluctuation. To exclude statistical noise, feature variances spanning all data sets were calculated. Plotting the feature variances against their frequency produced a right skewed histogram (**Fig. 4.2.3 A**). All features with a variance smaller than the total median variance were excluded from concentration-response fits. PCA supported the variance-based feature filtering approach (**Fig. 4.2.3 B**). Low variance features localized at the center of the loadings plot, whereas the interesting features represented the outliers of the loadings plot.

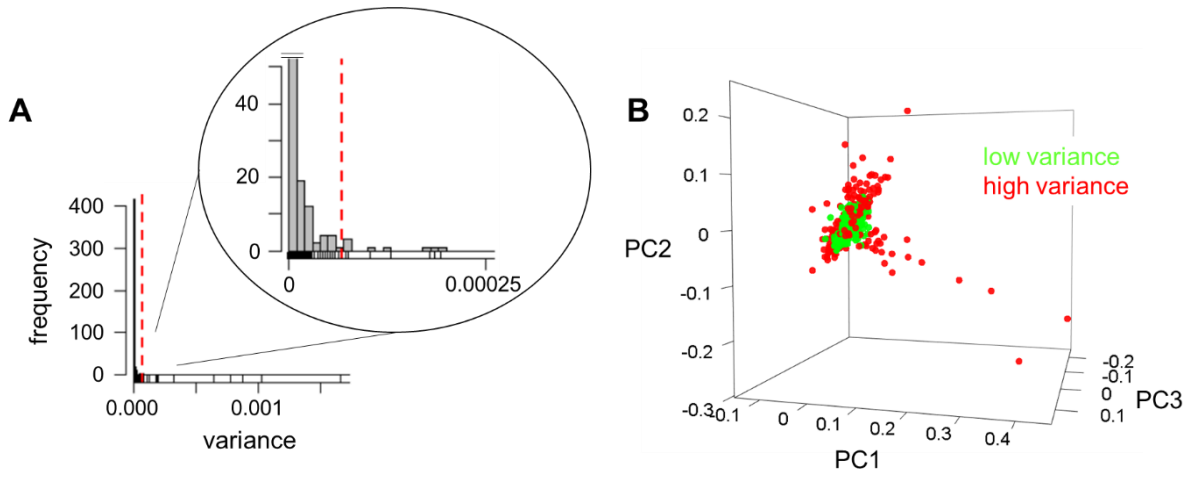

Figure 4.2.3: Variance-based feature filtering. A,B) Spectra acquired on an ultrafleXtreme were exported as text-files and loaded into R. Mass features exposing variances lower than the median variance of all features were excluded. These features fall to the left of the red dashed line in a variance histogram (A) and are typically located in the center of a loadings plot (B) while outliers (illustrated in red) are chosen for concentration response curve fits (This figure was adapted with some modifications from Weigt *et al.*, 2018 [121]).

Besides the necessity of a filtering step, additional valuable conclusions were drawn from the development of a data analysis pipeline based on the example of imatinib treated K562 cells. The initial data processing pipeline aimed at the discovery of features that exposed a good fit to either an ascending or a descending concentration-response curve. An *m/z* value was fitted to a decreasing concentration-response if its intensity (I) was greater at the control treated sample (ctr) compared to the sample treated with the highest inhibitor concentration (cmax) and vice versa:

$$\text{Descending curve fit: } I_{ctr} > I_{cmax}$$

$$\text{Ascending curve fit: } I_{ctr} < I_{cmax}$$

This approach enabled to extract *m/z* 826.6 as a marker for a descending concentration-response (**Fig. 4.2.4 A**). The descending concentration response model fitted best for the signal intensities of *m/z* 826.6, among several *m/z* values that showed an imatinib concentration-dependent decrease, rated by R^2 value. The extraction of features that increase upon imatinib treatment only revealed an $R^2 > 0.9$ for the compound imatinib (*m/z* 494.2) itself (**Fig. 4.2.4 B**) but no signals related to a treatment effect. This derived the hypothesis that eventual marker molecules are induced at low concentrations whereas no response is observed at high concentrations because of cell death. This kind of biphasic [126] or inverted U-shaped [127] concentration-response has been previously observed. The hypothesis was supported by a descending cellular viability of K562 cells, determined by MTT assay, at high

concentrations of imatinib treatment. The identification of biphasic concentration-response markers was based on a new criterion that the maximum feature intensity (I_{max}) was reached somewhere between the control group and the highest concentration, cmax. All feature intensities greater I_{max} were excluded and the remaining features were fitted to an ascending curve, which had to be defined by at least 5 data points. The approach enabled the extraction of *m/z* 616.2, which displayed a biphasic concentration response in three biological replicates **(Fig. 4.2.4 C)**.

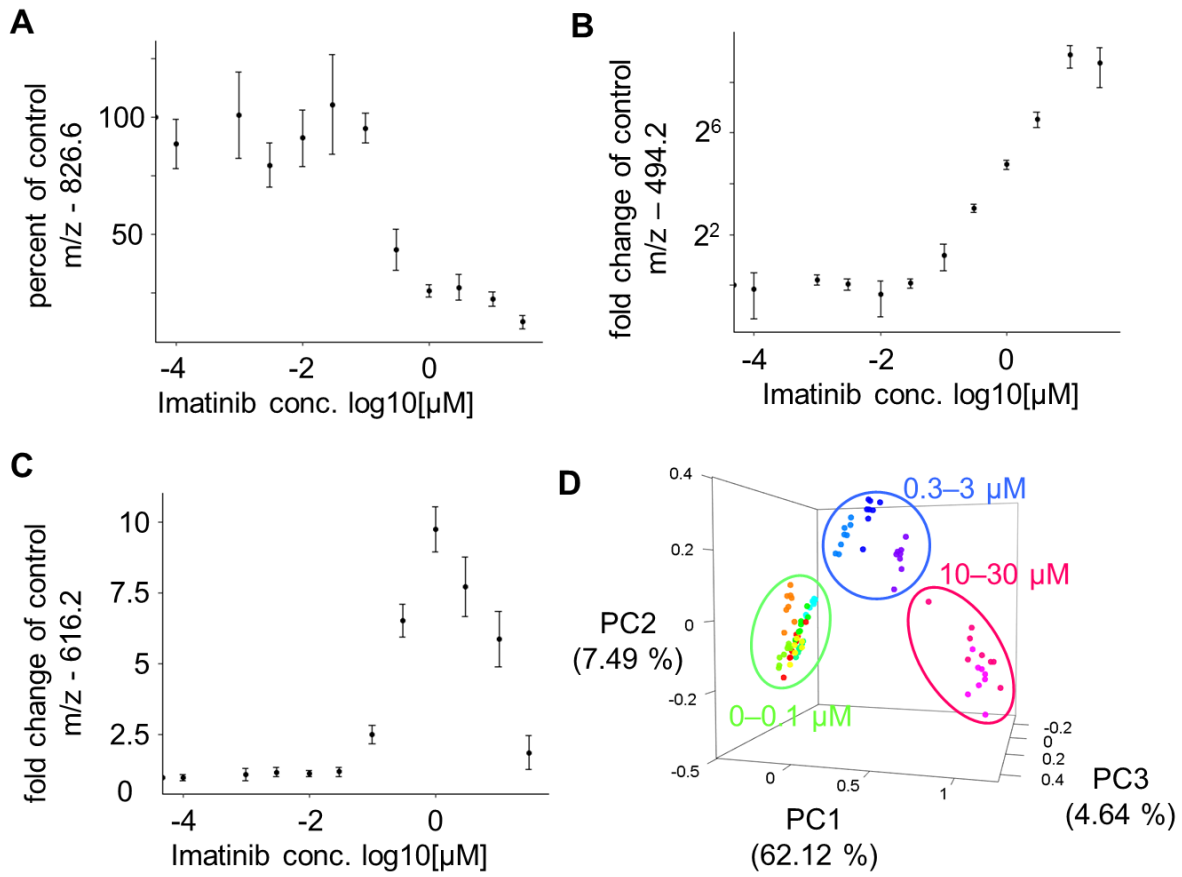

Figure 4.2.4: Small molecular features extracted from K562 fingerprints enable monitoring of imatinib concentration response. K562 cells were treated with various concentrations of imatinib and measured by an ultrafleXtreme. A data processing pipeline developed in R enabled the extraction of features that exposed descending (A), ascending (B) and biphasic (C) concentration-responses (mean ± SD of n = 3 biological replicates with 8 technical replicates each). D) Multivariate data analysis revealed groups of spectra of cells treated with similar concentrations of imatinib. Different imatinib concentrations are highlighted by a rainbow color scheme starting from the lowest concentration in red to highest concentration in violet (n = 8 technical replicates).

Interestingly, multivariate data analysis revealed that groups of spectra form clusters in PCA space related to imatinib concentration (**Fig. 4.2.4 D**): the spectra can be divided into low (0 – 0.1 µM), intermediate (0.3 – 3 µM) and high (10 – 30 µM) drug treated groups. This supports

the notion that biological effects, which in this case originate from the inhibitor treatment, outweigh technically attributed variances.

4.2.2 MARKER IDENTIFICATION USING MALDI-FTICR

The two extracted response marker *m/z* were subjected to molecular elucidation. As part of the response marker workflow, both features were remeasured using an ultra-high resolution 7T solariX FTICR (**Fig. 4.2.5**). Sample spots that had displayed highest feature of interest signal intensities during earlier MALDI-TOF analysis were used for MALDI-FTICR remeasurements and revealed more precise *m/z* 616.1767 and *m/z* 826.5722 for the low-resolution mass features *m/z* 616.2 and *m/z* 826.6, respectively.

Fortunately, the MALDI-FTICR remeasurements did only reveal a single high-resolution *m/z* feature underlying each low-resolution response marker. Noteworthy, it is likely that one low-resolution *m/z* feature harbors two or more molecular species, which would hamper its use as a response marker in fast MALDI-TOF analysis. An example from unrelated work are the phosphatidyl cholines (PC), PC(36:4) + H^+ (*m/z* 782.5694) and PC(34:1) + Na^+ (*m/z* 782.5670) which are distinguishable by MALDI-FTICR but not by MALDI-TOF MS.

Interestingly, the increase of *m/z* 616.2 (**Fig. 4.2.5 A**) and the decrease of *m/z* 826.6 (**Fig. 4.2.5 B**) upon 1 µM imatinib treatment was also observed in high-resolution measurements. This comparable sensitivity of low and high-resolution features to imatinib is another observation supporting the hypothesis that the detected high-resolution features correspond to the extracted low-resolution response markers.

High-resolution *m/z* features were subjected to database search using the human metabolome database (www.hmdb.ca). Search results with a mass accuracy better than 3 ppm were included. The list of potential adduct forming ions included protons, sodium and potassium. Moreover, search results proposing lipids with uneven carbon numbers in the fatty acid chain were excluded. The only result fulfilling these criteria for the search of *m/z* 616.1767 was heme B (*m/z* 616.1767, Δm = 0.03 ppm). The search of *m/z* 826.5722 revealed the potassium adduct of PC(36:1) (*m/z* 826.5723, Δm = 0.1 ppm) as the most promising candidate. Distribution of lipid chain length as well as position and stereo isomers of double bonds, which are notoriously difficult to analyze by MALDI MS [128] were not differentiated.

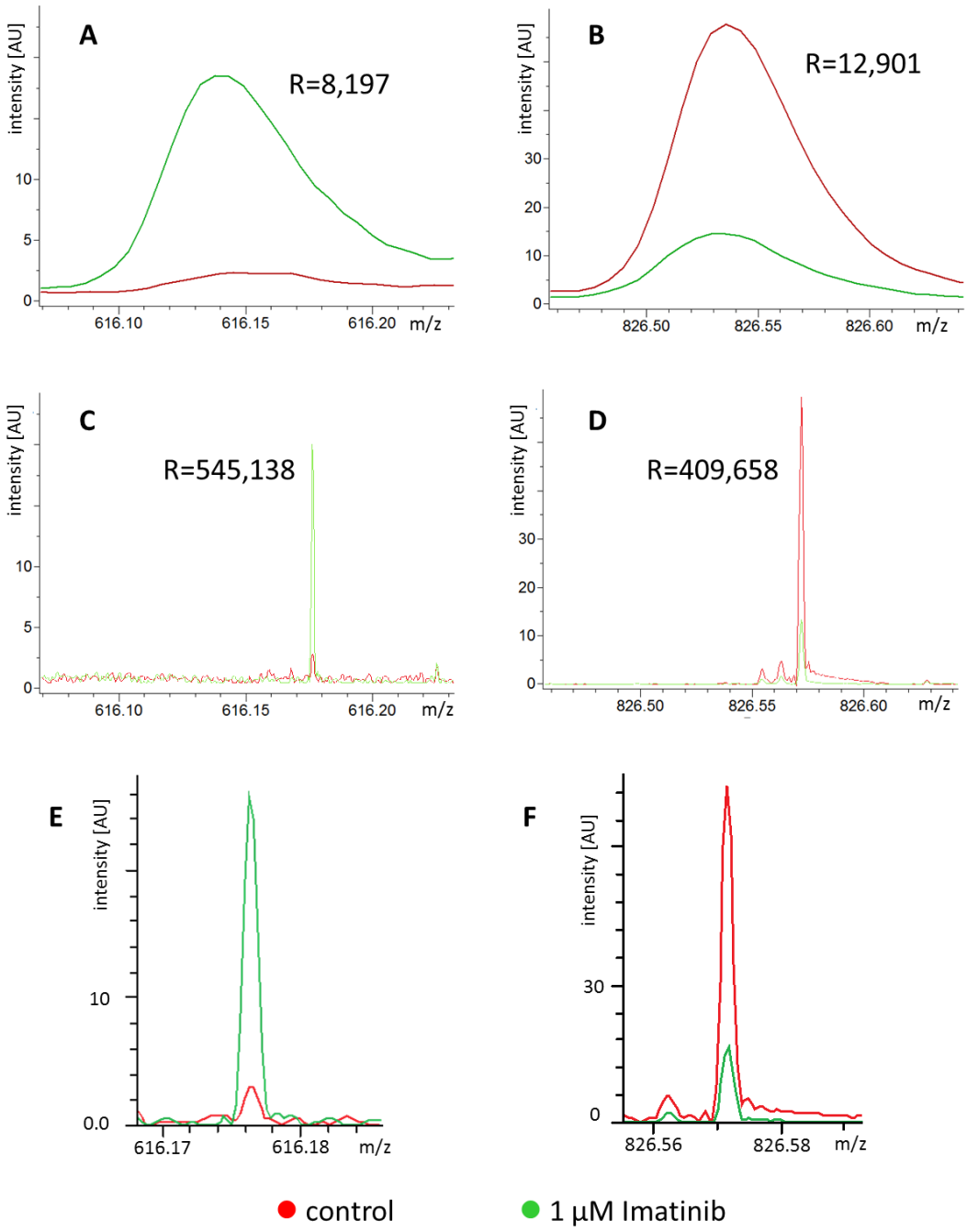

Figure 4.2.5: Remeasurement of low-resolution, putative *m/z* features by ultra-high resolution solariX MALDI-FTICR MS. Spots containing mock-treated cells (control; red spectra) and cells treated with 1 µM imatinib (green spectra) were measured using both MALDI-TOF (A,B) and MALDI-FTICR MS (C-F). For the low-resolution feature *m/z* 616.2 (A), a more precise *m/z* 616.1767 was obtained using high resolution MS (C,E). The low resolution feature *m/z* 826.6 (B) corresponds to the high resolution *m/z* 826.5722 (D,F).

The proposed molecular candidates underwent structural elucidation by MALDI-FTICR MS/MS. Fragmentation of the high resolution feature *m/z* 616.1767 confirmed the signal as heme B by revealing signals corresponding to the loss of the CH2COOH carboxylic acid side

chains (**Fig. 4.2.6 A**). High resolution MS/MS also confirmed *m/z* 826.5722 as the potassium adduct of PC(36:1) (**Fig. 4.2.6 B**). Signals corresponding to the loss of trimethylamine and the PC head group as well as a signal corresponding to a cyclophosphane ring (*m/z* 162.96) were detected. The fragments assignable to the PC were all detected as potassium adducts.

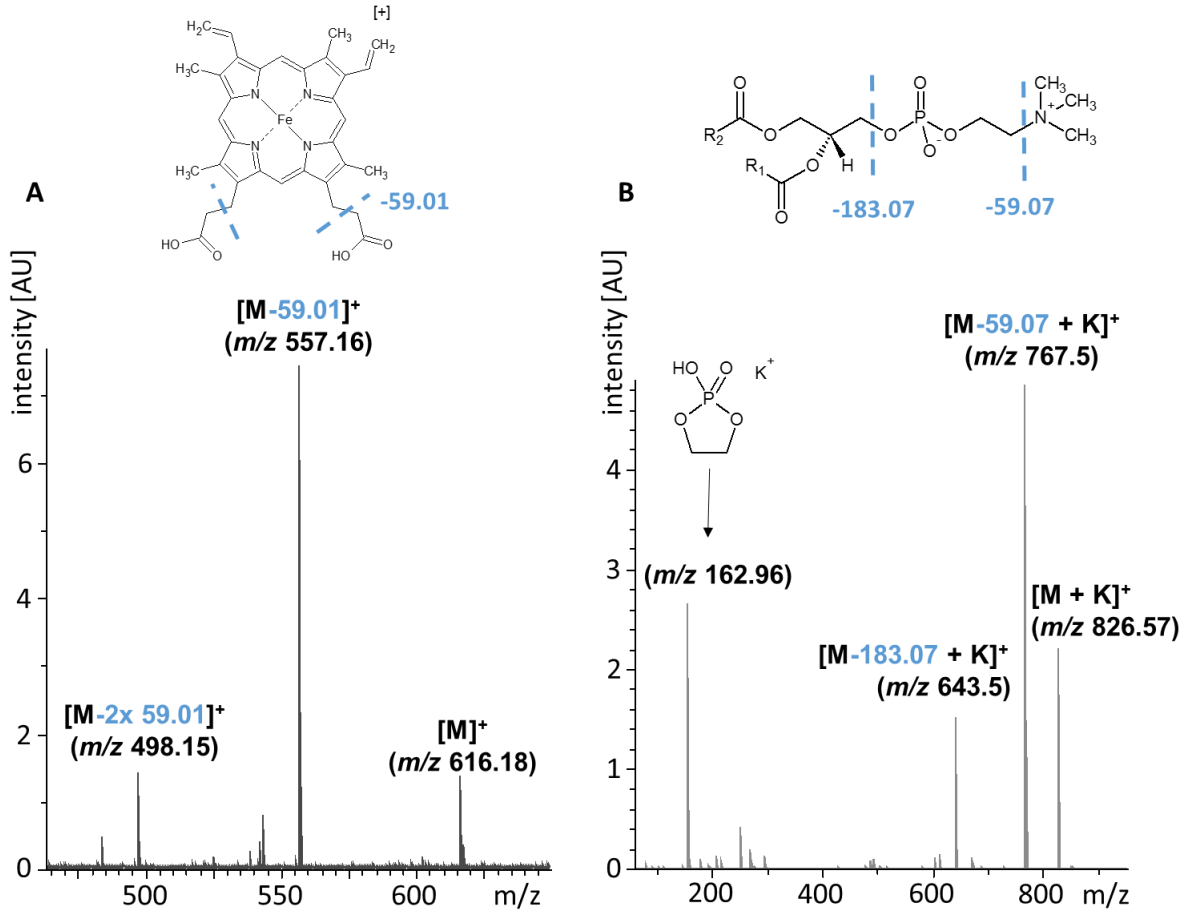

Figure 4.2.6: Identification of candidate response markers using MALDI-FTICR MS/MS. Spots that show highest feature of interest intensity were remeasured using a MALDI solariX 7T FTICR. Mass features were isolated using the instruments quadrupole and subjected to fragmentation. A) A spot containing 1 µM imatinib-treated cells exposed highest intensity of the feature *m/z* 616.1767. B) A spot containing DMSO-treated cells exposed highest intensity of the feature *m/z* 826.5722 (This figure was adapted with some modifications from Weigt *et al.*, 2018 [121]).

4.2.3 USE OF CONCENTRATION-RESPONSE MARKERS TO COMPARE DRUG POTENCIES

Heme B is the prosthetic group of heme proteins, which is produced in K562 cells during erythropoiesis. Erythropoiesis is a known indicator of redifferentiation of CML cells and thus a known indicator of successful action of Bcr-Abl inhibitors [129]. Heme B synthesis and degradation in K562 cells is tightly regulated due to the toxicity of free heme B [130]. PC(36:1) is a phospholipid molecule that is predominantly found in the plasma membrane. The decrease of PC(36:1) + K^+ in imatinib-treated K562 cells may be related to cell viability for two reasons: On the one hand apoptosis has been described to induce the expression of lipid degrading enzymes [131]. Additionally, apoptotic events are associated with a dysfunction of the Na/K-ATPase, which maintains membrane resting potential and indirectly cellular osmosis [132]. A loss of intracellular potassium might cause a pronounced decrease in potassium adduct formation during the MALDI process.

Since the whole cell fingerprint enables a simultaneous readout of both erythropoiesis and a process that is hypothesized to be apoptosis, it was important to test if the response of these molecules was specific for imatinib treatment or whether their readout was of a broader applicability.

A variety of inhibitors was chosen including the second line and second generation BCR-Abl specific inhibitors nilotinib and dasatinib as well as vandetanib that was designed as an EGFR and VEGFR inhibitor but also targets BCR-Abl [133, 134]. The drug sunitinib was chosen as a drug that inhibits multiple receptor tyrosine kinases but not BCR-Abl [135]. The anti-malaria drug chloroquine was chosen as a non-tyrosine kinase inhibitor drug.

In concentration-dependence experiments both heme B and PC(36:1) + K^+ responded to all inhibitors that have been described to target BCR-Abl (**Fig. 4.2.7**). Among the tested inhibitors, the strongest response was observed for dasatinib, followed by nilotinib, imatinib and vandetanib. No heme B induction was observed for sunitinib or chloroquine. The marker molecules proofed as valuable measures to perform drug potency evaluation in K562 cells and appear selective for BCR-Abl inhibitors.

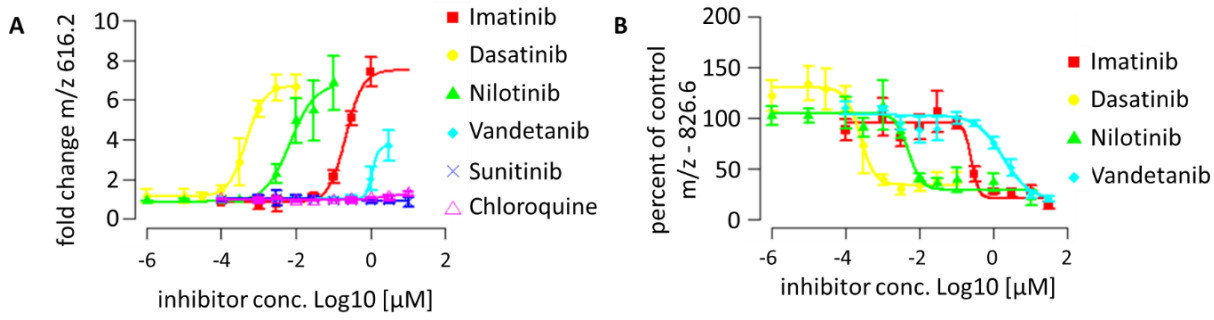

Figure 4.2.7: Drug potency evaluation using Heme B and PC(36:1) + K⁺. K562 cells were treated with various concentrations of the indicated inhibitors and analyzed by an ultrafleXtreme MS. The applied amounts of inhibitor were plotted against the signal intensities of heme B (*m/z* 616.2, **A**) and PC(36:1) + K^+ (*m/z* 826.6, **B**) (mean ± SD of n = 3 biological replicates with 8 technical replicates each, this figure was adapted with some modifications from Weigt *et al.*, 2018 [121]).

Since the decrease of PC(36:1)+K^+ was assumed to be related to apoptosis the use of *m/z* 826.6 as a viability marker was assessed. The descending curve shapes of *m/z* 826.2 were used to extract pIC50 values and compare these to viability data measured by MTT assay (**Fig. 4.2.8**). Standard deviations of pIC50 values derived from three biological replicates by MS experiments were comparable to those obtained by MTT assay (≤ 0.2) suggesting good experimental repeatability. Moreover, the pIC50 values obtained by MS and MTT were comparable (ΔpIC50 ≤ 0.4), suggesting usability of *m/z* 826.6 as a marker for viability in K562 cells.

A

Inhibitor	*m/z* – 826.6 pIC_{50}	MTT pIC_{50}
Imatinib	6.6 ± 0.1	7 ± 0.2
Dasatinib	9.6 ± 0.1	9.8 ± 0.1
Nilotinib	8.3 ± 0.1	8.5 ± 0.2
Vandetanib	5.8 ± 0.2	5.9 ± 0.2
Sunitinib	5.2 ± 0.2	5.6 ± 0.1
Chloroquine	-	-

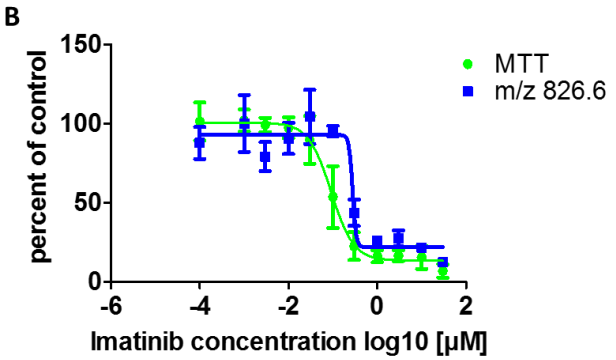

Figure 4.2.8: Use of PC(36:1) + K^+ to monitor viability of K562 cells. (A,B) K562 cells were treated with various concentrations of the indicated inhibitors and analyzed in parallel by an ultrafleXtreme MS and MTT assay. (A) pIC50 values derived from the concentration-response of *m/z* 826.6 were compared to MTT viability data. (B) Overlay of concentration response of *m/z* 826.6 and MTT data for imatinib treatment (mean ± SD of n = 3 biological replicates with 8 technical replicates each).

4.3 Development of a label-free cell-based mechanistic MALDI MS FASN assay

The previous section described the discovery of lipid marker molecules, which enabled the comparison of drug potencies. Since increases or decreases of phospholipid species can be induced by several stimuli, the readout becomes rather unspecific and may at best qualify as a phenotypic assay readout.

The fatty acid synthase (FASN) is a relevant drug target that has been associated with several diseases including cardiovascular diseases [105], neurodegenerative diseases [106] and cancer [103]. The FASN catalyzes the following reaction:

$$\text{Acetyl-CoA} + 7\ \text{Malonyl-CoA} + 14\ \text{NADPH} \rightarrow$$

$$\text{Palmitate} + 14\ \text{NADP}^{+} + 7\ \text{CO}_2 + 8\ \text{CoA}$$

The design of a MALDI MS enzyme assay demands some considerations that are going to be discussed in the following section. An MS-based cell assay requires at least one PD biomarker molecule from which a specific readout can be obtained. For enzyme assays these are the reaction educts or products. In the case of a FASN enzyme inhibition assay, method development towards the optimized detection of the reaction educts is justified by the expected dynamic range of the readout. FASN inhibition causes the accumulation of the educt malonyl-CoA which increases its signal readily by factor 100 [76]. Monitoring the reaction product, palmitate is expected to result in a readout with a poor dynamic range due to the poor detection of endogenous fatty acids via MALDI [136]. Among the educts of the FASN reaction, acetyl-CoA is involved in many biochemical reactions of cellular metabolism and has been proposed to be drawn to other pathways upon inhibition of the FASN [76]. Since the majority of metabolic enzymes requires NADH, NADPH is rather specific for the FASN reaction. Nevertheless, NADPH is also consumed by enzymes involved in purine biosynthesis, which diminishes its accumulation. A malonyl-CoA-based readout is proposed to be the most specific. Malonyl-CoA has not been described to be involved in any other metabolic pathways in human metabolism. Several studies previously demonstrated that cellular malonyl-CoA levels increase upon inhibition of the FASN [76, 137, 138]. Therefore, a malonyl-CoA-based readout is most desired for a FASN inhibition assay. To boost endogenous fatty acid synthesis, cells were seeded in lipid-free medium supplemented with 10 % charcoal-stripped FCS 16 h prior to all inhibitor treatment experiments as described by Hopcroft *et al*. [76].

4.3.1 Optimization and standardization of a malonyl-CoA-based FASN assay

The sample preparation workflow was optimized to improve the detection of endogenous malonyl-CoA. A commercially available standard was used to test various preparation parameters including matrix, pH, MS ion mode and cell number. A sweet spot was reached when supplementing DHB matrix with 2.5 % TFA (**Fig. 4.3.1**). Detection of 1 fmol malonyl-CoA was improved when using 2.5 % TFA compared to 0.5 % TFA, whereas no malonyl-CoA was detected at 5 % TFA. Interestingly, the best limit of detection was obtained in positive ion mode even though the molecular structure of malonyl-CoA would suggest preferred detection in negative ion mode.

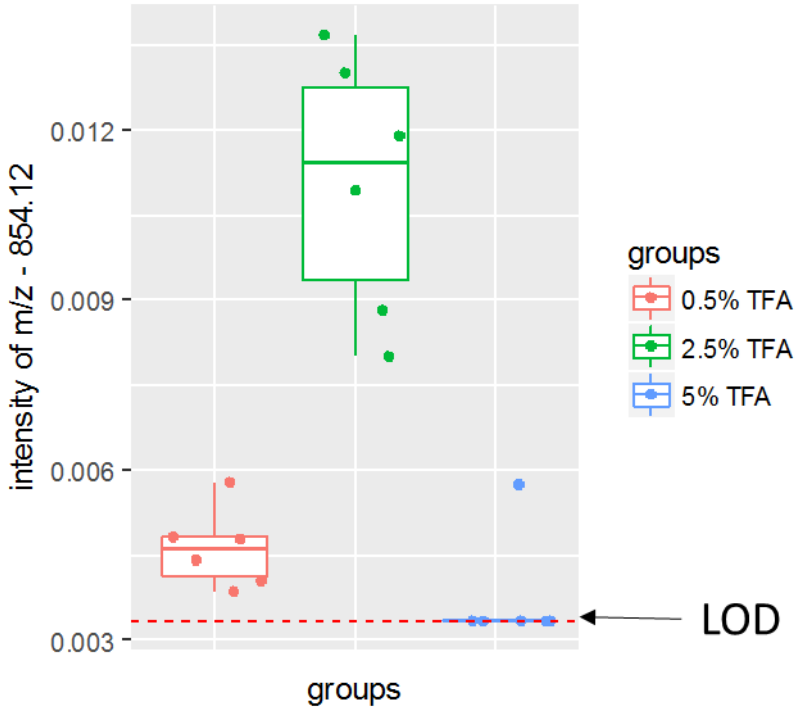

Figure 4.3.1: Optimized detection of malonyl-CoA standard using 2.5 % TFA. K562 cells were resuspended at 5,000 cells/µl in acetonitrile/H_2O (1/1) supplemented with 1 nM malonyl-CoA. 1 µL was applied on a ground steel MTP. The plate was spray coated with DHB matrix (20 mg/ml in acetonitrile/H_2O) supplemented with 0.5 %, 2.5 % or 5 % TFA. Sample spots were analyzed using an ultrafleXtreme (n = 6 technical replicates).

The optimized matrix composition was used for revised establishment of the malonyl-CoA--based FASN assay. Additionally, a potent, commercially available FASN inhibitor, GSK2194069, first described by Hardwicke *et al*. [109], was employed. Testing of GSK2194069 in K562 and A549 cells enabled detection of endogenous malonyl-CoA in both cell lines for the first time (**Fig. 4.3.2**). Malonyl-CoA ion intensity acquired on the ultrafleXtreme

MS reached a signal-to-noise ratio of 9.9 and 9.6 for A549 and K562 cells respectively (**Fig. 4.3.2 A,B**). Remeasurements using the solariX FTICR MS showed a more pronounced response to inhibitor treatment (**Fig. 4.3.2 C,D**). The obtained S/N ratio of malonyl-CoA on the FTICR were 78.6 and 64.7 for A549 and K562 cells respectively. Importantly, no interfering signals were detected in high-resolution remeasurements. The superior detection of malonyl-CoA in FTICR remeasurements is proposed to be due to the higher background observed in TOF data, which is in line with the higher specificity of the FTICR.

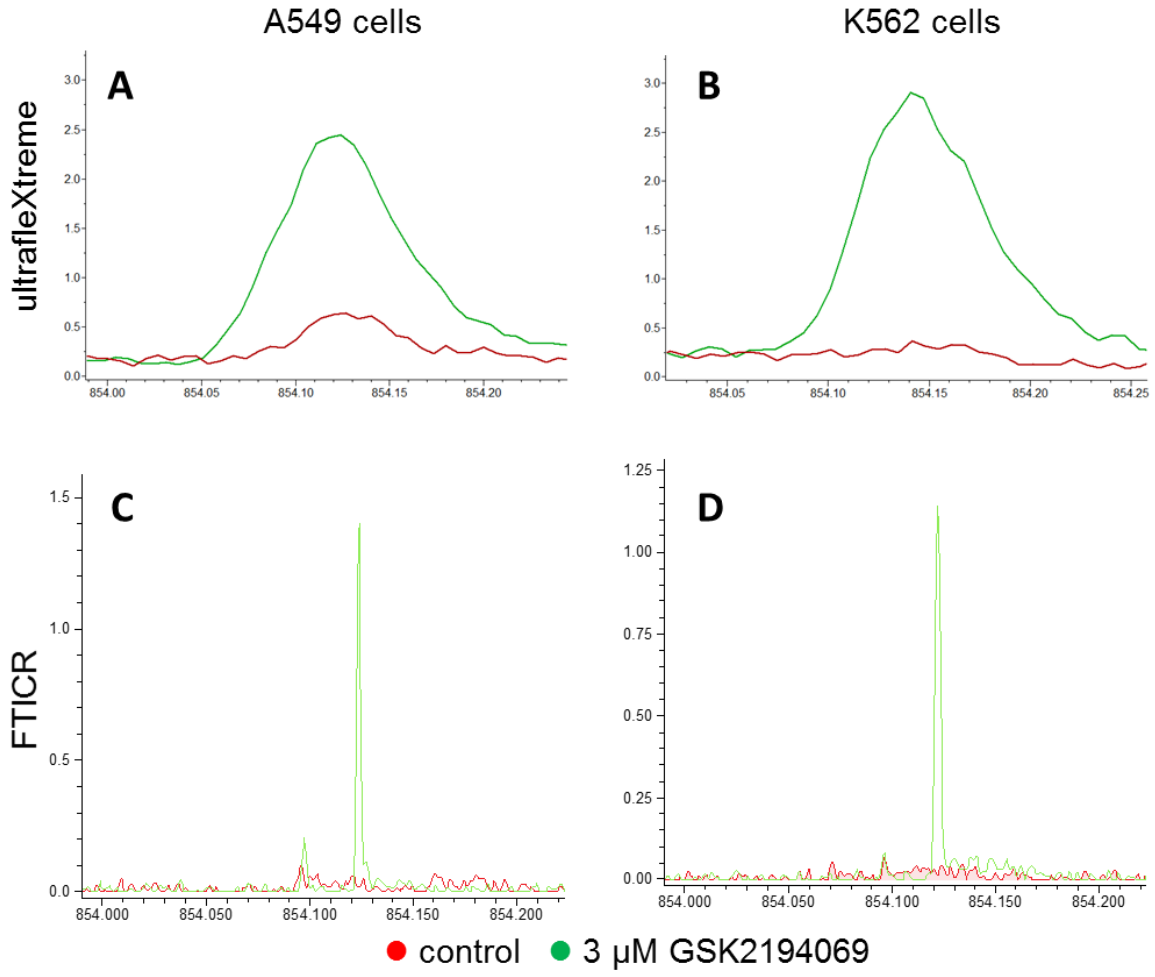

Figure 4.3.2: GSK2194069 induces malonyl-CoA accumulation. A549 (A, C) and K562 cells (B,D) were treated for 48 h with 3 µM concentrations of GSK2194069 (green spectra) and vehicle controls (red spectra). Cell pellets were resuspended in acetonitrile/H_2O and applied on a ground steel MTP. The target was spray-coated with DHB matrix (20 mg/ml in acetonitrile/H_2O/TFA (50/50/2.5)). Sample spots were measured by an ultrafleXtreme MS (A, B) and remeasured by a solariX FTICR MS (C,D).

In FTICR MS, the putative malonyl-CoA ion was subjected to fragmentation (**Fig 4.3.3**), which enabled the assignment of several malonyl-CoA-specific fragments originating from the breaking of the high-energy anhydride bond and the neutral loss of adenosine diphosphate.

Similar fragmentation patterns have been described in the literature for the LC-MS/MS fragmentation of 3-hydroxyisobutyryl-CoA [139].

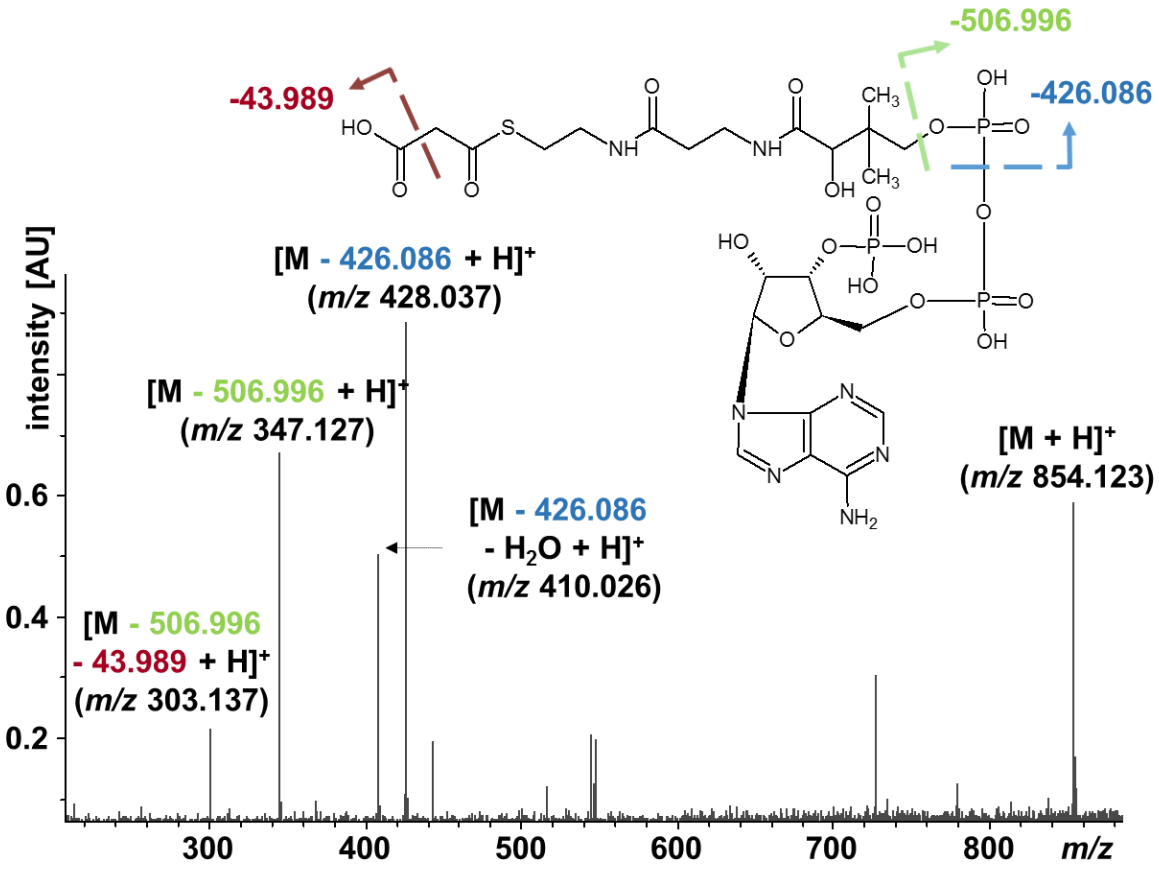

Figure 4.3.3: Fragmentation of endogenous cellular malonyl-CoA. A sample spot containing K562 cells treated with 3 µM GSK2194069 displayed highest ion intensity of the feature *m/z* 854.1229 and was used for FTICR MS/MS analysis.

To further optimize the MALDI-TOF-based readout, measurements were consigned from the ultrafleXtreme to the rapifleX MALDI-TOF MS that exposed greater sensitivity and measurement speed. To further standardize the measurements, a commercially available malonyl-CoA standard with a $^{13}C_3$-labeled malonyl-moiety was employed.

Application of an internal standard using a spray device is common practice in mass spectrometry imaging [140]. Fingerprinting experiments enable to directly spike the standard to the solvent used for sample resuspension. This harbors the advantage that the standard not only compensates measurement related inaccuracies but also variances induced by an error-prone spray process.

Dilution of the internal standard in a cell background revealed that spiking 5 µM labeled standard to the solvent used for sample resuspension, yielded a signal, which was about twice as high as the maximum endogenous signal induced by GSK2194069 treatment. Therefore, samples subjected to malonyl-CoA analysis by MS were henceforth resuspended in solvent supplemented with 5 µM malonyl-$^{13}C_3$-CoA internal standard (**Fig. 4.3.4 A**).

To determine the linearity of the assay readout, a dilution series of malonyl-CoA was spiked to a background of K562 cells, in which no endogenous malonyl-CoA was detected. Additionally, 5 µM malonyl-$^{13}C_3$-CoA was spiked into each sample for normalization. MS analysis revealed a good linear correlation (R^2 = 0.975) of the amount of spiked malonyl-CoA and the normalized signal at *m/z* 854.1 (**Fig. 4.3.4 B**). The concentration range in which a good linear correlation was observed exceeded 3 fmol/cell, suggesting that endogenous signal intensities wouldn't exceed the linear detection range.

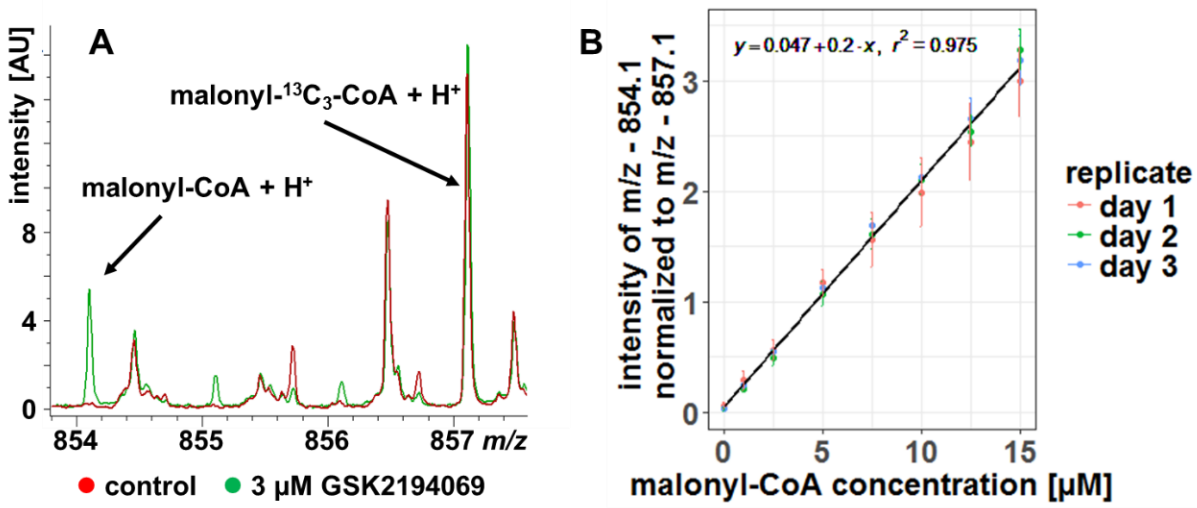

Figure 4.3.4: Linear range of malonyl-CoA detection between 0.2 – 3 fmol/cell. A) K562 cells were treated with 3 µM GSK2194069 (green spectra) and vehicle controls (red spectra) for 24 h. Cell pellets were resuspended in acetonitrile/H_2O supplemented with 5 µM malonyl-$^{13}C_3$-CoA. The suspension was applied on a MTP in 8-fold replicates and spray coated with DHB matrix (20 mg/ml in acetonitrile/H_2O/TFA (50/50/2.5)). Samples were analyzed using a rapifleX MS. B) K562 cells were resuspended at 5,000 cells/µl in acetonitrile/H_2O supplemented with various concentrations of malonyl-CoA and 5 µM of malonyl-$^{13}C_3$-CoA. 1 µl of the suspension was applied on a ground steel MTP in 8-fold replicates and spray-coated with DHB matrix (20 mg/ml in acetonitrile/H_2O/TFA (50/50/2.5)). Sample spots were measured by a rapifleX MS. Concentrations of the internal standard were plotted against the signal intensity of its protonated adduct (*m/z* – 854.1) normalized to the signal intensity of the ^{13}C-labeled standard (*m/z* – 857.1). Application of 1 µl of a 1 µM malonyl-CoA solution results in 1 pmol malonyl-CoA/spot. Division by 5,000 cells/spot results in an estimated 0.2 fmol malonyl-CoA/cell (n = 3 technical replicates, prepared and measured on different days).

The inhibitor incubation period was studied as the next step of assay establishment. A time course of GSK2194069 concentration response studies revealed that strongest malonyl-CoA accumulation was observed after 48 h (**Fig. 4.3.5 A**). Interestingly, a slight response and a more pronounced response are already observed after 6 and 12 h. In addition, the obtained pIC50 values increase with increasing inhibitor incubation periods. This implies an increased sensitivity with increased compound incubation time (**Fig 4.3.5 B**).

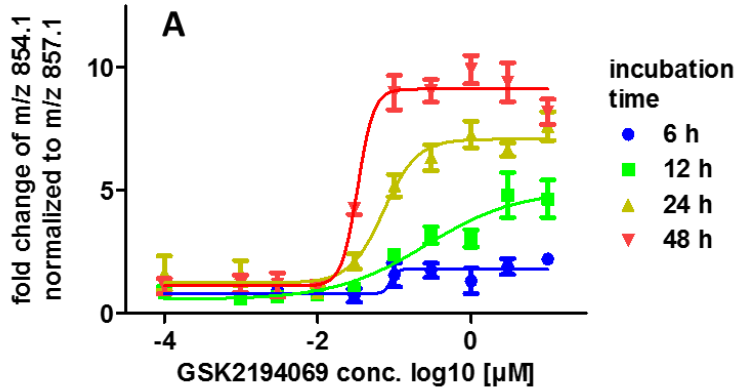

B

inhibitor incubation time [h]	pIC_{50} *m/z - 854.1 normalized to m/z - 857.1*
6	6.5
12	6.7
24	7.2
48	7.5

Figure 4.3.5: Time course of GSK2194069 concentration-response. K562 cells were treated with various concentrations of GSK2194069 for 6, 12, 24 and 48 h. Cell pellets were resuspended in acetonitrile/H_2O supplemented with 5 µM malonyl-$^{13}C_3$-CoA. The suspension was applied on a MTP in 8-fold replicates and spray coated with DHB matrix (20 mg/ml in acetonitrile/H_2O/TFA (50/50/2.5)). Samples were analyzed using a rapifleX MS. A) The GSK2194069 concentration was plotted against the endogenous malonyl-CoA signal normalized to the internal standard (mean ± SD, n = 8 technical replicates). B) pIC50 values were calculated from non-linear fittings to the concentration response curves.

To examine a homogenous distribution of the internal standard, a tool was written in R that displays the raw signal intensities allocated according to their arrangement on the target plate. Visualization of the distribution of the endogenous malonyl-CoA intensities revealed stronger signal intensities upon 48 h inhibitor treatment compared to 24 h inhibitor treatment (**Fig. 4.3.6 A**). As expected, malonyl-CoA signal intensities decreased with decreasing inhibitor concentration. Interestingly, visualization of the distribution of the malonyl-$^{13}C_3$-CoA standard revealed the same trend (**Fig. 4.3.6 B**). Samples treated for 48 h with GSK2194069 displayed a strong concentration-dependent increase of the internal standard, while the intensity of the internal standard was more homogenously distributed in samples treated for 24 h. Longer inhibitor incubation induced downstream effects beyond FASN inhibition, in particular cell death [137].

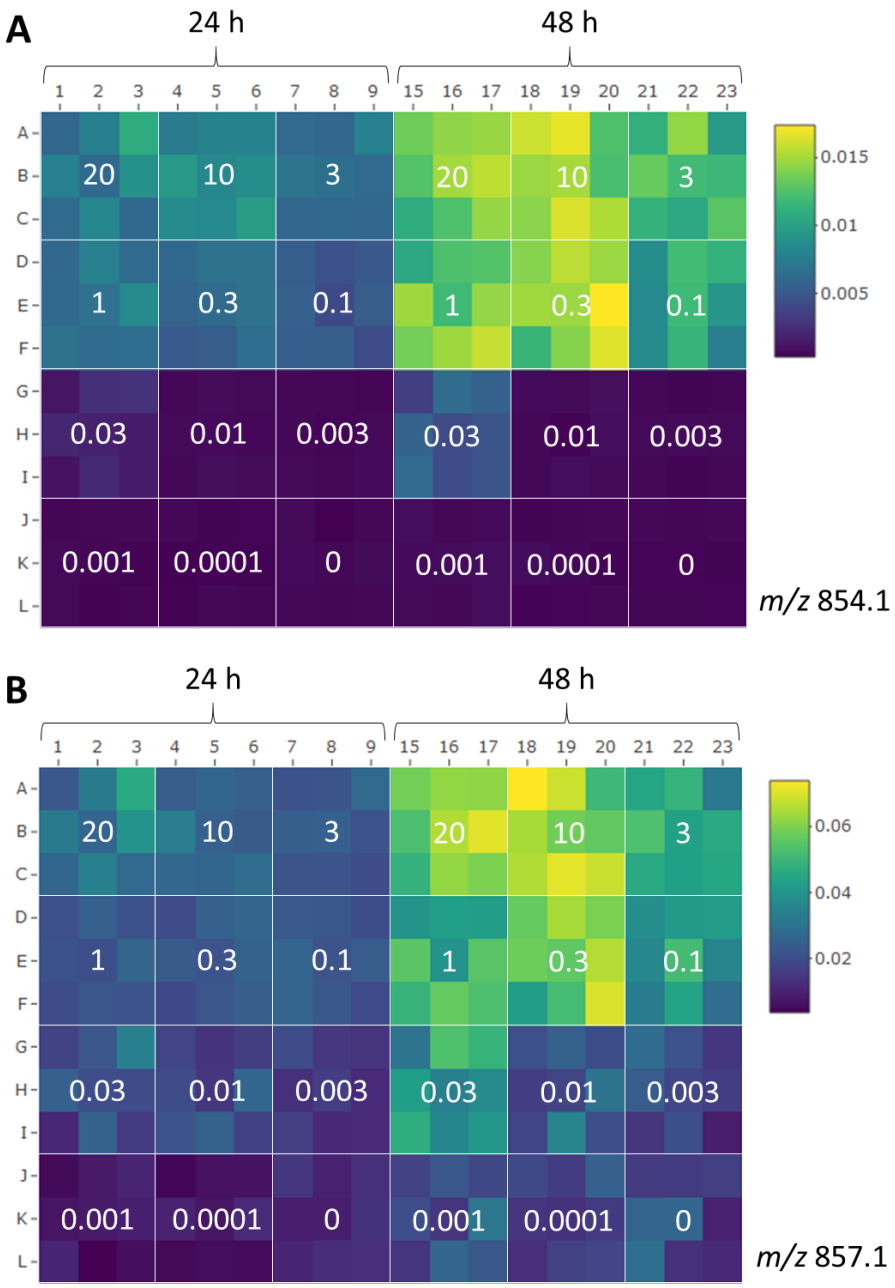

Figure 4.3.6: FASN-inhibitor incubation time affects signal intensities of both endogenous malonyl-CoA and malonyl-$^{13}C_3$-CoA standard. K562 cells were seeded in assay medium and incubated with various concentrations of GSK2194069 for 24 h (left) or 48 h (right). Cell pellets were resuspended at 5,000 cells/µl (cell number in control sample) in acetonitrile/H_2O (1/1) supplemented with 5 µM malonyl-$^{13}C_3$-CoA. The target plate was spray-coated with DHB matrix (20 mg/ml in acetonitrile/H_2O/TFA (50/50/2.5)). Samples were analyzed using a rapifleX MALDI-TOF mass spectrometer. The distribution of the raw signal intensities of *m/z* 854.1 (A) and *m/z* 857.1 (B) were extracted and plotted in R. Signal intensities are illustrated as a heat map, assigned to positions on the target plate. White numbers indicate the micromolar GSK2194069 concentrations.

Cell death reduces the amount of biological material possibly resulting in less molecules that can suppress the ionization of the internal standard. The strong increase of the malonyl-$^{13}C_3$-CoA standard therefore was taken as an indication to perform the assay with a shorter inhibitor incubation time of 24 h instead of 48 h. Nevertheless, the inhibitor incubation time depends on the expectations of the assay user. A user preferring a high S/N would probably choose a longer inhibitor incubation time, whereas a user preferring a more standardized readout rather prefers shorter incubation time.

It is also important to take into consideration that the addition of the internal standard does not reduce variances induced by the loss of cellular material, even though this is a potentially huge source of variation. The standard was added to reduce day-to-day variances in the matrix application as well as variances in the mass spectrometer's ionization and detection process. Intraday variances regarding, for example, the amount of cellular material would require an additional normalization step such as the performance of a Bradford assay. In fact, an internal standard can aggravate the loss of biologic material, since the resulting smaller endogenous signal is normalized to (i.e. divided by) an increased standard signal.

The FASN assay contained several modifications compared to the BCR-Abl assay including 1) cell cultivation in lipid-free medium, 2) shorter inhibitor incubations of 24 h, 3) sample resuspension in a solvent supplemented with ^{13}C-labelled internal standard, 4) use of a more acidic matrix solvent and 5) data acquisition on a faster mass spectrometer. The final workflow was tested using GSK2194069 as an exemplary compound in three different weeks. The data enabled reproducible pIC50 determination of 7.2 ± 0.1 suggesting good repeatability of the workflow and suitability as an assay (**Fig. 4.3.7**).

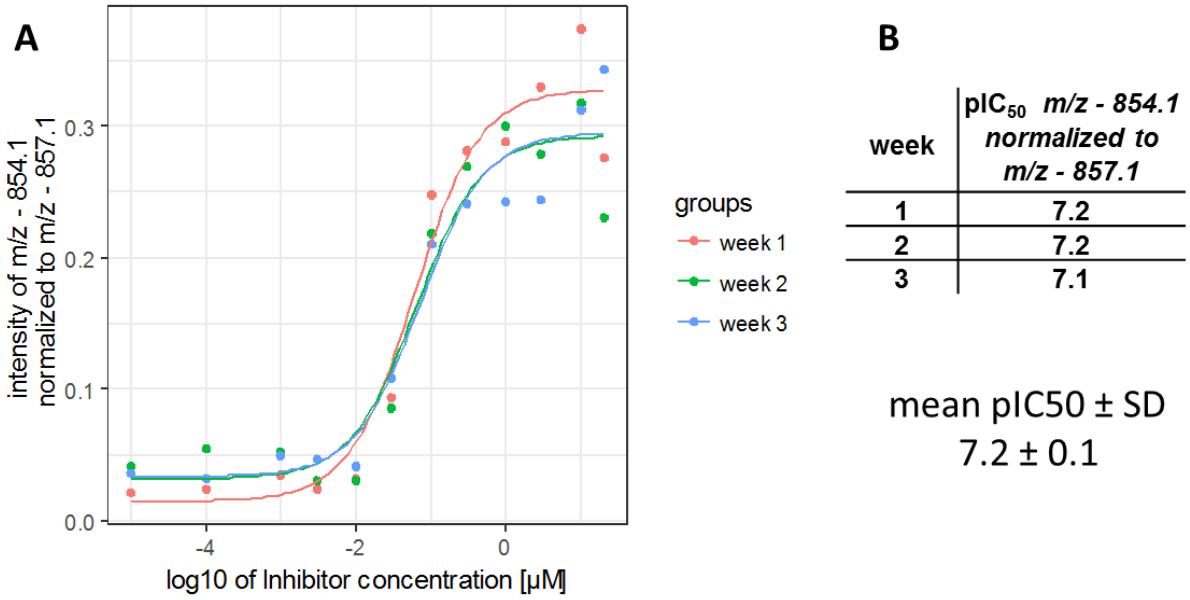

Figure 4.3.7: Mechanistic FASN-assay enables reproducible monitoring of FASN inhibition. K562 cells were seeded in assay medium and incubated with various concentrations of GSK2194069 for 24 h. Cell pellets were resuspended in acetonitrile/H_2O (1/1) supplemented with 5 µM malonyl-$^{13}C_3$-CoA. The target plate was spray-coated with DHB matrix (20 mg/ml in acetonitrile/H_2O/TFA (50/50/2.5)). Samples were analyzed using a rapifleX MALDI-TOF mass spectrometer. Data extraction, plotting and pIC50 calculation was performed in R. A) The GSK2194069 concentration was plotted against the endogenous malonyl-CoA signal normalized to the internal standard. B) pIC50 values were calculated from non-linear fittings to the concentration response curves. The experiment was performed in three different weeks "week 1", "week 2" and "week 3" (n = 3 biological replicates with 9 technical replicates each prepared in different weeks).

4.3.2 Application of the mechanistic malonyl-CoA-based FASN assay

The workflow was applied to compare the potency of different FASN inhibitors described in the literature. Orlistat is an FDA-approved drug for treating obesity. Orlistat acts as a lipase inhibitor and prevents the uptake of fats from the human diet in the intestine [141]. Kridel *et al*. suggested orlistat as a rather selective FASN inhibitor-based on a hydrolase screen in prostate cancer cells, making use of a fluorescent probe that competes for binding to the thioesterase domain of the FASN [142]. The potent FASN inhibitor, BI 99179 (pIC50 biochemical assay = 7.1), was discovered by Kley *et al*. using an *in vitro* HTS at Boehringer Ingelheim, which measures NADPH consumption in a biochemical assay [112]. Its optical antipode, BI 99990, exposes no FASN activity (pIC50 biochemical assay < 5.5) and was chosen as a control compound. It is important to note that the BI-compounds were tested in a separate tissue culture batch.

MTT analysis revealed no toxicity of the BI-compounds or GSK2194069 upon 24 h treatment (**Fig. 4.3.8**). However, viability was reduced by ~ 50 % upon treatment with 60 µM orlistat for 24 h.

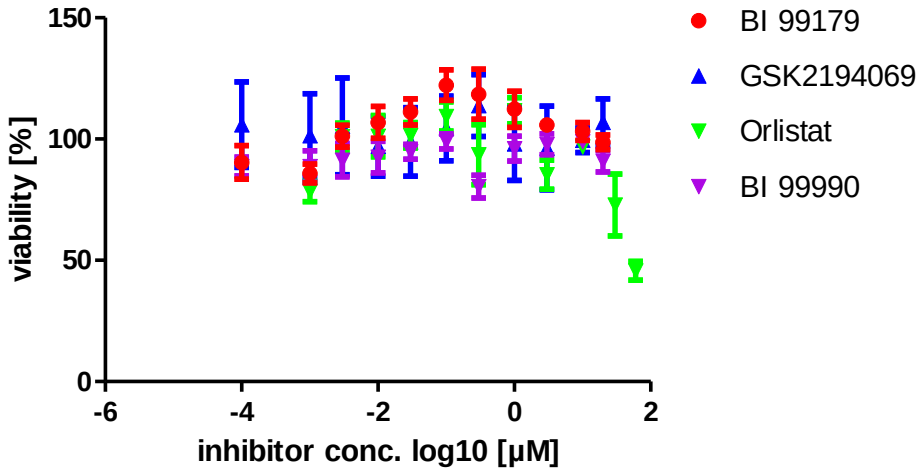

Figure 4.3.8: Viability of inhibitor-treated K562 cells. K562 cells were treated with various concentrations of BI 99179 (red), GSK2194069 (blue), Orlistat (green) and BI 99990 (purple) for 24 h prior to viability determination by MTT assay (mean ± standard deviation for n = 3 technical replicates).

The FASN inhibition assay revealed strongest malonyl-CoA accumulation upon treatment with BI 99179 (pIC50 = 7.6), followed by GSK2194069 (pIC50 = 7.2) and Orlistat (pIC50 = 5.2, **Fig. 4.3.9**). No inhibitory effect was observed for BI 99990, which confirmed that the optical antipode of BI 99179 exposes no inhibitory activity of the FASN. A comparison of the determined pIC50 values with values reported in the literature as well as the chosen assay conditions are addressed in more detail in the discussion section.

A

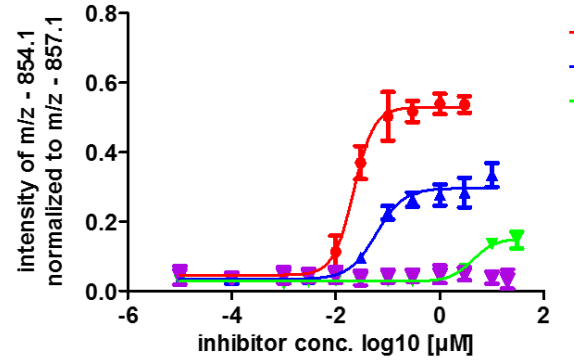

B

inhibitor	pIC_{50} *m/z - 854.1 normalized to m/z - 857.1*
BI 99179	7.6 ± 0.1
GSK2194069	7.2 ± 0.1
Orlistat	5.2 ± 0.2
BI 99990	n.c.

Figure 4.3.9: FASN assay enables potency evaluation of different FASN inhibitors. K562 cells were seeded in assay medium and incubated with various concentrations of BI 99179, GSK2194069, orlistat or BI 99990 for 24 h. Inhibitor treatments with the BI-compounds were performed in a separate cell batch. Cell pellets were resuspended in acetonitrile/H_2O (1/1) supplemented with 5 µM malonyl-$^{13}C_3$-CoA. The target plate was spray-coated with DHB matrix (20 mg/ml in acetonitrile/H_2O/TFA (50/50/2.5)). Samples were analyzed using a rapifleX MALDI-TOF mass spectrometer. Data extraction was performed in R. A) Inhibitor concentrations were plotted against the endogenous malonyl-CoA signal normalized to the internal standard. B) pIC50 values were calculated from non-linear fittings to concentration response curves (mean ± standard deviation for n = 3 biological replicates with 9 technical replicates each prepared on 3 different days, n.c. - not computable).

The compound BI 99179 exceeded both the potency of the GSK compound determined by IC50 calculation as well as the relative amount of accumulated malonyl-CoA. Since the experiments were performed in different cell culture batches, it was not clear whether the observed differences originated from the compound potency itself or variances in the response of different cell culture batches. The aim to develop this assay with a high focus on standardization justified to perform all comparisons of inhibitor potencies in the same tissue culture batch. The parallel evaluation of four compounds in a concentration response - including the required replicates - easily exceeds the workload of a single laboratory member. Therefore, the assay constituted a suitable example to establish an automation approach.

4.3.3 Automation of the mechanistic FASN assay

The conclusion that a standardized assay requires the comparison of multiple inhibitors to be performed in the same cell culture batch, confirmed the need for a faster and facilitated workflow. The aim was to develop an automated liquid handling workflow that also strengthens the perception of MALDI MS cell-based assays as a suitable tool for routine drug profiling.

HTS platforms rely on the performance assays in 384, 1536-well format and beyond [80]. As a proof of concept, the assay was established in 96-well format, an assay format common in compound profiling during lead optimization, which enables the performance of 8 concentration-response curves, defined by 12 points each, in parallel. The assay consists of multiple parallelized steps (**Fig. 4.3.10**). In the first step K562 cells are seeded into the wells of a 96-well "culture-plate". The previously established seeding density of 0.25 * 10^6 cells/ml was kept, since best drug responses were observed at this density. The seeding volume was reduced to 200 µl per well. The subsequent inhibitor treatment step was automated using the CyBio FeliX pipetting platform. Compounds were dissolved and diluted in a 96-well "compound-plate". When performing a dilution series with the CyBio FeliX, tips had to be exchanged after each dilution step, since carry over of the compound could not be ruled out. 1 µl of each well of the compound-plate was transferred to a respective well of the tissue culture plate using the CyBio 96-well 60 µL tip tray. Cell harvest was performed 24 h after inhibitor

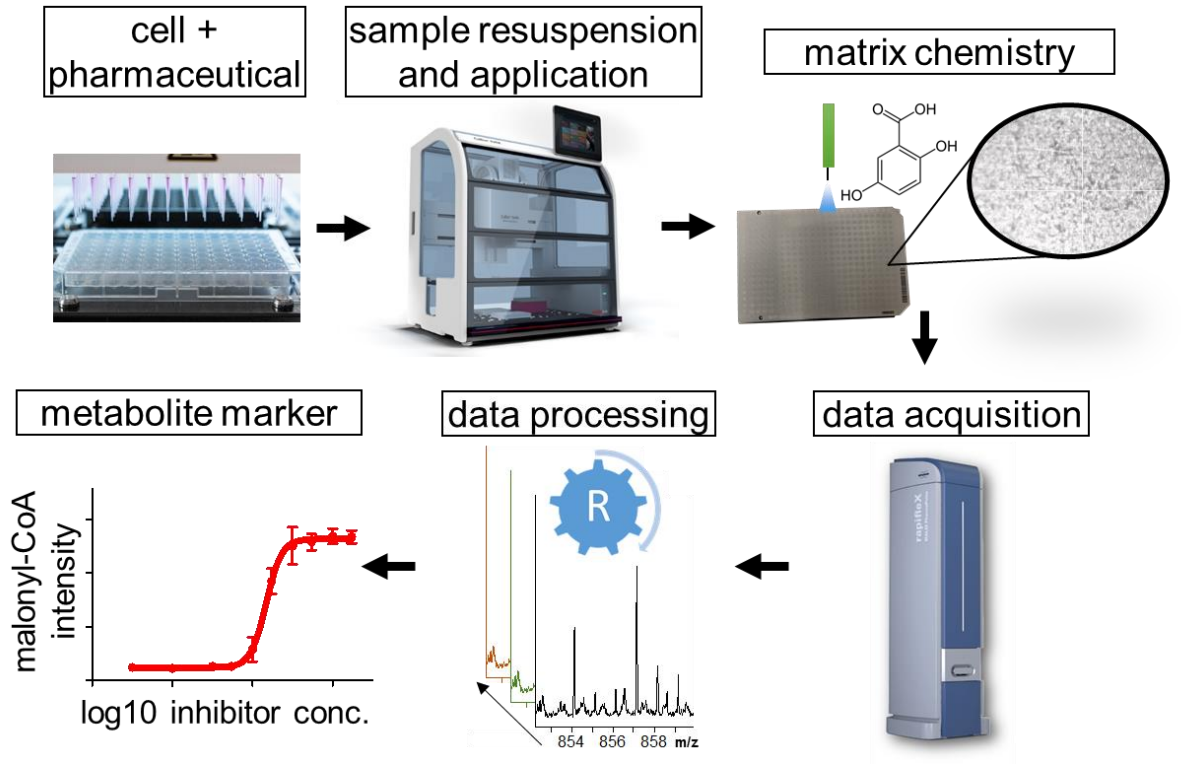

Figure 4.3.10: Automated FASN assay workflow. K562 cells were seeded in the wells of a 96-well plate and treated with inhibitors. 24 h after inhibitor treatment culture-plates are centrifuged and culture supernatants are removed. Culture plates are snap-frozen. The CyBio FeliX pipetting platform is used to resuspend cell pellets in acetonitrile/H_2O (1/1) supplemented with 5 µM malonyl-$^{13}C_3$-CoA and to apply the suspensions to a 384-well MALDI target plate. Sample spots were spray coated with DHB matrix (20 mg/ml in acetonitrile/H_2O/TFA (50/50/2.5)) using a HTX spray device. Sample spots are automatically analyzed using a rapifleX MALDI-TOF MS. Data processing and malonyl-CoA feature extraction is performed in R.

treatment by centrifuging the culture-plates and aspirating the supernatants. Dry culture plates were snap-frozen.

24 h inhibitor incubation period corresponded to approximately one doubling cycle of the K562 cells resulting in 200,000 cells/well. To remain the established 5,000 cells per measuring spot, cells were resuspended in 40 µl solvent, of which 1 µl was applied to the MALDI target. As well as the cell number, the previously established solvent, 50 % acetonitrile in water supplemented with 5 µM malonyl-$^{13}C_3$-CoA, was kept. Several aspects were of importance for the implementation of the CyBio FeliX. On the one hand, sample resuspension was not sufficiently obtained solely by up and down pipetting of the solvent. Sample resuspension was improved by shaking 96-well culture-plates for 3 seconds at 2000 rpm using the instrument's thermal mixer, BioShake. Moreover, the gas phase above the liquid in the pipetting tips was saturated by introducing a 5 s pause upon sample aspiration, which reduced the proportion of either dispersed or empty sample spots to less than 1 % in three independent preparations. A hypothetically critical aspect is the difference in viscosity of the pure solvent used for sample resuspension compared to the resuspended cell pellet. Greater losses of cellular material caused by either highly toxic compounds or inaccuracies in the sample processing might increase the proportion of dispersing sample spots. Additionally, the FeliX CyBio does not fully eject the liquid remaining in the pipette tips. This might lead to a contamination of the instrument's pistons in a sequence of several pipetting steps. To omit this scenario, 10 µl air were aspirated prior to each pipetting step.

Application of samples in 96-well format to a 384-well MALDI target plate enabled to apply four technical replicates of each sample. The sample spots were equally dispersed across the whole target plate (**Fig. 4.3.11 A**). A HTX spray device was employed to spray-coat the dried sample spots, since the instrument has a superior design to spray whole MALDI target plates compared to the SunCollect sprayer. A heated spray nozzle enabled matrix application at a higher flow rate, obtaining a homogenously coated target plate (**Fig. 4.3.11 B**). The previously established autoExecute function on the rapifleX MS was employed to analyze the sample spots.

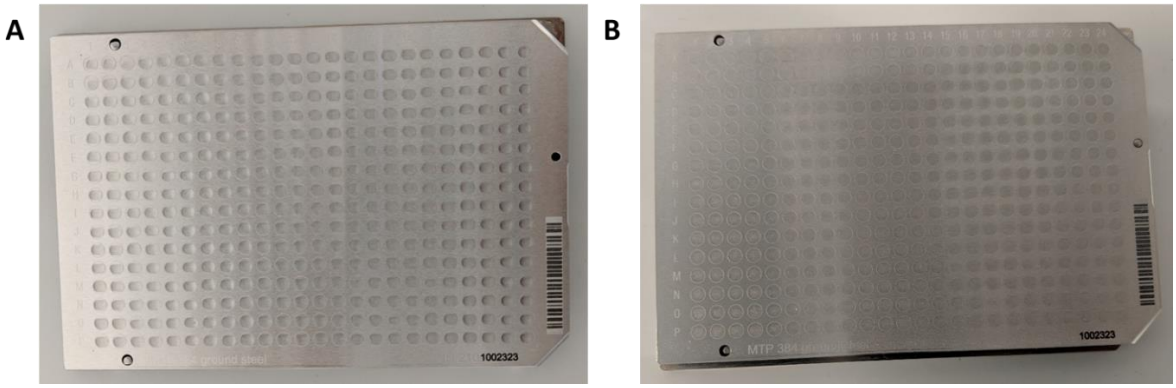

Figure 4.3.11: Automation retains homogenous application of sample spots and MALDI matrix to a ground steel target plate. (A,B) The following liquid handling steps were performed using the CyBio FeliX pipetting platform: A 96-well plate containing 200,000 K562 cells per well were resuspended in 40 µl acetonitrile/H_2O (1/1) supplemented with 5 µM malonyl-$^{13}C_3$-CoA. 1 µl per measuring spot of the suspension were applied to a 384-well ground steel MTP in 4-fold replicates (A). The target plate was spray-coated with DHB matrix (20 mg/ml in acetonitrile/H_2O/TFA (50/50/2.5)) using a HTX sprayer (B).

The automated workflow was applied to repeat the potency evaluation of the inhibitors BI 99179, GSK2194069, orlistat and BI 99990. Additionally, the compound triclosan was included for the study. Triclosan has been described to display a superior cytotoxic profile compared to the FASN inhibitors Orlistat and C75 [143]. A trend that triclosan might expose a superior cytotoxicity compared to orlistat in K562 cells was observed in an MTT assay (**Fig. 4.3.12**).

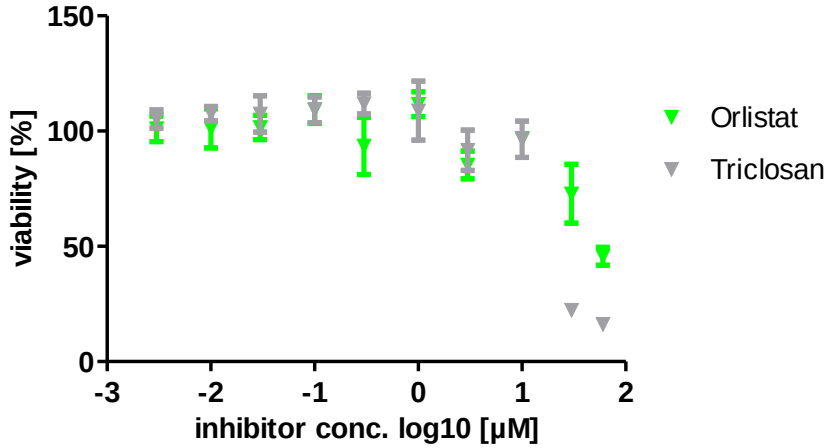

Figure 4.3.12: Viability of inhibitor-treated K562 cells. K562 cells were treated with various concentrations of Orlistat (green) and Triclosan (grey) for 24 h prior to viability determination by MTT assay (mean ± standard deviation for n = 3 technical replicates).

The automated MALDI MS FASN assay revealed that malonyl-CoA accumulation induced by GSK2194069 and BI 99179 is comparable when the inhibitor treatments were performed in the same cell culture batch (**Fig. 4.3.13 A**). Potency evaluation of the inhibitors revealed that comparable pIC50 values were obtained by the manual and the automated workflow (**Fig. 4.3.13 B**). Additionally, the error of the pIC50 value determination is comparable for both workflows with a standard deviation in the range of 0.1 – 0.2. Interestingly, no response was observed for triclosan. Previous biochemical, *in vitro* studies suggested that triclosan inhibits the ER-domain of the FASN [144]. Moreover, cell-based studies found that triclosan affects lipid content and lipid enzyme expression [143]. However, no study proved target engagement of triclosan in a cell-based context. This point is addressed with more detail in the discussion section of this thesis.

A further step of assay standardization included the determination of appropriate controls to judge whether the response of the assay is large enough. DMSO-treated K562 cells were chosen as negative control. The ideal positive control would induce highest malonyl-CoA accumulation with minimal cytotoxic effects. The best available positive control constituted 0.3 µM BI 99179 or 1 µM GSK2194069 treated K562 cells, a treatment with a low concentration of a potent compound that induces malonyl-CoA accumulation in its plateau-phase. For this thesis, the GSK compound was chosen, since it is commercially available. Signal intensities of three replicate measurements of negative and positive control were used for Z-factor calculation. The Z-factor was calculated according to the equation:

$$Z - factor = 1 - \frac{3 \bullet \mathrm{SD}_{NegativeControl} + 3 \bullet SD_{PosiiveControl}}{\left|\mu_{NegativeControl} - \mu_{PositiveControl}\right|}$$

where SD is the standard deviation and µ are the means of the normalized readout, i.e. malonyl-CoA signal intensity. The obtained Z-factor was 0.61 ± 0.06 (mean ± SD for n = 3 independent preparations (0.54/0.65/0.65)), which is considered an excellent assay related to screening [145].

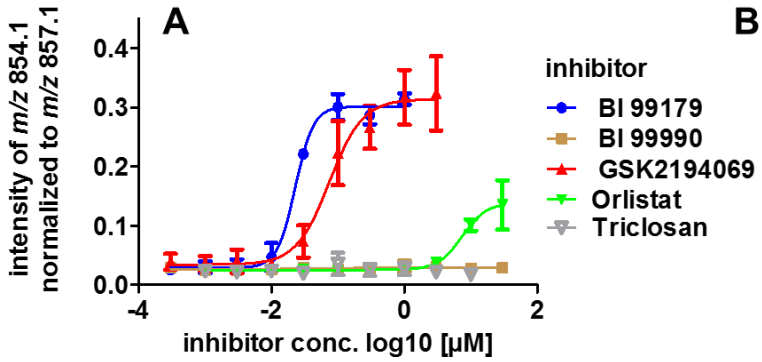

inhibitor	pIC_{50} *m/z - 854.1 normalized to m/z - 857.1*
BI 99179	7.6 ± 0.1
GSK2194069	7.1 ± 0.2
Orlistat	< 5.5
BI 99990	< 4.5
Triclosan	n.c.

Figure 4.3.13: Automated FASN assay enables reproducible potency evaluation of different FASN inhibitors. K562 cells were seeded in assay medium in 96-well plates and incubated with various concentrations of BI 99179, GSK2194069, orlistat, triclosan and BI 99990 for 24 h. All inhibitor treatments were performed in the same cell batch. Cell pellets were resuspended in acetonitrile/H_2O (1/1) supplemented with 5 µM malonyl-$^{13}C_3$-CoA and applied to a 384-well MTP using the CyBio FeliX pipetting platform. The target plate was spray-coated with DHB matrix (20 mg/ml in acetonitrile/H_2O/TFA (50/50/2.5)) using an HTX sprayer. Samples were analyzed using a rapifleX MALDI-TOF mass spectrometer. Data extraction was performed in R. A) Inhibitor concentrations were plotted against the endogenous malonyl-CoA signal normalized to the internal standard. B) pIC50 values were calculated from non-linear fittings to concentration response curves (mean ± standard deviation for n = 4 biological replicates with 4 technical replicates each prepared in different weeks, n.c. - not computable).

The saving of time during sample preparation for the automated workflow is enormous. Resuspension of 96 samples and application to a 384-well plate (4-fold replicates) takes less than 1 minute, whereas manual resuspension of 42 samples and application to a 384-well plate (9-fold replicates) takes an experienced PhD student more than 1 hour. Additionally the automated workflow reduces the amount of required solvents and consumables. The amount of required assay medium per data point, i.e. treatment condition, is reduced by a factor 5. The use of one 96 plate for cultivation and cell harvest replaces four 24-well plates for cultivation and 96 Eppendorf tubes for cell harvest.

4.3.4 CDP-CHOLINE AS A MARKER FOR LIPID PATHWAY INHIBITION

The next step, aimed at extracting additional information from MALDI full scan mass spectra to further elucidate drug-action of the tested inhibitors. MALDI-TOF MS data of samples treated for 48 h with the confirmed FASN-inhibitors BI 99179, GSK2194069 and orlistat revealed an additional drug response signal at *m/z* 511.1, which appeared most prominently when samples

were spray-coated with a less acidic matrix solution. The signal clearly followed a concentration-dependent response (**Fig. 4.3.14 A**).

A sum formula generated by MALDI-FTICR remeasurements gave evidence that the main underlying molecular species might be the sodium adduct of CDP-choline ($C_{14}H_{26}N_4O_{11}P_2 + Na^+$, *m/z* 511.0966, mass accuracy > 0.02 ppm, **Fig. 4.3.14 B**). This signal displayed a huge dynamic range in FTICR data. FTICR remeasurements also revealed two signals at *m/z* 511.0755 and *m/z* 511.1145 in close proximity to CDP-choline, which were not resolved in lower resolution TOF-MS measurements.

Due to the high abundance of the CDP-choline signal, the mass feature was isolated using the quadrupole of the solariX FTICR and subjected to fragmentation. These MS/MS remeasurements enabled assignment of several CDP-choline specific fragments, including fragments corresponding to the formation of the cyclophosphane ring, loss of the CDP-residue and breakage of the reactive pyrophosphate bond **(Fig. 4.3.14 C)**. Due to the low abundance of the features at *m/z* 511.0755 and *m/z* 511.1145 structural elucidation was not feasible. The feature at *m/z* – 511.0755 may presumably be a derivate of CDP-choline, since the mass corresponds well to the potassium adduct of CDP-choline upon loss of a hydroxyl moiety ($C_{14}H_{27}N_4O_{10}P_2 + K^+$, mass accuracy > 0.02 ppm). The identity of *m/z* 511.1145 is presently unknown. The presence of these features is the reason why relative quantification of CDP-choline is advised to be performed using MALDI-FTICR MS.

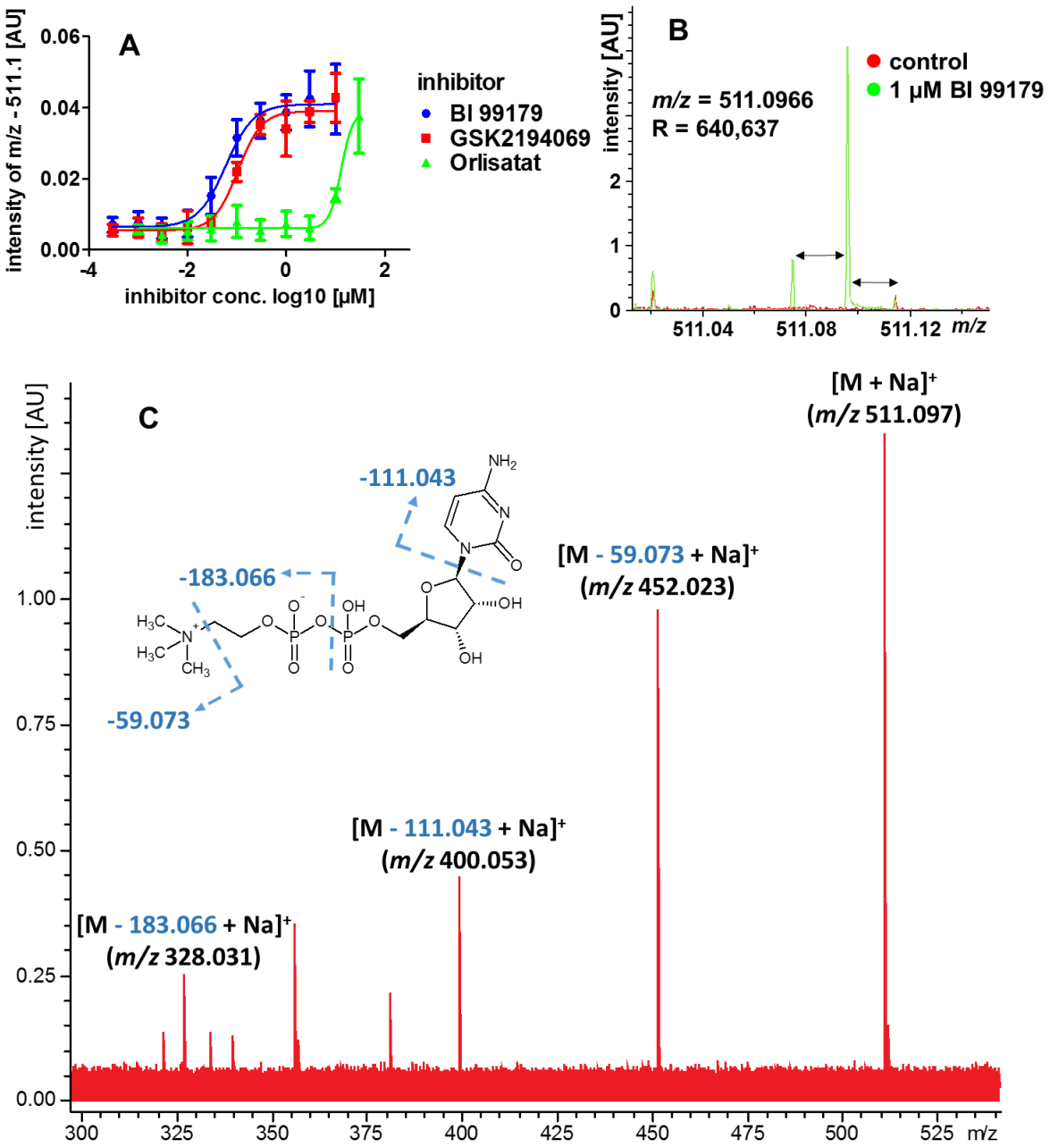

Figure 4.3.14: FASN inhibitors induce CDP-choline accumulation. A) K562 cells were treated with various concentrations of BI 99179, GSK2194069 and Orlistat for 48 h. Cell pellets were resuspended in acetonitrile/H_2O (1/1) and applied to a 384-well MALDI target plate using a CyBio FeliX pipetting platform. The target plate was spray-coated with DHB matrix (20 mg/ml in acetonitrile/H_2O/TFA (50/50/0.5)). Samples were analyzed using a rapifleX MALDI-TOF mass spectrometer. Inhibitor concentrations were plotted against the signal at *m/z* 511.1 (mean ± standard deviation for n = 4 biological replicates with 4 technical replicates each prepared in different weeks). B) FTICR mass spectra of 1 µM BI 99179 (green) and control-treated (red) K562 cells reveal the presence of mass features that interfere with low resolution TOF-MS measurements. C) A sample spot containing 1 µM BI 99179 treated K562 cells exposed highest feature intensity of *m/z* 511.1 and was used for FTICR MS/MS remeasurements.

The link between CDP-choline accumulation and FASN inhibition was found in the literature. The enzyme CDP-choline phosphotransferase (CPT) catalyzes the final step of phosphatidylcholine synthesis using diacylglycerol (DAG) and CDP-choline as its substrates (**Fig. 4.3.15,** [146]). Inhibition of fatty acid synthesis at any step in the pathway causes decreased levels of DAG, resulting in an accumulation of not converted CDP-choline. Therefore, CDP-choline constitutes an interesting phenotypic marker for lipid pathway inhibition in K562 cells rather than a mechanistic target-specific marker.

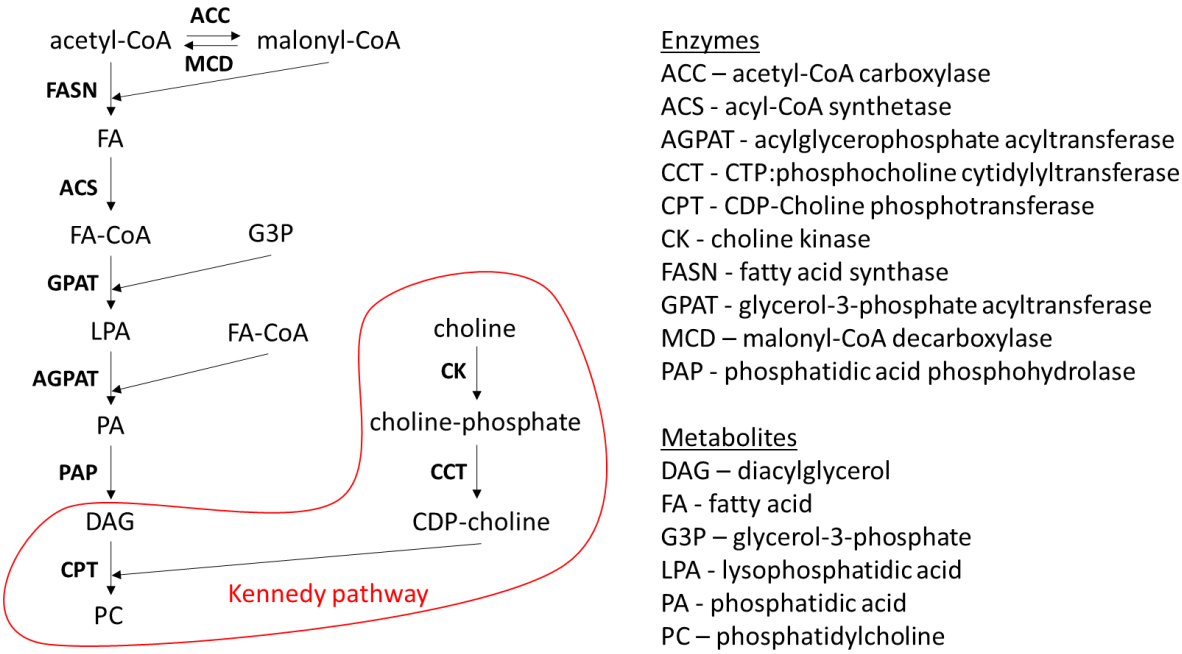

Figure 4.3.15: Membrane lipid synthesis and the Kennedy pathway. Lipid synthesis and the Kennedy pathway are brought together by the CDP-choline phosphotransferase (CPT). The enzyme catalyzes the reaction of diacylglycerol (DAG) and CDP-choline to phosphatidylcholine (PC). DAG is formed from acetyl-CoA by the successive action of acetyl-CoA carboxylase (ACC), fatty acid synthase (FASN), acyl-CoA synthetase (ACS), glycerol-3-phosphate acyltransferase (GPAT), acylglycerophosphate acyltransferase (AGPAT) and phosphatidic acid phosphohydrolase (PAP). CDP-choline is formed from choline by successive action of choline kinase (CK) and CTP:phosphocholine cytidylyltransferase (CCT).

CDP-choline accumulation is an interesting marker to provide additional evidence that the FASN-reaction was indeed inhibited. A conceivable counterargument might be that malonyl-CoA accumulation was observed due to an induced overproduction of malonyl-CoA. However, CDP-choline accumulation gives further evidence that the target was indeed the lipid synthesis. Therefore, all compounds that were previously examined for malonyl-CoA accumulation were re-evaluated. Moreover, the fact that DAG is not the direct product of the

FASN reaction gave rise to the hypothesis that CDP-choline accumulation might also be caused by other inhibitors of the lipid synthesis pathway. Therefore, the rather specific acetyl-CoA carboxylase (ACC) inhibitor 5-(tetradecyloxy)-2-furoic acid (TOFA) [147] was tested in addition to the previously tested inhibitors.

CDP-choline accumulation was observed not only for the FASN inhibitors BI 99179, GSK2194069 and orlistat but also for the acetyl-CoA carboxylase inhibitor TOFA, another inhibitor of the lipid synthesis pathway (**Fig 4.3.16**). A trend of CDP-choline accumulation was also observed for triclosan, but it consistently occurred at concentrations where the cellular viability was below 50 %.

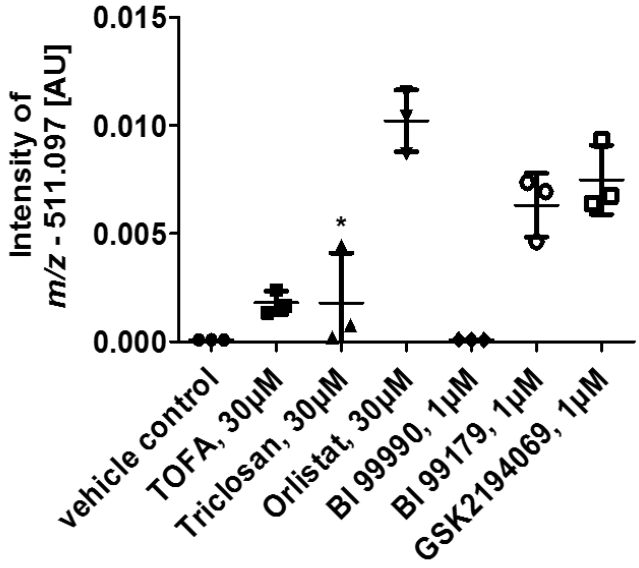

Figure 4.3.16: Inhibition of lipid synthesis causes CDP-choline accumulation. K562 cells were treated with 30 µM of TOFA, triclosan and orlistat as well as 1 µM of BI 99990, BI 99179 and GSK2194069 and analyzed using a solariX MALDI-FTICR mass spectrometer. Treatment conditions were plotted against the intensity of the signal at *m/z* 511.097 (mean ± standard deviation for n = 3 biological replicates prepared in different weeks, asterisk indicates that cellular viability was below 50 %).

With the combined detection of malonyl-CoA and CDP-choline the developed assay constitutes a relevant example for the diversity of the metabolite-based MALDI MS cell assay readouts. On the one hand, the malonyl-CoA signal provides mechanistic information on the drug action while CDP-choline is a rather phenotypic marker for drug action.

4.3.5 ADAPTATION OF THE DEVELOPED MECHANISTIC FASN ASSAY FOR A549 CELLS

Over the past years, the discovery of potent FASN-inhibitors has been a relevant research topic in the pharmaceutical industry [148]. Since CML and, hence, K562 cells are not relevant for FASN inhibitor discovery, which rather targets solid tumors, the automated FASN assay was implemented for the adherent lung cancer A549 cell line as well.

Since the A549 cell line is an adherently growing cell line, minor modifications were implemented in the automated workflow: Cell detachment was achieved by snap-freezing the 96-well “culture plates” and vigorous vortexing during sample resuspension. These two steps were already implemented for the K562 cell-based assay. However, A549 cells could not be seeded at similar cell numbers as the K562 cells. If A549 cells were seeded at 0.25 x 10^6 cells/ml, they were already confluent on the day of inhibitor treatment and overly confluent upon cell harvest. The seeding volume of 200 µl/well was not reduced on purpose to keep the concentration of the vehicle, DMSO, as low as possible. Therefore, the seeding density was reduced to 0.1 x 10^6 cells/ml. This measure resulted in a lower amount of cellular material per measuring spot and a hardly acceptable Z-factor of 0.06. This effect was counteracted by the application of 2 µl sample per measuring spot which drastically improved the Z-factor to 0.58.

The developed FASN assays for K562 and A549 cells were used for a compound profiling in parallel. The less specific FASN-inhibitor C75 [149] and G 28UCM [150] were included to assess whether the mechanistic FASN cell assay uncovered these kinds of inhibitors as well. Moreover, we decided to include the previously tested inhibitor GSK2194069 as quality measure whether the assay performed well and the previously determined pIC50 value was reproduced. We also decided to test the previously published inhibitor GSK837149A which was published as a potent inhibitor of the purified human FASN with impaired cellular permeability [73].

All inhibitors were evaluated in three biological replicates (**Fig. 4.3.17**). The pIC50 value of 7.1 for GSK2194069 previously determined in K562 cells was accurately reproduced (**Fig. 4.3.17 A**). The Z-factors of the assay performed in K562 cells (Z-factor = 0.56, 0.82, 0.41) were lower than for the previous set of experiments but still in an acceptable range. Z-factors determined in A549 cells (Z-factor = 0.85, 0.65, 082) were excellent, suggesting a reliable evaluation of the compounds (**Fig. 4.3.17 B**).

For GSK837149A no FASN inhibition was observed, supporting the hypothesis that this compound was not membrane permeable and displayed no cellular activity despite its high potency in a biochemical enzyme assay (pIC50 = 7.8 [73]). For C75 and G 28UCM no pIC50 values were determinable in either of the tested cell lines. The presumably low cellular potency

and selectivity of these inhibitors may require an evaluation using different inhibitor concentrations and incubation times. Interestingly, the pIC50 values for GSK2194069 determined in K562 cells (pIC50 = 7.1 ± 0.1) were slightly higher in A549 cells (pIC50 = 7.5 ± 0.1), indicating a stronger response of the A549 cells. The underlying reason can only be hypothesized and will be addressed in more detail in the discussion section. Finally, the aim was to confirm that the increased malonyl-CoA levels indeed originate from an increased inhibition of the FASN and consequently an inhibition of lipid synthesis. Therefore, accumulation of the previously established marker for lipid pathway inhibition, CDP-choline, was measured using a MALDI-FTICR MS (**Fig. 4.3.17 C, D**). CDP-choline accumulation was confirmed in both cell lines for GSK2194069.

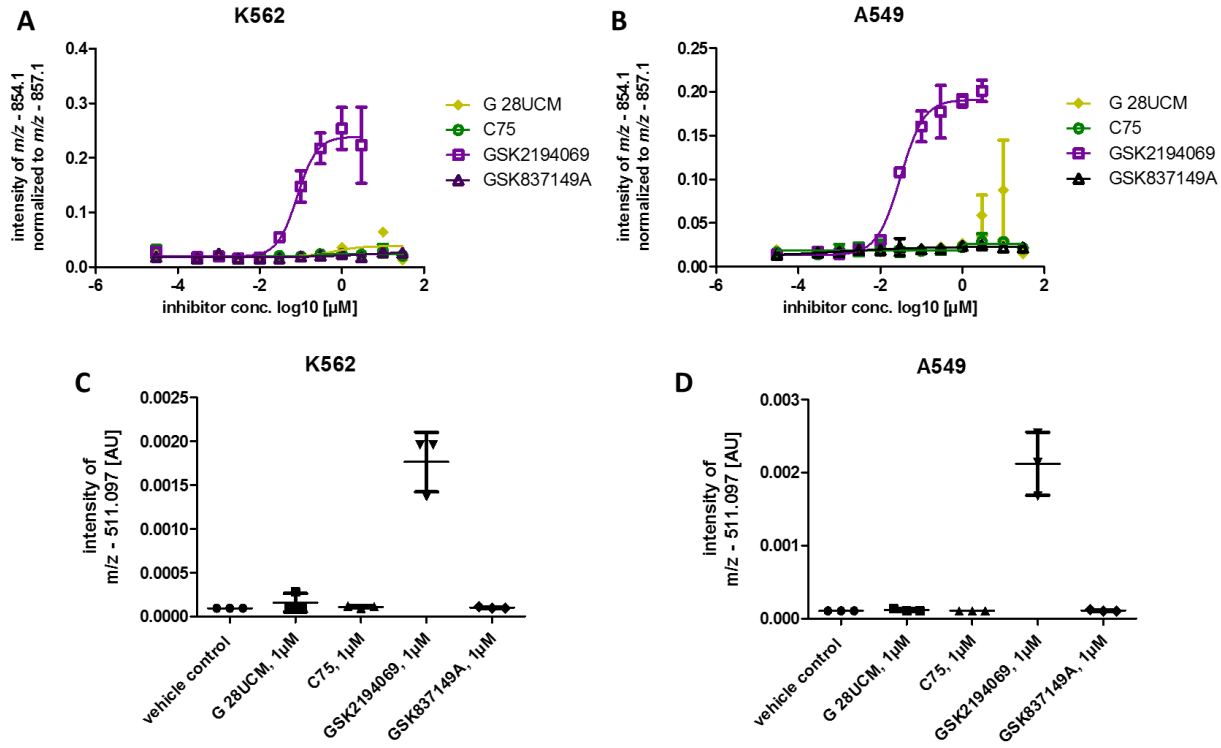

Figure 4.3.17: Transferability of mechanistic cell assay from K562 cells to adherently growing A549 cells. K562 (A) and A549 cells (B) cells were seeded in assay medium in 96-well plates and incubated with various concentrations of G 28UCM, C75, GSK2194069 and GSK837149A for 24 h. Cell pellets were supplemented with 5 µM malonyl-$^{13}C_3$-CoA and applied to a 384-well MTP using the CyBio FeliX pipetting platform. The target plate was spray-coated with DHB matrix (20 mg/ml in acetonitrile/H_2O/TFA (50/50/2.5)) using an HTX sprayer. Samples were analyzed using a rapifleX MALDI-TOF mass spectrometer. Data extraction was performed in R. Inhibitor concentrations were plotted against the endogenous malonyl-CoA signal normalized to the internal standard (mean ± standard deviation for n = 3 biological replicates with 4 technical replicates each prepared on different days). C,D) Sample spots containing 1 µM inhibitor treated K562 cells (C) and A549 cells (D) were spray-coated with DHB matrix (20 mg/ml in acetonitrile/H_2O/TFA (50/50/0.5)) and remeasured using a solariX MALDI-FTICR mass spectrometer. Treatment conditions were plotted against the intensity of the CDP-choline signal (mean ± standard deviation for n = 3 technical replicates).

5 DISCUSSION

5.1 A METABOLITE-BASED IC-MALDI MS FINGERPRINTING WORKFLOW

AlMasoud *et al.* described that the establishment of a new MALDI MS method including the evaluation of matrices, solvent additives and application methods, requires the performance of several thousands of experiments, which they could reduce to several hundred key experiments by fractional factorial design [46]. The remaining several hundreds of experiments still constitute a considerable expenditure of resources, which in this thesis was omitted by adapting and prospering from MALDI sample preparation methods described in the literature. Three cancer cell lines were prepared according to multiple preparation protocols. Score-based method evaluation was performed to develop a reproducible and sensitive IC-MALDI MS fingerprinting workflow.

The discipline of metabolite-based MALDI MS cell assays is still in its infancy. Prior to the publication of this work, three publications outlined in the introduction described preparation protocols for whole cell lipid measurements by MALDI MS [31, 33, 34]. Both Angelini *et al.* as well as Lobasso *et al.* used 9-amino acridine (9-AA) as a vacuum stable matrix, suitable for IC-MALDI MS measurements, enabling the detection of multiple negatively charged lipid classes. Since 9-AA is a DNA-intercalating ligand, which is known to cause mutations [151], the use of 9-AA is often not a viable option. Especially the aim for larger scale sample preparations and matrix application using spray devices affirmed the search for alternative matrix preparation protocols. Sakai et al, relied on the use of 2,6 dihydroxyacetophenone (DHAP). DHAP is a non-vacuum stable matrix [152]. DHAP might be suited for the analysis of relatively small sample sizes, as in the study done by Sakai *et al.* for the analysis of single concentration and single drug treatment or for MALDI instruments with atmospheric pressure ion sources. The aim to develop a workflow applicable for the analysis in 384-well format required a more vacuum stable matrix. 6-aza-2- thiothymine (ATT) has been described as a superior matrix for the detection of glycosphingolipid species in lipid extracts [38]. The ATT matrix also revealed good results for the discrimination of three cancer cell lines as evaluated by $J_{overlap}$ score. However, DHB matrix was chosen as the preferred matrix as elaborated by $J_{overlap}$ and MSE_{mod} scores.

MALDI MS imaging (MSI) is a rapidly growing technology [153], which is mostly applied for the analysis of tissue sections in a clinical or pharmacological context. The discipline's increased awareness for a need of standardization [47] and improved sensitivity [154] provided valuable

ideas that were repeatedly tested for implementability into a MALDI MS fingerprinting workflow during the course of this thesis. The use of a matrix sprayer, which is used to coat tissue sections with matrix for MSI experiments, worked well for the coating of ground steel MALDI target plates and led to the formation of homogenously distributed matrix and analyte signals. The adaptation of the scores $J_{overlap}$ [47] and *MSE* [49] which also were first described in publications related to MS imaging were swiftly implemented and highly valuable for a standardized method development. An approach to monitor reproducible matrix application by digital microscopy was presented. Future developments, ideally of the development of a pattern recognizing software, are going to be required to standardize this quality measure.

The biologic starting material for method development were harvested cell pellets of three cancer cell lines, including the gastrointestinal stroma tumor cell line GIST T1 and the two leukemia cell lines K562 and HL60. With the aim to develop a method that reproducibly detects as many metabolites as possible from these specimens, $J_{overlap}$ and MSE_{mod} optimization was performed. Gastrointestinal tumor cells and leukemia cells are expected to expose striking metabolic differences. However, these differences were diminished and altered by cultivation in cell culture media mainly supplemented with FCS. Previous work showed that cultivating the gastrointestinal cell line SGC7901 in both RPMI1640 and DMEM already caused distinct changes of the metabolome [155]. Moreover, an additional study reported that cultivation of cells in a developed human plasma like medium caused widespread changes in the metabolome compared to cultivation in traditional medium [124]. The authors reference to multiple studies that describe the influence of environmental metabolites on the cellular metabolome. In summary, these results suggest that a more pronounced separation in PCA space is expected if, for example, primary gastrointestinal and primary blood cells are subjected to the developed fingerprinting workflow.

Furthermore, the developed method had a strong focus on an exploratory metabolome analysis and therefore was of interest for the discovery of unknown response markers. A contrasting example constitutes the development of an assay to monitor the inhibition of the fatty acid synthase, which required malonyl-CoA as its readout. In this scenario, a method that detects as many metabolites as possible, but only poorly detects malonyl-CoA would not be conducive. Therefore, it is important to note that while the chosen method development approach was relevant for exploratory metabolome analysis. Analysis with a different scientific expectation might require a different method development approach, e.g. the employment of a commercially available standard for targeted measurements. Moreover, the condition of the MALDI instrument, including system purity and laser fluence have been described to cause differences in the acquired mass spectra [156], which aggravates the reproducible acquisition of mass spectra. Especially the chosen laser fluence affects the full scan mass spectrum,

shifting signals of intact analytes to signals of fragmented analytes at high laser fluence [136], which again highlights the need for internal standards in targeted MALDI MS measurements.

Direct infusion ESI MS experiments have been described to detect 4720 *m/z* features which were annotated to 962 metabolites by matching the accurate mass [157]. The focus of this thesis was not a comprehensive identification of all observed *m/z* features. A typical MALDI-FTICR spectrum of K562 cells contained 10,000 *m/z* features (4 M AMP transient, *m/z* 150 – 5,000) of which 15 metabolites were annotated by matching the accurate mass. Moreover, 4 metabolites were confirmed by FTICR MS/MS remeasurements. Further studies are required to assess to which extend the entirety of features observed in a full-scan FTICR spectrum covers the human metabolome. Since all MS analyses for this thesis were conducted in positive ion mode, metabolite coverage might be increased by implementing novel matrices described for negative ion mode [158, 159] or the use of dual polarity matrices that have been described for both positive and negative ion mode [160]. Additionally, optimized sensitivity harbors the potential to broaden the coverage of detected metabolites. Even though MALDI MS has been described as a rather impurity tolerant method [8], highest sample purity would be required for maximum sensitivity [161].

A central challenge during the development of a metabolite-based MALDI-fingerprinting workflow was the presence of interfering matrix ions as elaborated by MSE_{mod} scores. Besides alternative surface ionization technologies like desorption electrospray ionization mass spectrometry (DESI) and secondary ion mass spectrometry (SIMS), which follow a different ionization mechanism, alternative energy absorbing materials to reduce the matrix background are being developed. Carbon nanotubes have been found to transfer energy upon laser irradiation and to eliminate interfering matrix ions [162]. Oxidation of these carbon nanotubes has been described to further advance desorption / ionization of an amino acid mixture. Moreover, the oxidized carbon nanotubes exposed greater solubility in aqueous solutions [163]. Also other nanomaterials like silica beads and fullerenes [164] as well as surfaces coated with inorganic particles like gold, iron, titanium oxide or zinc oxide have been described as substitutes for established MALDI matrices [165]. In light of this great variety, it remains to be elucidated which of these emerging technologies will prevail. Conceivable is also a combination of surface coating and MALDI matrices, to further enhance sensitivity. A former high throughput biochemical HDAC assay made use of gold-coated surfaces in combination with MALDI mass spectrometry. The enzyme substrate was immobilized to the gold particles via a thiolate bond enabling on target washing and efficient desorption upon laser irradiation [166].

Spray-coating of DHB matrix was chosen since matrix applied as a liquid droplet formed crystals at its outer ring; a phenomenon commonly known as the coffee stain effect. The coffee

stain can also be prevented by electrowetting where an electric field generates an internal flow that counteracts the evaporation-driven flow and depins analytes from the outer contact line of the droplet. Kudina *et al.* published that an electrowetting MALDI approach enabled 2-30 fold enhanced MALDI MS signals [41]. Currently no electrowetting MALDI capable and Bruker instrument compatible MALDI target plates are available and might thus be an interesting approach for future experiments. Moreover, addition of benzoic acid has been observed to lead to a homogenous matrix crystallization without the need for a matrix sprayer. However, similar to the published DHAP matrix, the benzoic acid approach was not further pursued since benzoic acid is not vacuum stable and therefore not applicable for time consuming analysis in 384-well format. Technological advances in data recording and data processing enable a faster sample readout. As described in the introduction section technological advances go hand in hand with advances in the development of novel assays and might therefore empower reevaluation of previously declined approaches.

5.2 The phenotypic BCR-Abl tyrosine kinase inhibition assay – an example of phenotypic drug discovery by MALDI MS?

The developed fingerprinting workflow was applied to monitor drug action of tyrosine kinase inhibitors in K562 cells in 384-well format. An automated data processing pipeline was developed to extract concentration response marker molecules. The putative marker molecules were structurally elucidated by high resolution MALDI-FTICR MS/MS.

The two features, heme B and PC(36:1) + K^+ were identified as ascending and descending concentration response marker molecules respectively. The induction of heme B was hypothesized to originate from erythropoiesis of K562 cells. Heme B is the prosthetic group of hemoglobin [167]. Hemoglobin synthesis has previously been linked to erythropoiesis in K562 cells [168]. In previous publications erythropoiesis was monitored by heme or hemoglobin detection using a specific reaction with benzidine / hydrogen peroxide solution [169]. Intracellular heme concentrations are tightly regulated due to the toxicity of free heme [170]. Hietakangas *et al.* reported that K562 cells lost resistance to TNFα induced apoptosis upon erythroid differentiation [171]. In contrast, Bonovolias *et al.* concluded that erythroid differentiation protects K562 cells from imatinib induced cell killing [172]. The antithetical study outcomes indicate that the differentiation state determines the sensitivity to different antiproliferative agents.

The reason why the most pronounced decrease was observed for PC(36:1) + K^+ of all features is likely linked to cell death. Cristea *et al.* previously described that cell death is accompanied by the expression of lipid degrading enzymes [131]. However, the spectra of imatinib treated K562 cells contain multiple lipid signals, most of which show no or no response comparable to PC(36:1) + K^+. The protonated adduct and the sodiated adduct of PC(36:1) were also observed but do not show a decrease of signal intensity comparable to the potassiated adduct. Another lipid that also showed a prominent decrease was the potassium adduct of PC(34:1). Wang *et al.* described that apoptotic events impair Na^+/K^+ ATPase activity [132]. This might cause a loss of intracellular potassium, leading to a significantly reduced amount of K^+ adduct formations during the MALDI process. It still remains to be elucidated if all isomeric species of PC(36:1) + K^+ are equally affected by the decrease. The answer of this question would require the implementation of novel analytical techniques like ion mobility. Future work might for example involve Bruker's trapped ion mobility MS (TIMS) TOF, which may enable separation of the isomeric lipid species 18:1 (Δ-9) PC and 18:1 (Δ-6) PC[11].

Breitkopf *et al.* performed a triomics study, which included metabolomic, lipidomic and phopsphoproteomic analysis on imatinib treated myeloma cells [102]. The authors observed a reduction of lipid biosynthesis and incorporation of fatty acids into lysophospholipids as well as upregulation of some phosphatidylethanolamine species. Metabolomic analysis revealed that few metabolite levels were significantly affected. The most striking increase was observed for precursors of the nucleotide synthesis whereas acetyl-CoA and NADPH levels were decreased. Moreover, in a more recent study Noel *et al.* compared the metabolome of wild type and imatinib resistant K562 cells [173]. The authors correlated increased levels of glycolytic intermediates including glucose 6-phosphate, fructose 6-phosphate and fructose 1,6-bisphosphate to an increased imatinib resistance. These results highlight negatively charged ions like phospatidylethanolamines, metabolites of the glycolysis and nucleotide precursors as putative marker molecules. In summary, MALDI MS cell-based assays harbor a broad range of target molecules as phenotypic concentration response markers.

The observed lipid marker molecules are a very indirect readout for BCR-Abl inhibition. A direct link between lipid synthesis and BCR-Abl signaling was provided by Burns *et al.* [174]. The authors observed an increased expression of the sphingomyelin synthase (SMS) in K562 cells. Since SMS knock down by siRNA inhibited the proliferation of BCR-Abl positive cells, they concluded that SMS is a downstream target of BCR-Abl. A similar study would not be feasible for PC synthesis since PCs are an essential component of the plasma membrane [175]. From a signaling pathway perspective, the primary pathways affected by BCR-Abl inhibition are the

[11] Meyer SW, Sander P, Michalski A, Suckau D Poster Note PN-31 High resolution trapped ion mobility mass spectrometry for analysis of isomeric compounds

(Pi3K)/AKT, the RAS and the MEK pathway as reviewed by Cilloni *et al.* [176]. The inhibition of survival promoting factors, like AKT, leads to a reduced phosphorylation of key apoptosis-regulatory proteins and thus activates the signaling cascade towards cell death [177]. At the end of a cascade involving death receptor activation, formation of a death inducing signaling complex and recruitment of caspases occurs the observed degradation of membrane lipids, accompanied by DNA fragmentation and other biochemical changes [176]. The multitude of involved enzyme cascades highlights that the observed treatment effect is highly indirect. Therefore, the observed markers can be considered as phenotypic markers.

Phenotypic drug discovery has strongly contributed to drug discovery in previous years [60]. The prerequisite for a phenotypic assay is the identification of an appropriate phenotypic readout. This thesis presents an exemplary workflow how MALDI MS can discover novel phenotypic markers in a cell-based assay. Therefore, the workflow rises expectations to enable the extraction of phenotypic, biomolecular markers from other cellular models relevant for drug discovery, including genetically engineered cells [178], induced pluripotent cells [179] and organoid cultures [180], in a throughput oriented approach. Especially challenging is the development of test systems for neurologic diseases and heterogeneous tumors [59]. Even though MALDI MS has been established as a versatile readout for complex biological samples [181], it remains to be elucidated if MALDI MS will provide pharmacologically predictive models for these diseases.

The feasibility of metabolite-based IC-MALDI MS drug assays has not been described before [121]. Our study demonstrates that the technology has the potential to support cell-based profiling for drug discovery. Additionally, the developed workflow enabled reproducible potency evaluation of selected BCR-Abl inhibitors. The awareness for the need of a higher specificity was elaborated in this thesis and addressed with the development of a FASN assay.

5.3 The mechanistic FASN inhibition assay – a perspective in drug discovery?

During this thesis an assay to monitor the inhibition of the fatty acid synthase (FASN) directly in whole cells was developed. Further method development enabled the standardized and reproducible detection of malonyl-CoA as the readout of the assay. Exploratory analysis of full-scan spectral data enabled the identification of CDP-choline as a marker for lipid pathway inhibition.

The observation of CDP-choline was an unexpected finding during FASN-assay establishment, supporting the potential of the developed, exploratory MALDI-TOF MS

workflow. Increased CDP-choline levels were previously observed in erythrocytes. In 1983, Paglia *et al.* first described the accumulation of CDP-choline in the erythrocytes from a woman with hemolytic anemia [182]. The authors hypothesized an inherited choline phosphotransferase (CPT) deficiency. Petersen *et al.* observed CDP-choline accumulation in another case of haemolysis and could provide evidence for a CPT defect using 31P-NMR spectroscopy and enzymatic analysis [183]. Boggs *et al.* observed an inhibition of the CDP-choline pathway along with reduced choline incorporation into phospholipids upon treatment with lysophosphatidylcholine [184]. However, CDP-choline was not yet described as a marker for lipid pathway inhibition. Moreover, CDP-choline has been described to accumulate in erythrocytes. Our study on A549 cells suggests that CDP-choline also functions as a marker for lipid pathway inhibition in epithelial cells. The marker might be valuable for exploratory studies on the lipid-synthesis pathway for example as a readout for rescue assays of inhibited lipid enzymes.

Sadowski *et al.* proposed triclosan as a FASN inhibitor to target prostate cancer [143]. The authors described a superior cytotoxic profile compared to orlistat, increased expression of genes involved in fatty acid metabolism and observed an overall decrease of lipid levels upon triclosan treatment. Still sufficient proof that triclosan indeed targets the intracellular FASN was not provided. Triclosan also exposed a higher cytotoxicity compared to orlistat in our hands but no detectable malonyl-CoA accumulation. The observed CDP-choline accumulation suggests that triclosan targets one or several enzymes in the lipid synthesis pathway. Since no malonyl-CoA accumulation was observed FASN inhibition was not confirmed. Interestingly, Sadowski *et al.* observed a rescue of triclosan induced growth inhibition by addition of palmitate. This rises the hypothesis that triclosan might target a step prior to fatty acid synthesis, namely the acetyl-CoA carboxylase mediated formation of malonyl-CoA. On the other hand, the comparably simple molecular structure of triclosan might be an evidence for a rather unspecific inhibitor of the lipid pathway.

The pIC50 value determined by the response of malonyl-CoA accumulation upon FASN inhibition has been observed to increase with inhibitor incubation time. Acyl-CoA esters have been described as an allosteric inhibitor of the malonyl-CoA producing enzyme acetyl-CoA carboxylase (ACC) [185]. A lower cellular lipid content, might decrease ACC inhibition and thus further activate malonyl-CoA accumulation via a positive feedback mechanism.

Potency evaluation of various FASN inhibitors was performed both manually in 24-well format and, with support of an automated pipetting platform, in 96-well format. Comparison of the results of both potency evaluations revealed almost identical pIC50 values. When experiments were performed manually, a separate culture batch originating from a different cryo-stock was used for treatment with Boehringer Ingelheim compounds. Even though the determined pIC50

value was not affected by the use of a separate cryo-stock, results indicated a more pronounced area under the curve (AUC), i.e. malonyl-CoA accumulation, upon treatment with BI 99179 compared to GSK2194069. Repeated evaluation performed in parallel revealed a comparable malonyl-CoA accumulation for both compounds. Previous studies tested various machine learning algorithms on publically available screening datasets to build a model that predicts drug-sensitivity of cancer cell lines[12]. The factor that affected the predictive outcome the most were the molecular features provided by different laboratories followed by the choice of the algorithm. In line with these findings is a critical review of the reproducibility in high throughput cancer drug screening [186]. The authors concluded a poor intralaboratory concordance in the drug response phenotypes and referenced to two HTS studies, namely the Cancer Cell Line Encyclopedia and the Cancer Genome project. Comparison of both projects revealed similar gene-expression profiles for the tested cell lines but inconsistent drug responses. Besides differences in the sample preparation protocol and compound storage, the authors name variations in cell cycle, passage number and growth rate as factors that can affect drug responsiveness. In summary, standardization is a key factor for reproducible assay performance. This requires on the one hand to always follow the same, comprehensively logged preparation protocol. Moreover, standardization requires testing of compounds under as comparable conditions as possible. This includes compound dispensing, storage [187] and application but also treatment time point and incubation time. Despite these standardization approaches, monitoring a quality assurance factor like Z-factor is vital to warrant that the assays response was sufficient. The pIC50 value of GSK2194069 (pIC50 = 7.1 ± 0.1) was reproduced in 6 manual and 6 automated preparations of K562 cells. The mean Z-factor for 6 automated preparations (0.61 ± 0.13) with only one Z-factor below 0.5, suggests excellent overall performance of the assay.

Interestingly, the pIC50 value generated for the potency of GSK2194069 in A549 cells (pIC50 = 7.5) agrees well with the value published by GSK (pIC50 = 7.8 [109]). To determine the pIC50 value, researchers at GSK measured phosphatidylcholine levels of A549 cells upon 48 h incubation of the compound. The GSK Company had chosen inhibitor treatment conditions which were comparable to the conditions elaborated in this thesis. Therefore the accordance of the generated pIC50 values was an important validation of the developed assay. Boehringer Ingelheim's platform (www.opnMe.com) provides a pIC50 of 6.7 for the cellular FASN inhibition by BI 99179. The specified pIC50 deviates by almost one order of magnitude from the pIC50 obtained in our assay (pIC50 = 7.6). This is likely due to the fundamentally different approaches to determine cellular FASN inhibition. Scientists at Boehringer Ingelheim measured the

[12] Jang S, Neto EC, Guinney J, Friend SH, Margolin AA (2014) Systematic Assessment of Analytical Methods for Drug Sensitivity Prediction from Cancer Cell Line Data. In: Pacific Symposium on Biocomputing. pp 63–74

incorporation rate of ^{14}C-acetate into cellular lipids upon inhibitor treatment, which is a more sensitive but also an indirect readout. Moreover, inhibitor incubation was performed for only 1 h using mouse hypothalamic N-42 cells [112]. Previous experiments revealed an increase of pIC50 values with increasing inhibitor incubation time (**Fig. 4.3.5**).

For automation purposes, cells were treated in 96-well plates. Cell harvest was performed by centrifuging the culture-plates and aspirating the supernatants. Centrifugation is notoriously difficult to implement into automated assay workflows. For the purpose of establishing such a workflow, removing culture supernatants by filtration might also be considered [188].

Noteworthy the A549-based assay exposed a stronger response to the tested inhibitor, GSK2194069, compared to the K562-based assay. The underlying reason can only be hypothesized. Responses of established cancer cell lines to anti-cancer drugs have been systematically studied as part of the NIH funded LINCS program (Library of Integrated Network-Based Cellular Signatures) [189]. Multiple genotypic markers have been identified whose presence was connected with drug responsiveness. Especially responses to drugs targeting intracellular signaling kinases have been found to be cell type specific [190]. Studies indicate that both the cellular localization and activity of the FASN is regulated by phosphorylation as well as protein-protein interactions [148]. Prominent kinases that have been described to phosphorylate FASN include the human epidermal growth factor receptor 2 (Her2) [191] and a nutrition-dependent phosphorylation by the mammalian target of rapamycin (mTOR) [192]. Additionally, a study conducted with sera from patients with different tumor types and healthy controls revealed that Non-Small Cell Lung Cancer tumors are associated with especially high FASN expression levels [148]. Moreover, during the course of this thesis was observed that pIC50 values depend on the inhibitor incubation time. A similar dependency might exist for the seeding density of the respective cell line and therefore systematically shift the observed pIC50. In summary, this study highlights that a precise drug-potency determination not only depends on the cell type but also on the cellular state and chosen assay conditions, which again highlights that a high degree of standardization is vital for the reproducibility of MALDI MS cell-based assays.

5 years ago Munteanu and Hopf raised the question if MALDI MS cell assays are going to be an emerging technology for HTS [3]. Although this question still cannot be answered with certainty, there are many indications of major advances in near future which will further promote the attractiveness of the technology. Cell cultivation for the assay reported in this thesis was performed in 96-well format. Further miniaturization of the assay is absolutely conceivable, as first publications already reported the use of MALDI MS on the single cell level [193, 194]. Additionally, a strength of the developed cell-based assay compared to biochemical assays was the intrinsic validation that the compound is cell permeable. Another advance will

be the throughput-oriented screening of active ingredients in organoid cultures. Several studies already opened up possibilities for the use of organoids on a chip for drug discovery, such as 3D cultures to model the intestinal physiology [195] or blood-brain-barrier organoids to investigate the permeability of therapeutics targeting the central nervous system [196]. Due to its versatile readout, MALDI MS has also been implemented into multiplexing and array technologies. MALDI MS arrays have previously been implemented to monitor biochemical, *in vitro* assays [197] as well as for the classification of tumor sections [198]. Considerations to develop chip-based MALDI MS cell arrays would go hand in hand with the previous approach of assay-miniaturization.

Overall the results of the developed mechanistic FASN assay are encouraging and suggest that the automated workflow could be established as a routine workflow for cell drug assays. The automated workflow also is of interest from an industrial HTS perspective. Long-term evaluations are going to be required to assess instrument reliability and robustness.

6 REFERENCES

1. Yergey JA (1983) A general approach to calculating isotopic distributions for mass spectrometry. Int J Mass Spectrom Ion Phys 52:337–349 . doi: 10.1016/0020-7381(83)85053-0
2. Kind T, Fiehn O (2010) Advances in structure elucidation of small molecules using mass spectrometry. Bioanal Rev 2:23–60 . doi: 10.1007/s12566-010-0015-9
3. Munteanu B, Hopf C (2013) Emergence of whole-cell MALDI-MS biotyping for high-throughput bioanalysis of mammalian cells? Bioanalysis 5:885–93 . doi: 10.4155/bio.13.47
4. El-Aneed A, Cohen A, Banoub J (2009) Mass spectrometry, review of the basics: Electrospray, MALDI, and commonly used mass analyzers. Appl Spectrosc Rev 44:210–230 . doi: 10.1080/05704920902717872
5. Murray KK, Boyd RK, Eberlin MN, Langley GJ, Li L, Naito Y (2013) Definitions of terms relating to mass spectrometry (IUPAC Recommendations 2013). Pure Appl Chem 85:1515–1609 . doi: 10.1351/PAC-REC-06-04-06
6. G Marshall A, T Blakney G, Chen T, K Kaiser N, M McKenna A, P Rodgers R, M Ruddy B, Xian F (2013) Mass resolution and mass accuracy: how much is enough? Mass Spectrom (Tokyo, Japan) 2:S0009 . doi: 10.5702/massspectrometry.S0009
7. Suizdak G (2004) An introduction to mass spectrometry ionization: An excerpt from The Expanding Role of Mass Spectrometry in Biotechnology, 2nd ed.; MCC Press: San Diego, 2005. J Assoc Lab Autom 9:50–63 . doi: 10.1016/j.jala.2004.01.004
8. Fuchs B, Süß R, Schiller J (2010) An update of MALDI-TOF mass spectrometry in lipid research. Prog Lipid Res 49:450–475 . doi: 10.1016/j.plipres.2010.07.001
9. Awad H, Khamis MM, El-Aneed A (2015) Mass spectrometry, review of the basics: Ionization. Appl Spectrosc Rev 50:158–175 . doi: 10.1080/05704928.2014.954046
10. Jaskolla TW, Karas M (2011) Compelling evidence for lucky survivor and gas phase protonation: The unified MALDI analyte protonation mechanism. J Am Soc Mass Spectrom 22:976–988 . doi: 10.1007/s13361-011-0093-0
11. Karas M, Glückmann M, Schäfer J (2000) Ionization in matrix-assisted laser desorption/ionization: Singly charged molecular ions are the lucky survivors. J Mass Spectrom 35:1–12 . doi: 10.1002/(SICI)1096-9888(200001)35:1<1::AID-JMS904>3.0.CO;2-0
12. Welker M (2011) Proteomics for routine identification of microorganisms. Proteomics 11:3143–3153 . doi: 10.1002/pmic.201100049
13. Aichler M, Walch A (2015) MALDI Imaging mass spectrometry: Current frontiers and perspectives in pathology research and practice. Lab Investig 95:422–431 . doi: 10.1038/labinvest.2014.156
14. Scigelova M, Hornshaw M, Giannakopulos A, Makarov A (2011) Fourier Transform Mass Spectrometry. Mol Cell Proteomics 10:1–66 . doi: 10.1074/mcp.M111.009431
15. Griffiths J (2008) A brief history of mass spectrometry. Anal Chem 80:5678–5683 . doi: 10.1021/ac8013065
16. McLafferty FW (2008) Mass spectrometry across the sciences. Proc Natl Acad Sci U S A 105:18088–18089 . doi: 10.1073/pnas.0800784105
17. Karas M, Bachmann D, Hillenkamp F (1985) Influence of the wavelength in high-irradiance ultraviolet laser desorption mass spectrometry of organic molecules. Anal Chem 57:2935–2939 . doi: 10.1021/ac00291a042
18. Vestal ML (2009) Modern MALDI time-of-flight mass spectrometry. J Mass Spectrom 44:303–317 . doi: 10.1002/jms.1537
19. Tanaka K, Waki H, Ido Y, Akita S, Yoshida Y, Yoshida T, Matsuo T (1988) Protein and polymer analyses up to m/z 100 000 by laser ionization time-of-flight mass spectrometry. Rapid Commun Mass Spectrom 2:151–153 . doi: 10.1002/rcm.1290020802
20. Singhal N, Kumar M, Kanaujia PK, Virdi JS (2015) MALDI-TOF mass spectrometry: an emerging technology for microbial identification and diagnosis. Front Microbiol 6:791 . doi: 10.3389/fmicb.2015.00791

21. Prentice BM, Caprioli RM (2016) The Need for Speed in Matrix-Assisted Laser Desorption/Ionization Imaging Mass Spectrometry. Postdoc J a J Postdr Res Postdr Aff 4:3–13 . doi: 10.1007/978-1-4614-5915-6
22. Anhalt JP, Fenselau C (1975) Identification of Bacteria using Mass Spectrometry. Anal Chem 47:219–225 . doi: 10.1021/ac60352a007
23. Santos IC, Hildenbrand ZL, Schug KA (2016) Applications of MALDI-TOF MS in environmental microbiology. Analyst 141:2827–2837 . doi: 10.1039/C6AN00131A
24. Zhang X, Scalf M, Berggren TW, Westphall MS, Smith LM (2006) Identification of mammalian cell lines using MALDI-TOF and LC-ESI-MS/MS mass spectrometry. J Am Soc Mass Spectrom 17:490–499 . doi: 10.1016/j.jasms.2005.12.007
25. Munteanu B, Von Reitzenstein C, Hänsch GM, Meyer B, Hopf C (2012) Sensitive, robust and automated protein analysis of cell differentiation and of primary human blood cells by intact cell MALDI mass spectrometry biotyping. Anal Bioanal Chem 404:2277–2286 . doi: 10.1007/s00216-012-6357-0
26. Povey JF, O'Malley CJ, Root T, Martin EB, Montague GA, Feary M, Trim C, Lang DA, Alldread R, Racher AJ, Smales CM (2014) Rapid high-throughput characterisation, classification and selection of recombinant mammalian cell line phenotypes using intact cell MALDI-ToF mass spectrometry fingerprinting and PLS-DA modelling. J Biotechnol 184:84–93 . doi: 10.1016/j.jbiotec.2014.04.028
27. Schwamb S, Munteanu B, Meyer B, Hopf C, Hafner M, Wiedemann P (2013) Monitoring CHO cell cultures: Cell stress and early apoptosis assessment by mass spectrometry. J Biotechnol 168:452–461 . doi: 10.1016/j.jbiotec.2013.10.014
28. Dong H, Shen W, Cheung MTW, Liang Y, Cheung HY, Allmaier G, Kin-Chung Au O, Lam YW (2011) Rapid detection of apoptosis in mammalian cells by using intact cell MALDI mass spectrometry. Analyst 136:5181 . doi: 10.1039/c1an15750g
29. Munteanu B, Meyer B, von Reitzenstein C, Burgermeister E, Bog S, Pahl A, Ebert MP, Hopf C (2014) Label-Free in Situ Monitoring of Histone Deacetylase Drug Target Engagement by Matrix-Assisted Laser Desorption Ionization-Mass Spectrometry Biotyping and Imaging. Anal Chem 86:4642–4647 . doi: 10.1021/ac500038j
30. Kober SL, Meyer-Alert H, Grienitz D, Hollert H, Frohme M (2015) Intact cell mass spectrometry as a rapid and specific tool for the differentiation of toxic effects in cell-based ecotoxicological test systems. Anal Bioanal Chem 407:7721–7731 . doi: 10.1007/s00216-015-8937-2
31. Sakai M, Martinez-Arguelles DB, Patterson NH, Chaurand P, Papadopoulos V (2015) In search of the molecular mechanisms mediating the inhibitory effect of the GnRH antagonist degarelix on human prostate cell growth. PLoS One 10:1–23 . doi: 10.1371/journal.pone.0120670
32. Angelini R, Vitale R, Patil V a., Cocco T, Ludwig B, Greenberg ML, Corcelli a. (2012) Lipidomics of intact mitochondria by MALDI-TOF/MS. J Lipid Res 53:1417–1425 . doi: 10.1194/jlr.D026203
33. Angelini R, Lobasso S, Gorgoglione R, Bowron A, Steward CG, Corcelli A (2015) Cardiolipin fingerprinting of leukocytes by MALDI-TOF/MS as a screening tool for Barth syndrome. J Lipid Res 56:1787–1794 . doi: 10.1194/jlr.D059824
34. Lobasso S, Tanzarella P, Vergara D, Maffia M, Cocco T, Corcelli A (2017) Lipid profiling of parkin-mutant human skin fibroblasts. J Cell Physiol 232:3540–3551 . doi: 10.1002/jcp.25815
35. Glückmann M, Pfenninger A, Krüger R, Thierolf M, Karasa M, Horneffer V, Hillenkamp F, Strupat K (2001) Mechanisms in MALDI analysis: Surface interaction or incorporation of analytes? Int J Mass Spectrom 210–211:121–132 . doi: 10.1016/S1387-3806(01)00450-X
36. Korte AR, Lee YJ (2014) MALDI-MS analysis and imaging of small molecule metabolites with 1,5-diaminonaphthalene (DAN). J Mass Spectrom 49:737–741 . doi: 10.1002/jms.3400
37. Groseclose MR, Laffan SB, Frazier KS, Hughes-Earle A, Castellino S (2015) Imaging MS in toxicology: An investigation of juvenile rat nephrotoxicity associated with dabrafenib administration. J Am Soc Mass Spectrom 26:887–898 . doi:

10.1007/s13361-015-1103-4
38. Ruh H, Sandhoff R, Meyer B, Gretz N, Hopf C (2013) Quantitative characterization of tissue globotetraosylceramides in a rat model of polycystic kidney disease by PrimaDrop sample preparation and indirect high-performance thin layer chromatography-matrix-assisted laser desorption/ionization-time-of-flight-. Anal Chem 85:6233–6240 . doi: 10.1021/ac400931u
39. Shanta SR, Zhou LH, Park YS, Kim YH, Kim Y, Kim KP (2011) Binary matrix for MALDI imaging mass spectrometry of phospholipids in both ion modes. Anal Chem 83:1252–1259 . doi: 10.1021/ac1029659
40. Wei Y, Zhang Y, Lin Y, Li L, Liu J, Wang Z, Xiong S, Zhao Z (2015) A uniform 2,5-dihydroxybenzoic acid layer as a matrix for MALDI-FTICR MS-based lipidomics. Analyst 140:1298–1305 . doi: 10.1039/C4AN01964D
41. Kudina O, Eral B, Mugele F (2016) E-MALDI: An Electrowetting-Enhanced Drop Drying Method for MALDI Mass Spectrometry. Anal Chem 88:4669–4675 . doi: 10.1021/acs.analchem.5b04283
42. Schwamborn K, Caprioli RM (2010) MALDI Imaging Mass Spectrometry - Painting Molecular Pictures. Mol Oncol 4:529–538 . doi: 10.1016/j.molonc.2010.09.002
43. Hankin JA, Barkley RM, Murphy RC (2007) Sublimation as a Method of Matrix Application for Mass Spectrometric Imaging. J Am Soc Mass Spectrom 18:1646–1652 . doi: 10.1038/nmeth.2250.Digestion
44. Schiller J, Süß R, Fuchs B, Müller M, Petković M, Zschörnig O, Waschipky H (2007) The suitability of different DHB isomers as matrices for the MALDI-TOF MS analysis of phospholipids: which isomer for what purpose? Eur Biophys J 36:517–527 . doi: 10.1007/s00249-006-0090-6
45. Jaskolla TW, Onischke K, Schiller J (2014) 2,5-Dihydroxybenzoic acid salts for matrix-assisted laser desorption/ionization time-of-flight mass spectrometric lipid analysis: Simplified spectra interpretation and insights into gas-phase fragmentation. Rapid Commun Mass Spectrom 28:1353–1363 . doi: 10.1002/rcm.6910
46. AlMasoud N, Correa E, Trivedi DK, Goodacre R (2016) Fractional Factorial Design of MALDI-TOF-MS Sample Preparations for the Optimized Detection of Phospholipids and Acylglycerols. Anal Chem 88:6301–6308 . doi: 10.1021/acs.analchem.6b00512
47. Erich K, Sammour DA, Marx A, Hopf C (2017) Scores for standardization of on-tissue digestion of formalin-fixed paraffin-embedded tissue in MALDI-MS imaging. Biochim Biophys Acta - Proteins Proteomics 1865:907–915 . doi: 10.1016/j.bbapap.2016.08.020
48. Knochenmuss R (2003) A quantitative model of ultraviolet matrix-assisted laser desorption/ionization including analyte ion generation. Anal Chem 75:2199–2207 . doi: 10.1021/ac034032r
49. Fülöp A, Porada MB, Marsching C, Blott H, Meyer B, Tambe S, Sandhoff R, Junker HD, Hopf C (2013) 4-phenyl-α-cyanocinnamic acid amide: Screening for a negative ion matrix for MALDI-MS imaging of multiple lipid classes. Anal Chem 85:9156–9163 . doi: 10.1021/ac4018154
50. Jollife IT, Cadima J (2016) Principal component analysis: A review and recent developments. Philos Trans R Soc A Math Phys Eng Sci 374:20150202 . doi: 10.1098/rsta.2015.0202
51. Yao I, Sugiura Y, Matsumoto M, Setou M (2008) In situ proteomics with imaging mass spectrometry and principal component analysis in the Scrapper-knockout mouse brain. Proteomics 8:3692–3701 . doi: 10.1002/pmic.200701121
52. Deininger SO, Ebert MP, Fütterer A, Gerhard M, Röcken C (2008) MALDI imaging combined with hierarchical clustering as a new tool for the interpretation of complex human cancers. J Proteome Res 7:5230–5236 . doi: 10.1021/pr8005777
53. Hinners P, O'Neill KC, Lee YJ (2018) Revealing Individual Lifestyles through Mass Spectrometry Imaging of Chemical Compounds in Fingerprints. Sci Rep 8:5149 . doi: 10.1038/s41598-018-23544-7
54. Portevin D, Pflüger V, Otieno P, Brunisholz RR, Vogel G, Daubenberger C (2015) Quantitative whole-cell MALDI-TOF MS fingerprints distinguishes human monocyte sub-populations activated by distinct microbial ligands. BMC Biotechnol 15:24 . doi:

10.1186/s12896-015-0140-1
55. Miranda AA, Le Borgne YA, Bontempi G (2008) New routes from minimal approximation error to principal components. Neural Process Lett 27:197–207 . doi: 10.1007/s11063-007-9069-2
56. Sodhi RNS (2004) Time-of-flight secondary ion mass spectrometry (TOF-SIMS): - Versatility in chemical and imaging surface analysis. Analyst 129:483–487 . doi: 10.1039/b402607c
57. Winter M, Bretschneider T, Kleiner C, Ries R, Hehn JP, Redemann N, Luippold AH, Bischoff D, Büttner FH (2018) Establishing MALDI-TOF as Versatile Drug Discovery Readout to Dissect the PTP1B Enzymatic Reaction. SLAS Discov Adv Life Sci R&D 23:561–573 . doi: 10.1177/2472555218759267
58. Eggert US (2013) The why and how of phenotypic small-molecule screens. Nat Chem Biol 9:206–209 . doi: 10.1038/nchembio.1206
59. Moffat JG, Vincent F, Lee JA, Eder J, Prunotto M (2017) Opportunities and challenges in phenotypic drug discovery: an industry perspective. Nat Rev Drug Discov 16:531–543 . doi: 10.1038/nrd.2017.111
60. Swinney DC, Anthony J (2011) How were new medicines discovered? Nat Rev Drug Discov 10:507–519 . doi: 10.1038/nrd3480
61. Patnaik S, Stevens KL, Gerding R, Deanda F, Shotwell JB, Tang J, Hamajima T, Nakamura H, Leesnitzer MA, Hassell AM, Shewchuck LM, Kumar R, Lei H, Chamberlain SD (2009) Discovery of 3,5-disubstituted-1H-pyrrolo[2,3-b]pyridines as potent inhibitors of the insulin-like growth factor-1 receptor (IGF-1R) tyrosine kinase. Bioorganic Med Chem Lett 19:3136–3140 . doi: 10.1016/j.bmcl.2008.12.110
62. Liu N, Scott WJ, Haegebarth A, Moenning U, Fricke R, Boemer U, Bruening M, Mumberg D, Brands M, Ziegelbauer K (2012) Abstract 2799: BAY 1082439, a highly selective and balanced PI3Kα/β inhibitor demonstrated potent activity in tumors with activated PI3Kα and loss-of-function of PTEN. Cancer Res 72:2799–2799 . doi: 10.1158/1538-7445.AM2012-2799
63. Hevener KE, Pesavento R, Ren J, Lee H, Ratia K, Johnson ME (2018) Hit-to-Lead: Hit Validation and Assessment. Methods Enzymol 610:265–309 . doi: 10.1016/bs.mie.2018.09.022
64. Perola E (2010) An analysis of the binding efficiencies of drugs and their leads in successful drug discovery programs. J Med Chem 53:2986–2997 . doi: 10.1021/jm100118x
65. Schneider G (2018) Automating drug discovery. Nat Rev Drug Discov 17:97–113 . doi: 10.1038/nrd.2017.232
66. Michelini E, Cevenini L, Mezzanotte L, Coppa A, Roda A (2010) Cell-based assays: Fuelling drug discovery. Anal Bioanal Chem 398:227–238 . doi: 10.1007/s00216-010-3933-z
67. Scannell JW, Blanckley A, Boldon H, Warrington B (2012) Diagnosing the decline in pharmaceutical R&D efficiency. Nat Rev Drug Discov 11:191–200 . doi: 10.1038/nrd3681
68. Lane RF, Friedman LG, Keith C, Braithwaite SP, Frearson JA, Lowe DA, Longo FM, Refolo LM, Watterson DM, Tsaioun K, Shineman DW, Fillit HM (2013) Optimizing the use of CROs by academia and small companies. Nat Rev Drug Discov 12:487–488 . doi: 10.1038/nrd4057
69. McKim Jr. J (2010) Building a Tiered Approach to In Vitro Predictive Toxicity Screening: A Focus on Assays with In Vivo Relevance. Comb Chem High Throughput Screen 13:188–206 . doi: 10.2174/138620710790596736
70. Wawer MJ, Li K, Gustafsdottir SM, Ljosa V, Bodycombe NE, Marton MA, Sokolnicki KL, Bray M-A, Kemp MM, Winchester E, Taylor B, Grant GB, Hon CS-Y, Duvall JR, Wilson JA, Bittker JA, Dan ik V, Narayan R, Subramanian A, Winckler W, Golub TR, Carpenter AE, Shamji AF, Schreiber SL, Clemons PA (2014) Toward performance-diverse small-molecule libraries for cell-based phenotypic screening using multiplexed high-dimensional profiling. Proc Natl Acad Sci 111:10911–10916 . doi: 10.1073/pnas.1410933111

71. Lindström S, Andersson-Svahn H (2011) Miniaturization of biological assays - Overview on microwell devices for single-cell analyses. Biochim Biophys Acta - Gen Subj 1810:308–316 . doi: 10.1016/j.bbagen.2010.04.009
72. Janzen WP (2014) Screening technologies for small molecule discovery: The state of the art. Chem Biol 21:1162–1170 . doi: 10.1016/j.chembiol.2014.07.015
73. Vázquez MJ, Leavens W, Liu R, Rodríguez B, Read M, Richards S, Winegar D, Domínguez JM (2008) Discovery of GSK837149A, an inhibitor of human fatty acid synthase targeting the β-ketoacyl reductase reaction. FEBS J 275:1556–1567 . doi: 10.1111/j.1742-4658.2008.06314.x
74. Zhang Z, Guan N, Li T, Mais DE, Wang M (2012) Quality control of cell-based high-throughput drug screening. Acta Pharm Sin B 2:429–438 . doi: 10.1016/j.apsb.2012.03.006
75. Holt TG, Choi BK, Geoghagen NS, Jensen KK, Luo Q, LaMarr WA, Makara GM, Malkowitz L, Ozbal CC, Xiong Y, Dufresne C, Luo M-J (2009) Label-Free High-Throughput Screening via Mass Spectrometry: A Single Cystathionine Quantitative Method for Multiple Applications. Assay Drug Dev Technol 7:495–506 . doi: 10.1089/adt.2009.0200
76. Hopcroft PJ, Fisher DI (2016) Development of a Medium-Throughput Targeted LCMS Assay to Detect Endogenous Cellular Levels of Malonyl-CoA to Screen Fatty Acid Synthase Inhibitors. J Biomol Screen 21:111–116 . doi: 10.1177/1087057115617894
77. Greis KD, Zhou S, Burt TM, Carr AN, Dolan E, Easwaran V, Evdokimov A, Kawamoto R, Roesgen J, Davis GF (2006) MALDI-TOF MS as a Label-Free Approach to Rapid Inhibitor Screening. J Am Soc Mass Spectrom 17:815–822 . doi: 10.1016/j.jasms.2006.02.019
78. Beeman K, Baumgärtner J, Laubenheimer M, Hergesell K, Hoffmann M, Pehl U, Fischer F, Pieck J-C (2017) Integration of an In Situ MALDI-Based High-Throughput Screening Process: A Case Study with Receptor Tyrosine Kinase c-MET. SLAS Discov Adv Life Sci R&D 22:247255521772770 . doi: 10.1177/2472555217727701
79. Heap RE, Hope AG, Pearson L-A, Reyskens KMSE, McElroy SP, Hastie CJ, Porter DW, Arthur JSC, Gray DW, Trost M (2017) Identifying Inhibitors of Inflammation: A Novel High-Throughput MALDI-TOF Screening Assay for Salt-Inducible Kinases (SIKs). SLAS Discov Adv Life Sci R&D 22:1193–1202 . doi: 10.1177/2472555217717473
80. Haslam C, Hellicar J, Dunn A, Fuetterer A, Hardy N, Marshall P, Paape R, Pemberton M, Resemannand A, Leveridge M (2016) The Evolution of MALDI-TOF Mass Spectrometry toward Ultra-High-Throughput Screening: 1536-Well Format and Beyond. J Biomol Screen 21:176–186 . doi: 10.1177/1087057115608605
81. Ritorto MS, Ewan R, Perez-Oliva AB, Knebel A, Buhrlage SJ, Wightman M, Kelly SM, Wood NT, Virdee S, Gray NS, Morrice NA, Alessi DR, Trost M (2014) Screening of DUB activity and specificity by MALDI-TOF mass spectrometry. Nat Commun 5:4763 . doi: 10.1038/ncomms5763
82. Cambridge SB, Gnad F, Nguyen C, Bermejo JL, Krüger M, Mann M (2011) Systems-wide proteomic analysis in mammalian cells reveals conserved, functional protein turnover. J Proteome Res 10:5275–5284 . doi: 10.1021/pr101183k
83. León Z, García-Cañaveras JC, Donato MT, Lahoz A (2013) Mammalian cell metabolomics: Experimental design and sample preparation. Electrophoresis 34:2762–2775 . doi: 10.1002/elps.201200605
84. Zhu M, Zhang H, Humphreys WG (2011) Drug metabolite profiling and identification by high-resolution mass spectrometry. J Biol Chem 286:25419–25425 . doi: 10.1074/jbc.R110.200055
85. Rodriguez-Cuenca S, Barbarroja N, Vidal-Puig A (2015) Dihydroceramide desaturase 1, the gatekeeper of ceramide induced lipotoxicity. Biochim Biophys Acta - Mol Cell Biol Lipids 1851:40–50 . doi: 10.1016/J.BBALIP.2014.09.021
86. Siddique MM, Li Y, Wang L, Ching J, Mal M, Ilkayeva O, Wu YJ, Bay BH, Summers SA (2013) Ablation of dihydroceramide desaturase 1, a therapeutic target for the treatment of metabolic diseases, simultaneously stimulates anabolic and catabolic signaling. Mol Cell Biol 33:2353–69 . doi: 10.1128/MCB.00226-13

87. Flowers MT, Ntambi JM (2008) Role of stearoyl-coenzyme A desaturase in regulating lipid metabolism. Curr Opin Lipidol 19:248–256 . doi: 10.1097/MOL.0b013e3282f9b54d
88. Ordóñez-Gutiérrez L, Benito-Cuesta I, Abad JL, Casas J, Fábrias G, Wandosell F (2018) Dihydroceramide Desaturase 1 Inhibitors Reduce Amyloid-β Levels in Primary Neurons from an Alzheimer's Disease Transgenic Model. Pharm Res 35: . doi: 10.1007/s11095-017-2312-2
89. Qiang L, Kon N, Zhao W, Jiang L, Knight CM, Welch C, Pajvani U, Gu W, Accili D (2015) Hepatic SirT1-Dependent Gain of Function of Stearoyl-CoA Desaturase-1 Conveys Dysmetabolic and Tumor Progression Functions. Cell Rep 11:1797–1808 . doi: 10.1016/j.celrep.2015.05.025
90. von Roemeling CA, Caulfield TR, Marlow L, Bok I, Wen J, Miller JL, Hughes R, Hazlehurst L, Pinkerton AB, Radisky DC, Tun HW, Kim YSB, Lane AL, Copland JA (2018) Accelerated bottom-up drug design platform enables the discovery of novel stearoyl-CoA desaturase 1 inhibitors for cancer therapy. Oncotarget 9:3–20 . doi: 10.18632/oncotarget.21545
91. Jabbour E, Kantarjian H (2018) Chronic myeloid leukemia: 2018 update on diagnosis, therapy and monitoring. Am J Hematol 93:442–459 . doi: 10.1002/ajh.25011
92. Stoklosa T, Poplawski T, Koptyra M, Nieborowska-Skorska M, Basak G, Slupianek A, Rayevskaya M, Seferynska I, Herrera L, Blasiak J, Skorski T (2008) BCR/ABL Inhibits Mismatch Repair to Protect from Apoptosis and Induce Point Mutations. Cancer Res 68:2576–2580 . doi: 10.1158/0008-5472.CAN-07-6858
93. Deininger M, Buchdunger E, Druker BJ (2005) The development of imatinib as a therapeutic agent for chronic myeloid leukemia. Blood 105:2640–2653 . doi: 10.1182/blood-2004-08-3097
94. Capdeville R, Buchdunger E, Zimmermann J, Matter A (2002) Glivec (ST1571, imatinib), a rationally developed, targeted anticancer drug. Nat Rev Drug Discov 1:493–502 . doi: 10.1038/nrd839
95. Hochhaus A, Larson RA, Guilhot F, Radich JP, Branford S, Hughes TP, Baccarani M, Deininger MW, Cervantes F, Fujihara S, Ortmann C-E, Menssen HD, Kantarjian H, O'Brien SG, Druker BJ (2017) Long-Term Outcomes of Imatinib Treatment for Chronic Myeloid Leukemia. N Engl J Med 376:917–927 . doi: 10.1056/NEJMoa1609324
96. Lasota J, Miettinen M (2006) KIT and PDGFRA mutations in gastrointestinal stromal tumors (GISTs). Semin Diagn Pathol 23:91–102 . doi: 10.1053/j.semdp.2006.08.006
97. Ma Y, Zeng S, Metcalfe DD, Akin C, Dimitrijevic S, Butterfield JH, McMahon G, Jack Longley B (2002) The c-KIT mutation causing human mastocytosis is resistant to STI571 and other KIT kinase inhibitors; kinases with enzymatic site mutations show different inhibitor sensitivity profiles than wild-type kinases and those with regulatory-type mutations. Blood 99:1741–1744 . doi: 10.1182/blood.V99.5.1741
98. Milojkovic D, Apperley JF (2009) Mechanisms of resistance to imatinib and second-generation tyrosine inhibitors in chronic myeloid leukemia. Clin Cancer Res 15:7519–7527 . doi: 10.1158/1078-0432.CCR-09-1068
99. Iqbal N, Iqbal N (2014) Imatinib: A Breakthrough of Targeted Therapy in Cancer. Chemother Res Pract 2014:1–9 . doi: 10.1155/2014/357027
100. Wylie AA, Schoepfer J, Jahnke W, Cowan-Jacob SW, Loo A, Furet P, Marzinzik AL, Pelle X, Donovan J, Zhu W, Buonamici S, Hassan AQ, Lombardo F, Iyer V, Palmer M, Berellini G, Dodd S, Thohan S, Bitter H, Branford S, Ross DM, Hughes TP, Petruzzelli L, Vanasse KG, Warmuth M, Hofmann F, Keen NJ, Sellers WR (2017) The allosteric inhibitor ABL001 enables dual targeting of BCR-ABL1. Nature 543:733–737 . doi: 10.1038/nature21702
101. Nagar B, Hantschel O, Young MA, Scheffzek K, Veach D, Bornmann W, Clarkson B, Superti-Furga G, Kuriyan J (2003) Structural basis for the autoinhibition of c-Abl tyrosine kinase. Cell 112:859–871 . doi: 10.1016/S0092-8674(03)00194-6
102. Breitkopf SB, Yuan M, Helenius KP, Lyssiotis CA, Asara JM (2015) Triomics Analysis of Imatinib-Treated Myeloma Cells Connects Kinase Inhibition to RNA Processing and Decreased Lipid Biosynthesis. Anal Chem 87:10995–11006 . doi: 10.1021/acs.analchem.5b03040

103. Menendez JA, Lupu R (2017) Fatty acid synthase (FASN) as a therapeutic target in breast cancer. Expert Opin Ther Targets 21:1001–1016 . doi: 10.1080/14728222.2017.1381087
104. Menendez JA, Vazquez-Martin A, Ortega FJ, Fernandez-Real JM (2009) Fatty acid synthase: Association with insulin resistance, type 2 diabetes, and cancer. Clin Chem 55:425–438 . doi: 10.1373/clinchem.2008.115352
105. Razani B, Zhang H, Schulze PC, Schilling JD, Verbsky J, Lodhi IJ, Topkara VK, Feng C, Coleman T, Kovacs A, Kelly DP, Saffitz JE, Dorn GW, Nichols CG, Semenkovich CF (2011) Fatty acid synthase modulates homeostatic responses to myocardial stress. J Biol Chem 286:30949–30961 . doi: 10.1074/jbc.M111.230508
106. Sato N, Morishita R (2015) The roles of lipid and glucose metabolism in modulation of β-amyloid, tau, and neurodegeneration in the pathogenesis of Alzheimer disease. Front Aging Neurosci 7:199 . doi: 10.3389/fnagi.2015.00199
107. Ventura R, Mordec K, Waszczuk J, Wang Z, Lai J, Fridlib M, Buckley D, Kemble G, Heuer TS (2015) Inhibition of de novo Palmitate Synthesis by Fatty Acid Synthase Induces Apoptosis in Tumor Cells by Remodeling Cell Membranes, Inhibiting Signaling Pathways, and Reprogramming Gene Expression. EBioMedicine 2:808–824 . doi: 10.1016/j.ebiom.2015.06.020
108. Vázquez MJ, Ashman S, Ramón F, Calvo D, Bardera A, Martín JJ, Rüdiger M, Tew D, Domínguez JM (2006) Utilization of substrate-induced quenching for screening targets promoting NADH and NADPH consumption. J Biomol Screen 11:75–81 . doi: 10.1177/1087057105283296
109. Hardwicke MA, Rendina AR, Williams SP, Moore ML, Wang L, Krueger JA, Plant RN, Totoritis RD, Zhang G, Briand J, Burkhart WA, Brown KK, Parrish CA (2014) A human fatty acid synthase inhibitor binds β-ketoacyl reductase in the keto-substrate site. Nat Chem Biol 10:774–779 . doi: 10.1038/nchembio.1603
110. Alwarawrah Y, Hughes P, Loiselle D, Carlson DA, Darr DB, Jordan JL, Xiong J, Hunter LM, Dubois LG, Thompson JW, Kulkarni MM, Ratcliff AN, Kwiek JJ, Haystead TAJ (2016) Fasnall, a Selective FASN Inhibitor, Shows Potent Anti-tumor Activity in the MMTV-Neu Model of HER2+ Breast Cancer. Cell Chem Biol 23:678–688 . doi: 10.1016/j.chembiol.2016.04.011
111. Dean EJ, Falchook GS, Patel MR, Brenner AJ, Infante JR, Arkenau H-T, Borazanci EH, Lopez JS, Pant S, Schmid P, Frankel AE, Jones SF, McCulloch W, Kemble G, O'Farrell M, Burris H (2016) Preliminary activity in the first in human study of the first-in-class fatty acid synthase (FASN) inhibitor, TVB-2640. J Clin Oncol 34:2512 . doi: 10.1200/JCO.2016.34.15_suppl.2512
112. Kley JT, MacK J, Hamilton B, Scheuerer S, Redemann N (2011) Discovery of BI 99179, a potent and selective inhibitor of type i fatty acid synthase with central exposure. Bioorganic Med Chem Lett 21:5924–5927 . doi: 10.1016/j.bmcl.2011.07.083
113. Lu T, Schubert C, Cummings MD, Bignan G, Connolly PJ, Smans K, Ludovici D, Parker MH, Meyer C, Rocaboy C, Alexander R, Grasberger B, De Breucker S, Esser N, Fraiponts E, Gilissen R, Janssens B, Peeters D, Van Nuffel L, Vermeulen P, Bischoff J, Meerpoel L (2018) Design and synthesis of a series of bioavailable fatty acid synthase (FASN) KR domain inhibitors for cancer therapy. Bioorganic Med Chem Lett 28:2159–2164 . doi: 10.1016/j.bmcl.2018.05.014
114. Chung CC, Ohwaki K, Schneeweis JE, Stec E, Varnerin JP, Goudreau PN, Chang A, Cassaday J, Yang L, Yamakawa T, Kornienko O, Hodder P, Inglese J, Ferrer M, Strulovici B, Kusunoki J, Tota MR, Takagi T (2008) A Fluorescence-Based Thiol Quantification Assay for Ultra-High-Throughput Screening for Inhibitors of Coenzyme A Production. Assay Drug Dev Technol 6:361–374 . doi: 10.1089/adt.2007.105
115. Ihaka R, Gentleman R (1996) R: A Language for Data Analysis and Graphics. J Comput Graph Stat 5:299–314 . doi: 10.1080/10618600.1996.10474713
116. Gibb S, Strimmer K (2012) MALDIquant: a versatile R package for the analysis of mass spectrometry data. Bioinformatics 28:2270–2271 . doi: 10.1093/bioinformatics/bts447
117. Wang W, Jüttler B, Zheng D, Liu Y (2008) Computation of rotation minimizing frames. ACM Trans Graph 27:1–18 . doi: 10.1145/1330511.1330513

118. Salonikios T (2017) Dissertation: Automatische Datenanalyse von massenspektrometrischen Signaturen zur Klassifikation von Krebszellen und Bestimmungen von Wirkstoffwirkungen. Universität Heidelberg
119. Mattson MP (2008) Hormesis defined. Ageing Res Rev 7:1–7 . doi: 10.1016/j.arr.2007.08.007
120. Stübiger G, Belgacem O, Rehulka P, Bicker W, Binder BR, Bochkov V (2010) Analysis of oxidized phospholipids by MALDI mass spectrometry using 6-Aza-2-thiothymine together with matrix additives and disposable target surfaces. Anal Chem 82:5502–5510 . doi: 10.1021/ac100280p
121. Weigt D, Sammour DA, Ulrich T, Munteanu B, Hopf C (2018) Automated analysis of lipid drug-response markers by combined fast and high-resolution whole cell MALDI mass spectrometry biotyping. Sci Rep 8:11260 . doi: 10.1038/s41598-018-29677-z
122. Smolira A, Wessely-Szponder J (2014) Importance of the Matrix and the Matrix/Sample Ratio in MALDI-TOF-MS Analysis of Cathelicidins Obtained from Porcine Neutrophils. Appl Biochem Biotechnol 175:2050–2065 . doi: 10.1007/s12010-014-1405-1
123. Donegan M, Tomlinson AJ, Nair H, Juhasz P (2004) Controlling matrix suppression for matrix-assisted laser desorption/ionization analysis of small molecules. Rapid Commun Mass Spectrom 18:1885–1888 . doi: 10.1002/rcm.1568
124. Cantor JR, Abu-Remaileh M, Kanarek N, Freinkman E, Gao X, Louissaint A, Lewis CA, Sabatini DM (2017) Physiologic Medium Rewires Cellular Metabolism and Reveals Uric Acid as an Endogenous Inhibitor of UMP Synthase. Cell 169:258–272.e17 . doi: 10.1016/j.cell.2017.03.023
125. Yang J, Caprioli RM (2011) Matrix sublimation/recrystallization for imaging proteins by mass spectrometry at high spatial resolution. Anal Chem 83:5728–5734 . doi: 10.1021/ac200998a
126. Huang YY, Chen AC-H, Carroll JD, Hamblin MR (2009) Biphasic dose response in low level lightherapy. Dose-Response 7:358–383 . doi: 10.2203/dose-response.09-027.Hamblin
127. Zuardi AW, Rodrigues NP, Silva AL, Bernardo SA, Hallak JEC, Guimarães FS, Crippa JAS (2017) Inverted U-shaped dose-response curve of the anxiolytic effect of cannabidiol during public speaking in real life. Front Pharmacol 8:259 . doi: 10.3389/fphar.2017.00259
128. Castro-Perez J, Roddy TP, Nibbering NMM, Shah V, McLaren DG, Previs S, Attygalle AB, Herath K, Chen Z, Wang SP, Mitnaul L, Hubbard BK, Vreeken RJ, Johns DG, Hankemeier T (2011) Localization of fatty acyl and double bond positions in phosphatidylcholines using a dual stage CID fragmentation coupled with ion mobility mass spectrometry. J Am Soc Mass Spectrom 22:1552–1567 . doi: 10.1007/s13361-011-0172-2
129. Beham-Schmid C, Apfelbeck U, Sill H, Tsybrovsky O, Höfler G, Haas OA, Linkesch W (2002) Treatment of chronic myelogenous leukemia with the tyrosine kinase inhibitor STI571 results in marked regression of bone marrow fibrosis. Blood 99:381–383 . doi: 10.1182/blood.V99.1.381
130. Alves LR, Costa ES, Sorgine MHF, Nascimento-Silva MCL, Teodosio C, Bárcena P, Castro-Faria-Neto HC, Bozza PT, Orfao A, Oliveira PL, Maya-Monteiro CM (2011) Heme-oxygenases during erythropoiesis in K562 and human bone marrow cells. PLoS One 6:e21358 . doi: 10.1371/journal.pone.0021358
131. Cristea IM, Degli Esposti M (2004) Membrane lipids and cell death: An overview. Chem Phys Lipids 129:133–160 . doi: 10.1016/j.chemphyslip.2004.02.002
132. Wang XQ (2003) Apoptotic insults impair Na+, K+-ATPase activity as a mechanism of neuronal death mediated by concurrent ATP deficiency and oxidant stress. J Cell Sci 116:2099–2110 . doi: 10.1242/jcs.00420
133. Wang J, Pendergast AM (2015) The Emerging Role of ABL Kinases in Solid Tumors. Trends in Cancer 1:110–123 . doi: 10.1016/j.trecan.2015.07.004
134. Annunziata CM, Walker AJ, Minasian L, Yu M, Kotz H, Wood BJ, Calvo K, Choyke P, Kimm D, Steinberg SM, Kohn EC (2010) Vandetanib, designed to inhibit VEGFR2 and EGFR signaling, had no clinical activity as monotherapy for recurrent ovarian cancer

and no detectable modulation of VEGFR2. Clin Cancer Res 16:664–672 . doi: 10.1158/1078-0432.CCR-09-2308
135. Papaetis GS, Syrigos KN (2009) Sunitinib: A multitargeted receptor tyrosine kinase inhibitor in the era of molecular cancer therapies. BioDrugs 23:377–389 . doi: 10.2165/11318860-000000000-00000
136. Ibrahim H, Jurcic K, Wang JS-H, Whitehead SN, Yeung KK-C (2017) 1,6-Diphenyl-1,3,5-hexatriene (DPH) as a Novel Matrix for MALDI MS Imaging of Fatty Acids, Phospholipids, and Sulfatides in Brain Tissues. Anal Chem acs.analchem.7b03284 . doi: 10.1021/acs.analchem.7b03284
137. Pizer ES, Thupari J, Han WF, Pinn ML, Chrest FJ, Frehywot GL, Townsend CA, Kuhajda FP (2000) Malonyl-coenzyme-A is a potential mediator of cytotoxicity induced by fatty-acid synthase inhibition in human breast cancer cells and xenografts. Cancer Res 60:213–218 . doi: 10.1158/0008-5472.can-2148-2
138. Thupari JN, Pinn ML, Kuhajda FP (2001) Fatty Acid Synthase Inhibition in Human Breast Cancer Cells Leads to Malonyl-CoA-Induced Inhibition of Fatty Acid Oxidation and Cytotoxicity. Biochem Biophys Res Commun 285:217–223 . doi: 10.1006/bbrc.2001.5146
139. Liu X, Sadhukhan S, Sun S, Wagner GR, Hirschey MD, Qi L, Lin H, Locasale JW (2015) High-Resolution Metabolomics with Acyl-CoA Profiling Reveals Widespread Remodeling in Response to Diet. Mol Cell Proteomics 14:1489–1500 . doi: 10.1074/mcp.M114.044859
140. Liu J, Ouyang Z (2013) Mass spectrometry imaging for biomedical applications. Anal Bioanal Chem 405:5645–5653 . doi: 10.1007/s00216-013-6916-z
141. Heck AM, Yanovski JA, Calis KA (2000) Orlistat, a new lipase inhibitor for the management of obesity. Pharmacotherapy 20:270–279 . doi: 10.1592/phco.20.4.270.34882
142. Kridel SJ, Axelrod F, Rozenkrantz N, Smith JW (2004) Orlistat Is a Novel Inhibitor of Fatty Acid Synthase with Antitumor Activity. Cancer Res 64:2070–2075 . doi: 10.1158/0008-5472.CAN-03-3645
143. Sadowski MC, Pouwer RH, Gunter JH, Lubik AA, Quinn RJ, Nelson CC (2014) The fatty acid synthase inhibitor triclosan: repurposing an anti-microbial agent for targeting prostate cancer. Oncotarget 5:1–20 . doi: 10.18632/oncotarget.2433
144. Liu B, Wang Y, Fillgrove KL, Anderson VE (2002) Triclosan inhibits enoyl-reductase of type I fatty acid synthase in vitro and is cytotoxic to MCF-7 and SKBr-3 breast cancer cells. Cancer Chemother Pharmacol 49:187–193 . doi: 10.1007/s00280-001-0399-x
145. Zhang JH, Chung TDY, Oldenburg KR (1999) A simple statistical parameter for use in evaluation and validation of high throughput screening assays. J Biomol Screen 4:67–73 . doi: 10.1177/108705719900400206
146. Gibellini F, Smith TK (2010) The Kennedy pathway-de novo synthesis of phosphatidylethanolamine and phosphatidylcholine. IUBMB Life 62:414–428 . doi: 10.1002/iub.337
147. Wang C, Xu C, Sun M, Luo D, Liao D, Cao D (2009) Acetyl-CoA carboxylase-α inhibitor TOFA induces human cancer cell apoptosis. Biochem Biophys Res Commun 385:302–306 . doi: 10.1016/j.bbrc.2009.05.045
148. Buckley D, Duke G, Heuer TS, O'Farrell M, Wagman AS, McCulloch W, Kemble G (2017) Fatty acid synthase – Modern tumor cell biology insights into a classical oncology target. Pharmacol Ther 177:23–31 . doi: 10.1016/j.pharmthera.2017.02.021
149. Landree LE, Hanlon AL, Strong DW, Rumbaugh G, Miller IM, Thupari JN, Connolly EC, Huganir RL, Richardson C, Witters LA, Kuhajda FP, Ronnett G V (2004) C75, a Fatty Acid Synthase Inhibitor, Modulates AMP-activated Protein Kinase to Alter Neuronal Energy Metabolism. J Biol Chem 279:3817–3827 . doi: 10.1074/jbc.M310991200
150. Puig T, Turrado C, Benhamu B, Aguilar H, Relat J, Ortega-Gutierrez S, Casals G, Marrero PF, Urruticoechea A, Haro D, Lopez-Rodriguez ML, Colomer R (2009) Novel Inhibitors of Fatty Acid Synthase with Anticancer Activity. Clin Cancer Res 15:7608–7615 . doi: 10.1158/1078-0432.CCR-09-0856
151. Ferguson LR, Denny WA (1991) The genetic toxicology of acridines. Mutat Res Genet

Toxicol 258:123–160 . doi: 10.1016/0165-1110(91)90006-H
152. Ogrinc Potočnik N, Porta T, Becker M, Heeren RMA, Ellis SR (2015) Use of advantageous, volatile matrices enabled by next-generation high-speed matrix-assisted laser desorption/ionization time-of-flight imaging employing a scanning laser beam. Rapid Commun Mass Spectrom 29:2195–2203 . doi: 10.1002/rcm.7379
153. Watrous JD, Alexandrov T, Dorrestein PC (2011) The evolving field of imaging mass spectrometry and its impact on future biological research. J Mass Spectrom 46:209–22 . doi: 10.1002/jms.1876
154. Schulz S, Becker M, Groseclose MR, Schadt S, Hopf C (2019) Advanced MALDI mass spectrometry imaging in pharmaceutical research and drug development. Curr Opin Biotechnol 55:51–59 . doi: 10.1016/j.copbio.2018.08.003
155. Huang Z, Shao W, Gu J, Hu X, Shi Y, Xu W, Huang C, Lin D (2015) Effects of culture media on metabolic profiling of the human gastric cancer cell line SGC7901. Mol Biosyst 11:1832–1840 . doi: 10.1039/c5mb00019j
156. Teearu A, Vahur S, Haljasorg U, Leito I, Haljasorg T, Toom L (2014) 2,5-Dihydroxybenzoic acid solution in MALDI-MS: ageing and use for mass calibration. J Mass Spectrom 49:970–979 . doi: 10.1002/jms.3395
157. Sévin DC, Fuhrer T, Zamboni N, Sauer U (2016) Nontargeted in vitro metabolomics for high-throughput identification of novel enzymes in Escherichia coli. Nat Methods 14:187–194 . doi: 10.1038/nmeth.4103
158. Weißflog J, Svatoš A (2016) 1,8-Di(piperidinyl)-naphthalene-rationally designed MAILD/MALDI matrix for metabolomics and imaging mass spectrometry. RSC Adv 6:75073–75081 . doi: 10.1039/c6ra17237g
159. Giampà M, Lissel MB, Patschkowski T, Fuchser J, Hans VH, Gembruch O, Bednarz H, Niehaus K (2016) Maleic anhydride proton sponge as a novel MALDI matrix for the visualization of small molecules (<250: M / z) in brain tumors by routine MALDI ToF imaging mass spectrometry. Chem Commun 52:9801–9804 . doi: 10.1039/c6cc02387h
160. Thomas A, Charbonneau JL, Fournaise E, Chaurand P (2012) Sublimation of new matrix candidates for high spatial resolution imaging mass spectrometry of lipids: Enhanced information in both positive and negative polarities after 1,5-diaminonapthalene deposition. Anal Chem 84:2048–2054 . doi: 10.1021/ac2033547
161. Rechthaler J, Pittenauer E, Schaub TM, Allmaier G (2013) Detection of amine impurity and quality assessment of the MALDI matrix α-cyano-4-hydroxy-cinnamic acid for peptide analysis in the amol range. J Am Soc Mass Spectrom 24:701–710 . doi: 10.1007/s13361-013-0614-0
162. Xu S, Li Y, Zou H, Qiu J, Guo Z, Guo B (2003) Carbon Nanotubes as Assisted Matrix for Laser Desorption/Ionization Time-of-Flight Mass Spectrometry. Anal Chem 75:6191–6195 . doi: 10.1021/ac0345695
163. Pan C, Xu S, Hu L, Su X, Ou J, Zou H, Guo Z, Zhang Y, Guo B (2005) Using oxidized carbon nanotubes as matrix for analysis of small molecules by MALDI-TOF MS. J Am Soc Mass Spectrom 16:883–892 . doi: 10.1016/j.jasms.2005.03.009
164. Rainer M, Qureshi MN, Bonn GK (2011) Matrix-free and material-enhanced laser desorption/ionization mass spectrometry for the analysis of low molecular weight compounds. Anal Bioanal Chem 400:2281–2288 . doi: 10.1007/s00216-010-4138-1
165. Kusano M, Kawabata S-I, Tamura Y, Mizoguchi D, Murouchi M, Kawasaki H, Arakawa R, Tanaka K (2014) Laser Desorption/Ionization Mass Spectrometry (LDI-MS) of Lipids with Iron Oxide Nanoparticle-Coated Targets. Mass Spectrom 3:A0026–A0026 . doi: 10.5702/massspectrometry.A0026
166. Gurard-Levin ZA, Scholle MD, Eisenberg AH, Mrksich M (2011) High-Throughput Screening of Small Molecule Libraries using SAMDI Mass Spectrometry. ACS Comb Sci 13:347–350 . doi: 10.1021/co2000373
167. Quigley JG, Yang Z, Worthington MT, Phillips JD, Sabo KM, Sabath DE, Berg CL, Sassa S, Wood BL, Abkowitz JL (2004) Identification of a human heme exporter that is essential for erythropoiesis. Cell 118:757–766 . doi: 10.1016/j.cell.2004.08.014
168. Hiep NC, Kinohira S, Furuyama K, Taketani S (2012) Depletion of glutamine enhances sodium butyrate-induced erythroid differentiation of K562 cells. J Biochem 152:509–519

. doi: 10.1093/jb/mvs097
169. Cortesi R, Gui V, Osti F, Nastruzzi C, Gambari R (1998) Human leukemic K562 cells treated with cytosine arabinoside: enhancement of erythroid differentiation by retinoic acid and retinol. Eur J Haematol 61:295–301 . doi: 10.1111/j.1600-0609.1998.tb01091.x
170. Khan AA, Quigley JG (2011) Control of intracellular heme levels: Heme transporters and heme oxygenases. Biochim Biophys Acta - Mol Cell Res 1813:668–682 . doi: 10.1016/j.bbamcr.2011.01.008
171. Hietakangas V, Poukkula M, Heiskanen KM, Karvinen JT, Sistonen L, Eriksson JE (2003) Erythroid differentiation sensitizes K562 leukemia cells to TRAIL-induced apoptosis by downregulation of c-FLIP. Mol Cell Biol 23:1278–91 . doi: 10.1128/MCB.23.4.1278
172. Bonovolias ID, Tsiftsoglou AS (2009) Hemin counteracts the repression of Bcl-2 and NrF2 genes and the cell killing induced by imatinib in human Bcr-Abl(+) CML cells. Oncol Res 17:535–547 . doi: 10.3727/096504009789745557
173. Noel BM, Ouellette SB, Marholz L, Navis C, Yang T-Y, Nguyen V, Parker SJ, Sachs Z, Parker LL (2018) Multi-omic profiling of TKI resistant K562 cells suggests metabolic reprogramming to promote cell survival. bioRxiv 308528 . doi: 10.1101/308528
174. Burns TA, Subathra M, Signorelli P, Choi Y, Yang X, Wang Y, Villani M, Bhalla K, Zhou D, Luberto C (2013) Sphingomyelin synthase 1 activity is regulated by the BCR-ABL oncogene. J Lipid Res 54:794–805 . doi: 10.1194/jlr.M033985
175. Watson H (2015) Biological membranes. Essays Biochem 59:43–69 . doi: 10.1042/bse0590043
176. Cilloni D, Saglio G (2012) Molecular pathways: BCR-ABL. Clin Cancer Res 18:930–937 . doi: 10.1158/1078-0432.CCR-10-1613
177. Kalimuthu S, Se-Kwon K (2013) Cell survival and apoptosis signaling as therapeutic target for cancer: Marine bioactive compounds. Int J Mol Sci 14:2334–2354 . doi: 10.3390/ijms14022334
178. Scott A (2018) A CRISPR path to drug discovery. Nature 555:S10–S11 . doi: 10.1038/d41586-018-02477-1
179. Grskovic M, Javaherian A, Strulovici B, Daley GQ (2011) Induced pluripotent stem cells — opportunities for disease modelling and drug discovery. Nat Rev Drug Discov 10:915–929 . doi: 10.1038/nrd3577
180. Takahashi T (2019) Organoids for Drug Discovery and Personalized Medicine. Annu Rev Pharmacol Toxicol 59:annurev-pharmtox-010818-021108 . doi: 10.1146/annurev-pharmtox-010818-021108
181. Norris JL, Caprioli RM (2013) Analysis of tissue specimens by matrix-assisted laser desorption/ionization imaging mass spectrometry in biological and clinical research. Chem Rev 113:2309–42 . doi: 10.1021/cr3004295
182. Paglia DE, Valentine WN, Nakatani M, Rauth BJ (1983) Selective accumulation of cytosol CDP-choline as an isolated erythrocyte defect in chronic hemolysis. Proc Natl Acad Sci 80:3081–3085 . doi: 10.1073/pnas.80.10.3081
183. Petersen A, Borregaard N (1997) A family with chronic haemolysis and selective accumulation of erythrocyte CDP-choline. Leukemia 11:1373–1376 . doi: 10.1038/sj.leu.2400689
184. Boggs KP, Rock CO, Jackowski S (1995) Lysophosphatidylcholine and 1-O-octadecyl-2-O-methyl-rac-glycero-3- phosphocholine inhibit the CDP-choline pathway of phosphatidylcholine synthesis at the CTP:phosphocholine cytidylyltransferase step. J Biol Chem 270:7757–7764 . doi: 10.1074/jbc.270.13.7757
185. Kim KH (1983) Regulation of Acetyl-CoA Carboxylase. Curr Top Cell Regul 22:143–176 . doi: 10.1016/B978-0-12-152822-5.50009-9
186. Hatzis C, Bedard PL, Birkbak NJ, Beck AH, Aerts HJWL, Stern DF, Shi L, Clarke R, Quackenbush J, Haibe-Kains B (2014) Enhancing reproducibility in cancer drug screening: How do we move forward? Cancer Res 74:4016–4023 . doi: 10.1158/0008-5472.CAN-14-0725
187. McDonald GR, Hudson AL, Dunn SMJ, You H, Baker GB, Whittal RM, Martin JW, Jha A, Edmondson DE, Holt A (2008) Bioactive contaminants leach from disposable

laboratory plasticware. Science (80-) 322:917 . doi: 10.1126/science.1162395
188. Bordag N, Janakiraman V, Nachtigall J, González Maldonado S, Bethan B, Laine JP, Fux E (2016) Fast filtration of bacterial or mammalian suspension cell cultures for optimal metabolomics results. PLoS One 11:e0159389 . doi: 10.1371/journal.pone.0159389
189. Keenan AB, Jenkins SL, Jagodnik KM, Koplev S, He E, Torre D, Wang Z, Dohlman AB, Silverstein MC, Lachmann A, Kuleshov M V., Ma'ayan A, Stathias V, Terryn R, Cooper D, Forlin M, Koleti A, Vidovic D, Chung C, Schürer SC, Vasiliauskas J, Pilarczyk M, Shamsaei B, Fazel M, Ren Y, Niu W, Clark NA, White S, Mahi N, Zhang L, Kouril M, Reichard JF, Sivaganesan S, Medvedovic M, Meller J, Koch RJ, Birtwistle MR, Iyengar R, Sobie EA, Azeloglu EU, Kaye J, Osterloh J, Haston K, Kalra J, Finkbiener S, Li J, Milani P, Adam M, Escalante-Chong R, Sachs K, Lenail A, Ramamoorthy D, Fraenkel E, Daigle G, Hussain U, Coye A, Rothstein J, Sareen D, Ornelas L, Banuelos M, Mandefro B, Ho R, Svendsen CN, Lim RG, Stocksdale J, Casale MS, Thompson TG, Wu J, Thompson LM, Dardov V, Venkatraman V, Matlock A, Van Eyk JE, Jaffe JD, Papanastasiou M, Subramanian A, Golub TR, Erickson SD, Fallahi-Sichani M, Hafner M, Gray NS, Lin JR, Mills CE, Muhlich JL, Niepel M, Shamu CE, Williams EH, Wrobel D, Sorger PK, Heiser LM, Gray JW, Korkola JE, Mills GB, LaBarge M, Feiler HS, Dane MA, Bucher E, Nederlof M, Sudar D, Gross S, Kilburn DF, Smith R, Devlin K, Margolis R, Derr L, Lee A, Pillai A (2018) The Library of Integrated Network-Based Cellular Signatures NIH Program: System-Level Cataloging of Human Cells Response to Perturbations. Cell Syst 6:13–24 . doi: 10.1016/j.cels.2017.11.001
190. Niepel M, Hafner M, Duan Q, Wang Z, Paull EO, Chung M, Lu X, Stuart JM, Golub TR, Subramanian A, Ma'Ayan A, Sorger PK (2017) Common and cell-type specific responses to anti-cancer drugs revealed by high throughput transcript profiling. Nat Commun 8:1186 . doi: 10.1038/s41467-017-01383-w
191. Jin Q, Yuan LX, Boulbes D, Baek JM, Wang YN, Gomez-Cabello D, Hawke DH, Yeung SC, Lee MH, Hortobagyi GN, Hung MC, Esteva FJ (2010) Fatty acid synthase phosphorylation: A novel therapeutic target in HER2-overexpressing breast cancer cells. Breast Cancer Res 12:R96 . doi: 10.1186/bcr2777
192. Jensen-Urstad APL, Song H, Lodhi IJ, Funai K, Yin L, Coleman T, Semenkovich CF (2013) Nutrient-dependent phosphorylation channels lipid synthesis to regulate PPARα. J Lipid Res 54:1848–1859 . doi: 10.1194/jlr.M036103
193. Amantonico A, Urban PL, Fagerer SR, Balabin RM, Zenobi R (2010) Single-cell MALDI-MS as an analytical tool for studying intrapopulation metabolic heterogeneity of unicellular organisms. Anal Chem 82:7394–7400 . doi: 10.1021/ac1015326
194. Boggio KJ, Obasuyi E, Sugino K, Nelson SB, Agar NYR, Agar JN (2012) Recent advances in single-cell MALDI MS imaging and potential clinical impact. Expert Rev Proteomics 8:591–604 . doi: 10.1586/epr.11.53.Recent
195. Short SP, Costacurta PW, Williams CS (2017) Using 3D Organoid Cultures to Model Intestinal Physiology and Colorectal Cancer. Curr Colorectal Cancer Rep 13:183–191 . doi: 10.1007/s11888-017-0363-8
196. Bergmann S, Lawler SE, Qu Y, Fadzen CM, Wolfe JM, Regan MS, Pentelute BL, Agar NYR, Cho CF (2018) Blood–brain-barrier organoids for investigating the permeability of CNS therapeutics. Nat Protoc 13:2827–2843 . doi: 10.1038/s41596-018-0066-x
197. Chang SH, Han JL, Tseng SY, Lee HY, Lin CW, Lin YC, Jeng WY, Wang AHJ, Wu CY, Wong CH (2010) Glycan array on aluminum oxide-coated glass slides through phosphonate chemistry. J Am Chem Soc 132:13371–13380 . doi: 10.1021/ja1046523
198. Mascini NE, Teunissen J, Noorlag R, Willems SM, Heeren RMA (2018) Tumor classification with MALDI-MSI data of tissue microarrays: A case study. Methods 151:21–27 . doi: 10.1016/j.ymeth.2018.04.004

7 ACKNOWLEGDEMENTS

Abschließend möchte ich meine Dankbarkeit zum Ausdruck bringen und mich an all die Leute wenden, die diese Arbeit ermöglicht haben.

Mein ganz besonderer Dank gilt Prof. Carsten Hopf, der mich in sein Team großartiger Wissenschaftler aufgenommen hat und mir dieses spannende Thema angeboten hat. Ich bin dankbar für seine unermüdliche Unterstützung und durchdachte Beratung während meiner Doktorarbeit. Des Weiteren möchte ich Prof. Britta Brügger danken, dass sie den Vorsitz der Begutachtung meiner Doktorarbeit übernommen hat. Ich bin dankbar für ihre ermunternde Begeisterung für meinen wissenschaftlichen Fortschritt im Verlauf meiner Doktorarbeit. Auch möchte ich Prof. Matthias Mayer dafür danken, dass er meine Arbeit begleitete. Darüber hinaus möchte ich Prof. Matthias Mack für das Einwerben des NanokatII Projektes, sowie die Begleitung meiner Arbeit in regelmäßigen Nanokat-Meetings danken. Ich möchte mich dafür bedanken, dass ich meine Arbeit im Labor von CeMOS an der Hochschule Mannheim durchführen durfte und danke CeMOS für die Bereitstellung der hervorragenden MS Infrastruktur.

Ganz ausdrücklich möchte ich mich auch bei den Mitgliedern des Hopf-Labors bedanken, die mich als vielseitiges und starkes Team in den letzten Jahren begleiteten. Dr. Bogdan Munteanu danke ich dafür, dass er mich in die Thematik der MALDI MS basierten Zellassays einarbeitete und stets beratend zur Seite stand. Ich möchte mich bei Denis-Abu Sammour und Timon Ulrich für ihre Expertise und Unterstützung beim Erstellen von R-Skripten bedanken. Dr. Annabelle Fülöp und Dr. Christian Marsching danke ich für wertvolle Diskussionen, insbesondere über die Chemie und Massenspektrometrie der Metabolite. Alexander Geisel danke ich für seine immer-kritischen Anmerkungen. Auch danke ich meinen weiteren Kollegen und Freunden Rebecca Brendel, Dr. Jinrui Gan, Dr. Carina Ramallo Guevara, Dr. Sandra Schulz, Melissa Unger, Dr. Quiquin Zhou, Robert Boll, Thomas Enzlein, Ralf Müller, Dr. Jan-Hinrich Rabe, Matthias Schwartz, Dr. Sebastian Schwolow und Dr. Diego Yepes für die Gestaltung einer angenehmen Arbeitsatmosphäre und ihre beispiellose Hilfsbereitschaft.

Mein Dank gilt zudem dem BMBF für die Finanzierung meiner Doktorandenstelle. Ich danke dem großartigen HBIGS Team, insbesondere Martina Galvan, Sandra Martini und Rolf Lutz für ihre durchweg zuvorkommende und freundliche Unterstützung. Auch danke ich Swen Tyrasa der Firma Analytik Jena für die gute wissenschaftliche Zusammenarbeit mit der Pipetrierplattform. Boehringer Ingelheim danke ich für die Bereitstellung von Wirkstoffen.

Zu guter Letzt möchte ich meiner Familie und meinen Freunden dafür danken, dass sie immer für mich da waren. Meinen Eltern danke ich für ihren unvergleichlichen Rückhalt in allen Lebenslagen. Meiner Freundin Hannah Henrich danke ich für ihre bedingungslose Liebe.